UNIVERSITÀ DEGLI STUDI DI MILANO

SCUOLA DI DOTTORATO DI RICERCA IN SCIENZE BIOCHIMICHE, NUTRIZIONALI E METABOLICHE

DOTTORATO DI RICERCA IN BIOCHIMICA
CICLO XXIII

TESI DI DOTTORATO DI RICERCA

Nanostructured biosensors for the detection of foodborne pathogens and toxins

Relatore: Ch. ma Prof.ssa Silvia Pagani

Correlatori: Ch.mo Prof. Gian Franco Greppi

Ch.mo Prof. Plinio Innocenzi

Dottorando: Stefania Mura

Matricola: R07807

Settore disciplinare: BIO10

Coordinatori: Ch. mo Prof. Sandro Sonnino

Ch.mo Prof. Francesco Bonomi

Anno accademico 2009/2010

A

Salvatore

e alla mia famiglia

che mi hanno accompagnato

incondizionatamente

in questo lungo

percorso

Abstract

New, fast, low cost and simple methods were developed to provide tools to detect a possible contamination of foodborne pathogens or environmental toxins, avoiding the diffusion of dangerous food. New biosensors were created using nanostructured thin films deposited on silicon wafers as substrates. In detail mesoporous materials (pores of 2-40 nm) of SiO_2, TiO_2, HfO_2, ZrO_2 were synthesized via "evaporation induced self assembly", and the behaviour of these materials was studied at different temperature and in PBS solution. Mesoporous titania thin films have been identified as the materials with the best properties and therefore were used for the development of the final devices. First of all a biosensor for the detection of dioxins was developed. Titania films were functionalized with APTES, an organic linker, and three peptides selective for Dioxins (TCDD) were linked to the amino-terminal groups. The peptides were bonded to a fluorescent marker, FITC, and the fluorescence variations were studied after the absorption of TCDD on the films. In this way it was possible to obtain a chip able to detect pM levels of TCDD. The second part of the work was based on the detection of pathogens with FTIR, using mesoporous titania as substrate for the development of the biosensor. This time titania thin films were functionalized with specific antibodies for the detection of E.coli O157:H7. The absorption of antibodies was carried out directly on the substrates and on the substrates functionalized with APTES and GA (Glutaraldehyde) used as cross linker. With the functionalized films were reached detection limits of $1x10^2$ CFU/ ml of E.coli. These results obtained with our devices have been competitive with the existing bioassay methods but with advantages compared to the old techniques as low cost, simplicity, speed of analysis, and possibility to use on-field. This methods can be effective for a screening of samples but, for more specific analysis, a better sensibility is required. To reach lower detection limits was used another vibrational technique, Raman spectroscopy, complementary to FTIR, taking advantage of new properties due to the SERS effect. This technique is based on the detection of analytes adsorbed, or in close proximity, of a special resonant surface of a noble metal (Ag). Starting from our materials (mesoporous titania thin films) were grown Ag^0 nanoparticles into the pores of titania films that worked as a mold for directing the size and the distribution of nanoparticles, avoiding nanoparticle dispersion and aggregation. The features were monitored to obtain a material able to detect analytes in very low concentration and the effectiveness of these materials was studied dipping titania-AgNPs thin films in Rhodamine B isothiocyanate (RhBITC) and Cytochrome C (CytC) solutions. The results obtained from raman measures revealed that films with the analyte (TiO_2 films without AgNPs) showed a Raman spectrum visible until a concentration of $1x10^{-3}$M; while with our new substrates (TiO_2 films with AgNPs) it was possible to discriminate the spectrum of RhITC and Cytocrome C until a concentration of $1x10^{-16}$ M, obtaining an analytical enhancement factor AEF of $1x10^{13}$. This is an excellent result that can be applied to the detection of different contaminants because each one has a characteristic fingerprint and can be discriminated with this technique with or without the use of labels. In this way will be possible to use these substrates for the detection of contaminants in very low concentration, until a single molecule level, opening the route to new ways of detection, simple, fast, low cost; achieving the objective of our work.

Introduction

Food safety and foodborne illness

Food safety is an important public health issue in developed and developing countries, for this reason there is a big interest in this field. In the last years there have been different problems related to food safety because new foodborne diseases appeared. There are different causes that have exacerbated this problem as the increase in international travel and trade that helped to spread the local pathogens into new geographic areas, the microbial adaptation, changes in microorganisms and in food production systems, changes in human population and in lifestyle, globalization of the food supply; all these behaviours have produced foodborne diseases. Foodborne illnesses are diseases derived by pathogens or environmental toxins that enter into the body with the consumption of food or water and can be infectious or toxic in nature. There are some studies that report how only in 2005 there has been a mortality of 1.8 million people in the world caused by diarrhoeal diseases, even if difficult to estimate, it seems that in industrialized countries the 30% of the population suffers for diseases related to food consumption [1]. These problems are accentuated in developing countries where the hygienic standards are low and parasites cause a big warning for food security. Most infections are not reported because of small dimensions but there have been several that involved a big number of individuals. The major microorganisms involved in these diseases have been identified as Salmonella, Campylobacter, Listeria, Escherichia coli, Vibrio cholerae. In particular, infections due to enterohaemorrhagic E. coli, have a relatively low incidence but produce severe and sometimes fatal health consequences, particularly among infants, children and the elderly, resulting among the most serious foodborne infections. In 1982 the first infection caused by Escherichia coli serotype O157:H7 has been described in literature; it can be contracted with the assumption of some particular food as lettuce, beef, cheese curd, raw milk, game meat and unpasteurized fruit juice and has been identified as the major cause of acute renal failure and bloody diarrhoea. Due to this hazards nowadays there is the need to avoid the diffusion of contaminated food and with this purpose led to focus a part of our work on the development of new detection methods to prevent the diffusion of foodborne pathogens, in order to improve food safety.

In addition to food diseases caused by microrganisms in the last years there have been several cases produced by cyanogenic glycosides, toxins contracted from poisonous mushrooms, natural

toxins as mycotoxins (ochratoxin A and aflatoxin), marine biotoxins, that frequently cause intoxications. There are also other agents that can be transmitted to humans with the consumption of bovine products and brain tissues as the bovine spongiform encephalopathy (BSE, or "mad cow disease") associated with the human variant Creutzfeldt-Jakob Disease (vCJD). Other toxic compounds of great hazard in food chain, and in particular in fishery, are metals, such as lead and mercury. As well as pathogens, metals and natural toxins, there are also other chemical agents that can enter in the food chain and cause diseases as the Persistent Organic Pollutants (POPs) compounds that can accumulate in the environment and enter into the human body as dioxins and polychlorinated biphenyls (PCBs) [1]. PCBs and Dioxins can be produced from waste incineration and as by-products of industrial processes; the chronic exposure to these agents can lead to dangerous effects in humans as cancer and death. These compounds and POPs contaminate food through pollution of air, water and soil and it is important to know their presence in food to prevent illnesses. For the great incidence of these compounds in our country and for the frequent food complaints was decided to develop a new, fast method of detection to prevent the diffusion of environmental toxins. On this theme will be developed another part of our work because the researcher has an important task: to provide the tools to detect a possible food contamination avoiding the development of diseases related to it.

The purpose of the first and second chapter is to describe the conventional methods to detect pathogens and environmental toxins and study new solutions to overcome the issues that these techniques pose (third chapter). In particular in the next chapters will be described the state of the art for the detection of microorganisms, as E.coli and, environmental toxins, as Dioxins that will be analyzed in detail in our work.

Foodborne pathogens

There are different bacteria that can be involved in foodborne illness, in particular Campylobacter, Salmonella, Listeria monocytogenes, and Escherichia coli O157:H7 are present in the majority of food-borne outbreaks [2,3] and most of the food products recalls are due to these pathogens [4]. In particular E. coli is a typical inhabitant of the human intestinal tract and can be a causative agent of intestinal and extra-intestinal infections [5]. E. coli O157:H7 is a rare strain of E. coli that is considered to be one of the most dangerous foodborne pathogens [6,7] because it can lead to death producing a dangerous toxin released in the intestine that can cause the haemolytic uremic

syndrome or hemorrhagic colitis [8]. It is extremely important to check, during the food production, any presence of this strain that can be found frequently in different food as chicken, ground beef, raw milk. Recently new measures have been taken to check the food healthiness as good agricultural and manufacturing practices [9, 10, 11], hazard analysis in critical control point (HACCP) [12, 13] and food barcode reader devices to determine the expiry date of the products [14] but it is not enough. For this reason the development of new detection methods today assumes a big importance to prevent and identify problems related to health and safety.

The purpose of the next section is to review the traditional methods employed for foodborne pathogen detection over the past decades to the recent year, by highlighting their strengths and weakness, to find a way to improve them.

Conventional detection methods

The conventional methods for the detection and identification of pathogens are mostly based on microbiological and biochemical identification; this methods are sensitive, inexpensive, can recognize, in a qualitative and quantitative way, the type of organism and the number of colonies, but they are not efficient because it is necessary a step of enrichment to detect low number of pathogens also in food and water samples [15].
Conventional methods are based on:

- culture and colony counting methods (that involve counting of bacteria)
- immunology - based methods (that involve antigen–antibody interactions)
- the polymerase chain reaction (PCR) method (which involves DNA analysis).

Culture and colony based methods

Culture and colony based methods are accurate and reliable techniques for the detection of pathogens. With these techniques it is possible to amplify the signal for the detection of single bacteria through the growth of a cell into a colony. All these procedures are time consuming because they require 72 h for the colony counts, about 18h for the growth of a colony of 10^6 organism and different steps of pre enrichment, selective enrichment, biochemical screening and serological confirmation. Also the interpretation of results takes long time and, to have a

confirmation, often there are required additional tests. These methods have been used for detection of L. monocytogenes [16], S. aureus, Salmonella, Coliforms, E. coli, [17], Campylobacter jejuni [18] and Yersinia enterocolitica [19], etc. The main problem of this technique is the time involved in the analysis: for example the detection of L. monocytogenes requires two-steps of cultural enrichment that take one week only for the biochemical identification of the colonies [20] and for the detection of Campylobacter are necessary 4–9 days for a negative result and 14-16 days for the confirmation of a positive result [21, 22]. Sometime it is possible to have an underestimation of pathogens because they can enter in a dormancy state, becoming non culturable and this is another point against this method. These techniques are not convenient in many industrial applications, in particular in food field; for this reason they are often combined with other methods to obtain better results.

Immunology-based methods

Immunological methods based on antigen–antibody bindings, that include heavy chain antibodies, polyclonal, monoclonal or recombinant antibodies for the detection of pathogens, have been largely employed for the detection of toxins, spores, virus, and bacterial cells [23,24] as Escherichia coli, Salmonella, L. monocytogenes, Staphylococcus, Campylobacter spp. The basic problem of this technique is that antibodies are limited for specificity and abundance. With the development of monoclonal antibodies, immunological detection of pathogen contamination has become more sensitive, specific, reproducible and reliable, because they provide a big amount of single antibodies. Thanks to these advances, lately, have been developed different immunoassays for the detection of a wide range of bacteria and their products [24] with the disadvantage that they are expensive to produce and they require a skilled technician and specialized growth apparatus. To solve this problem there have been created recombinant antibodies that can be produced in reasonable quantities in short periods of time from bacterial expression systems [22], and have been used in different protocols.

Between the immunological techniques for pathogen detection in food there have been reported different techniques: the enzyme linked immunosorbent assay (ELISA), enzyme-linked immunomagnetic chemiluminescence (ELIMCL), enzyme immunoassay (EIA), radio-immunoassays (RIA), flow injection immuno-assay, enzyme-linked fluorescent assay (ELFA), bioluminescent enzyme immunoassay (BEIA), immunomagnetic separation, immuno-precipitation assay, immunochromatography (ICG) strip test, agglutination test, western blot test, and

technically modified western blot that includes the line immunoassay (LIA) and the recombinant immunoblot assay (RIBA). All these techniques are due to the fact that antibody-based detection technique requires less assay time compared to traditional culture techniques, permitting to detect microorganisms in "real-time". These methods are not as specific and sensitive as nucleic acid-based detection, but they are more robust, faster and able to detect not only contaminating organisms but also their biotoxins that may not be expressed in the genome of the organisms [23]. The problems associated are the potential interference of contaminants, low sensitivity of the assays and low affinity between antibody and pathogen or with other analytes measured [25].

Polymerase chain reaction (PCR)

The polymerase chain reaction (PCR) is a technique realized about 20 years ago that can be used to amplify small quantities of genetic material to determine the presence of bacteria. The PCR method is extremely sensitive, in fact it is possible to detect a single pathogenic bacterium in food because a target sequence of DNA can be amplified 1-million-fold in less than an hour. This method is widely used because it has a low percentage of false-positives and can be used to enhance the sensitivity of nucleic acid-based assays. PCR has an advantage in relation to other methods because it is a sensitive, specific, rapid technique, with high accuracy and it is able to detect small amounts of target nucleic acid in a sample. Sometimes it is possible to have false-positives for the interference with target-cell lysis, necessary for nucleic acid extraction, nucleic acid degradation and/or direct inhibition of the PCR, and for this reason it is necessary to use appropriate controls [26]. This technique has been used for the detection of different pathogens like S. aureus, L. monocytogenes, Salmonella, Bacillus cereus, Escherichia coli O157: H7, Yersinia enterocolitica, C. jejuni. There are different PCR based methods for pathogen detection: real-time PCR, multiplex PCR and reverse transcriptase PCR (RT-PCR). In the last years there has been a development in PCR techniques, as reported in literature with multiplex PCR that permitted to detect simultaneously several pathogens with different primers that amplify DNA regions coding for specific genes of each bacterial strain targeted [27]. PCR is a valuable alternative to traditional detection methods for its speed, good detection limit, selectivity, specificity, sensitivity, potential for automation, quick results with low manipulation, but it is not able to distinguish between viable and non-viable cells, since DNA is always present in the cell dead or alive; this limitation can be overcome with Reverse Transcriptase PCR (RT-PCR). The principal issue for

the detection of microbes using PCR is that it is expensive, complicated to use, and requires pure samples, time for processing, expertise in molecular biology and skilled workers.

From all these assays we can deduct how today there is the need of a new device for an in situ, simple, inexpensive and quick detection, that does not require skilled workers, with high sensitivity, for a fast screening of different samples and that gives an immediate response.

Dioxins

The term “dioxins” includes a family of chlorinated aromatic hydrocarbons [28] polychlorinated dibenzo para dioxins (PCDDs), polychlorinated biphenyls (PCBs) and polychlorinated dibenzofurans (PCDFs) that are chemically and structurally related (Fig. 1). The group includes 210 theoretically possible congeners with 75 polychlorinated dibenzo-p-dioxins (PCDDs) and 135 polychlorinated dibenzofurans (PCDFs). Certain dioxin-like polychlorinated biphenyls (PCBs) with similar toxic properties are also included under the term “dioxins” even if they have a different molecular structure and can be divided into different groups according to their biochemical and toxicological properties. The most widely known and most toxic congener of dioxins is 2,3,7,8- tetrachlorodibenzo-para-dioxin (TCDD).

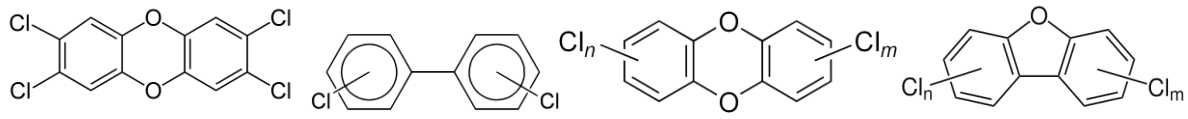

TCDD PCB PCDD PCDF

Fig.1 Dioxins and dioxin like molecules

Dioxins and dioxin-like PCBs have dangerous effects on human health as endocrine disrupting effects, reproductive system effects, immunotoxicity, dermal toxicity, teratogenicity, and carcinogenicity [29].

Sources of dioxins

Dioxins and PCB are by-products of industrial processes but can also result from volcanic eruptions or forest fires and can be produced also in different activities as manufacturing of certain chemicals, incineration of municipal waste, bleaching of wood pulp [30-33]. In terms of release the worst production is due to incomplete burning of uncontrolled waste incinerators from solid and hospital waste. Dioxins are very stable against chemical and microbiological degradation and therefore persistent in the environment. Polychlorinated biphenyls (PCBs) have been largely used in different industrial and commercial applications for their physical and chemical properties, as chemical stability, high boiling point, non-flammability, low heat conductivity and high dielectric constants [34]. They are called "dioxin-like PCBs" because some substituted compounds show toxicological properties that are similar to dioxins. Other PCBs termed "non-dioxin-like PCBs" do not have a toxicological behaviour similar to dioxins. In 1985 these toxic products have been banned from the market but it is possible to find large amounts in plastic products, electrical equipment, and buildings (e.g. plastic carpeting and sealing materials). The most dangerous dioxin-like compounds have in common some chlorine substitutions and a high number of chlorine atoms in the molecule that, if assumed, presents a high stability in the body and a slow metabolism, for this reason once entered it accumulates in the organisms. Dioxins were found in some soils, air, sediments and water through which they enter in the food chain; therefore large quantities were found in food, especially dairy products, fish and shellfish, meat and plants [35, 36]. Although the formation of dioxins is local, the environmental distribution is global, for this reason dioxins are found throughout the world in the environment.

Dioxin contamination incidents

The World Health Organization set 1-4 pg ITEQ/kg/day as the tolerable daily intake TDI of dioxins in the diet of European population that has been noted usually to exceed this value if we consider also PCBs. There are different examples in the last decade of declared food contaminations due to too high levels of dioxins for an uncontrolled production of animal feed and contamination of clays, citrus pulp pellets, fats or tainted ingredients, with dioxins used for their production. A serious accident happened in our country in 1976 in a chemical factory in Seveso, Italy, when large amounts of dioxins were released. A cloud of toxic chemicals, including 2,3,7,8-

Tetrachlorodibenzo-p-dioxin TCDD, was released into the air and contaminated an area of 15 square kilometres where 37 000 people lived. A recent contamination event that has been more significant was in 2008 in Ireland where many tons of pork meat and pork products were recalled. In this case up to 200 times more dioxins than the safe limit were detected in samples of pork. This finding led to one of the largest food recalls related to a chemical contamination. Extensive studies in the affected population are continuing to determine the long-term human health effects from this incident [35]. In July 2007, the European Commission issued a health warning to its member States after high levels of dioxins were detected in a food additive, guar gum, used largely in meat, dairy and dessert products. Other incidents of food contamination have been reported in other parts of the world and frequent is the alarm-dioxin for the production of mozzarella cheese in the Naples area. Although all countries can be affected, most contamination cases have been reported in industrialized countries where adequate food contamination monitoring is available and where a greater awareness of the hazard and better regulatory controls for the detection of dioxin problems exist.

Toxicity of dioxins

The toxicity of dioxins and dioxin-like PCBs is related to the binding to the aryl hydrocarbon (Ah) receptor thereby inducing protein synthesis. The toxicity of all the dioxin classes that includes dibenzodioxin, dibenzofuran and PCB congeners differs considerably. Considering the 210 possible congeners of dioxin and furan, only those substituted in each of the 2-, 3-, 7- and 8-positions of the two aromatic rings are of toxicological concern. These 17 congeners exhibit a similar toxicological profile, with 2,3,7,8-tetrachlorodibenzo-p-dioxin (2,3,7,8-TCDD) the most toxic congener [37, 38]. Also considering the 209 possible PCB congeners, only 12 can easily adopt a coplanar structure that allows binding to the Ah receptor, showing dioxin-like toxicity [39, 40]. In general dioxins are more toxic than the PCBs, but the quantities of PCBs released to the environment are several times higher, and for this reason often there are much higher levels in food and feed than dioxins. The toxicity of these compounds is due to the property of "dioxins" to be fat soluble and to accumulate in organs and systems, once entered into the body, in fact their half-life in the body is estimated to be seven to eleven years. Their chemical stability and the absorption in fat tissues permits to endure a long time into the body of human and animals, biomagnifying through the food chain. They are generally not absorbed by plants, but can stay on the surfaces of the leaves, except some members of the cucurbit family [41]. Recent international studies show how around 95% of human exposure comes from the consumption of food of animal origin [36]; other ways of contamination are through breathing in air contaminated by dioxins and

dioxin-like PCBs from smoke, factory or incinerator emissions or from uncontrolled hazardous waste sites. Dioxins are reputed to be among the most toxic of organic compounds. Short-term exposure may result in skin lesions (chloracne and patchy darkening of the skin) and altered liver function, while long-term exposure is linked to impairment of the immune system, problems to the nervous system, the endocrine system and reproductive functions. Chronic exposure of animals to dioxins has resulted in several types of cancer. Based on both animal studies and epidemiologic evidence 2,3,7,8-TCDD was classified as a "known human carcinogen" (class 1) by the World Health Organisation (WHO) and International Agency for Research on Cancer (IARC). However, 2,3,7,8-TCDD does not directly affect genetic material and there is a level of exposure below which cancer risk would be negligible. Dioxins and dioxin-like PCBs in general contain complex mixtures of different PCDD, PCDF and PCB congeners and to describe the cumulative toxicity of these mixtures and establish the risk it has been introduced the concept of toxic equivalency (TEQ) [37]. Individual toxicity equivalency factors (TEFs) have been assigned to the PCDD, PCDF, and PCB congeners for their relative toxicity compared to 2,3,7,8-TCDD, which is considered as the reference congener (TEF=1).

Mechanism of action of dioxins

All the bioassays used for TCDD and related halogenated aromatic hydrocarbons (HAHs) are based on the molecular mechanism by which these chemicals produce their biological and toxic effects and focus on the ability of these chemicals to activate the Ah receptor (AhR) and AhR signal transduction pathway. The AhR is an intracellular transcription factor ligand-dependent that is responsible for mediating the effects of TCDD, TCDD-like HAHs and other ligands in a different range of species [42-44]. The current reported mechanism model of AhR action is presented in figure 2. TCDD and related HAHs enter into the responsive cell and bind with high affinity to the cytosolic AhR which exists as a multi-protein complex containing the chaperone protein hsp90 [45, 46], XAP2 [47], and the co-chaperone protein p23 [48]. After the ligand binding, the AhR seems to have a conformational change that results in its accumulation in the nucleus, release of the ligand AhR from its associated proteins and dimerization of the AhR with a related nuclear protein called Ah receptor nuclear translocator (Arnt). AhR-Arnt complex converts the AhR into its high affinity DNA binding form. Binding of the heteromeric ligand AhR-Arnt complex to its specific DNA recognition site, the dioxin responsive element (DRE), upstream of a responsive gene (such as cytochrome P4501A1 (CYP1A1)), stimulates its transcription and leads to an increase in production and accumulation of CYP1A1 [49]. Not only the AhR is important to

regulate gene expression, but it is also responsible for mediating the toxicity of TCDD and related HAHs. The good correlation between the toxic potency of a HAH congener and its ability to activate the AhR and AhR-dependent gene expression led to the development and utilization of AhR-based bioassay systems for the detection of dioxin and related HAHs [50].

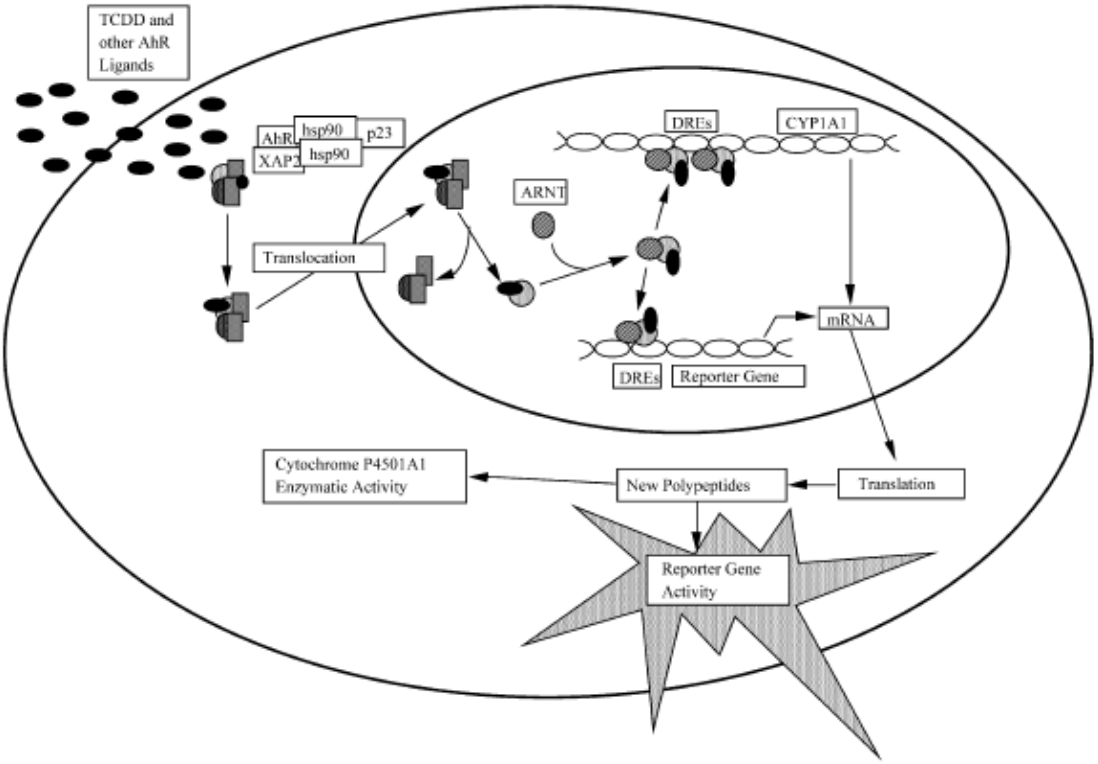

Fig. 2 Molecular mechanism of induction of gene expression by TCDD and related AhR agonists. Reproduced by [50]

Conventional detection methods

TCDD and its related compounds induce dangerous effects, as previously described; this has generated considerable concern worldwide. In the last years many analytical techniques have been developed for the detection and quantification of HAHs in environmental, biological, and food samples, but, the ‘‘golden standard’’ for HAHs analysis uses high-resolution gas chromatography / mass spectrometry (HRGC/MS).

Classical chemical analysis

These methods are based on the separation and quantification of dioxin-like compounds from matrices for their difference in molecular size, charge, mass, polarities, and redox potentials. The

advantages are the accurate measurement of the known isomers and congeners in sample extracts, the possibility to know the conformation of the structure, the congener and the pattern specificity, the calculation of the TEQ and the international standardization. Possible disadvantages include potential loss in specificity, not all the standards of interest are available, high cost, a long time for analysis, the limited information of the biological potency and potential interactions in complex mixture of dioxin-like compounds, complicated separating process and expensive equipments for the analysis. This technique is not suitable for a rapid screening and for the analysis of a big number of samples because the cost of dioxin analysis is much higher than any other analytical methods; for this reason low cost immuno- and bio-assay methods were developed. These methods can reduce the cost of 50% or more and can be used to analyze food samples where an analysis is necessary.

Cell culture-based bioassays

There is a good correlation between the affinity that HAHs have to bind to the AhR and their potency to induce toxicity, for this reason most assays are based on the AhR-dependent mechanism of actions [51]. Cell bioassay systems, in particular, for the detection and quantification of TCDD and other AhR ligands, measure AhR-dependent gene expression occurring in eukaryotic cells, each at the desired endpoint. Also a recombinant yeast cell bioassay system and a variety of mammalian cell culture bioassays that use endogenous and/or transfected reporter genes have been described [44]. The AhR-based bioassays integrate the possible interactions of all congeners in a complex mixture. This is the major advantage of the bioassays because the results give directly a measure of the total sum of dioxin toxic equivalency (TEQ) [52]. With in vitro bioassays it is possible to select between easily biodegradable compounds and more persistent AhR agonists, by different sample incubation times (in vitro luciferase bioassays: 4–48 h; possible test strategy: 4–6 h; EROD bioassays: 24–72 h), while the more persistent dioxin-like compounds are responsible for effects at 24–48 h incubation time [53, 54]. Cell culture-based bioassays with recombinant cell lines that stably transfected the firefly luciferase gene, such as the chemically activated luciferase expression (CALUX) [55] and the green fluorescent protein-based cell bioassay [56], are extremely sensitive and suitable as screening methods for the estimation of AhR-dependent potential of pure compounds and extracts from environmental and biological matrices. However, these assays require equipments for cell cultures and a luminometer/ fluorometer for a multiple-well microtiter plate. Furthermore, it has been described that there is no applicability to tissues or primary cultured cells isolated from experimental animals. For these

reasons a chemical separation of HAHs and dioxins is the most useful, easiest and quickest strategy.

Immunoassays

The enzyme-linked immunoassay has been used for dioxin detection; it is a receptor immuno-chemical assay that analyzes the total toxicity potential of dioxin and dioxin-like compounds. The analysis of toxicity is possible by measuring the capability of these compounds to bind to a cytosolic aryl-hydrocarbon receptor protein (AhR). The mechanism of action is based on an activated AhR protein that binds an exogenous ARNT protein to form an activated protein complex, which is able to bind an ELISA plate-bound oligonucleotide "dioxin responsive element (DRE)" and is then detected by an immunoassay-based colour reaction or fluorometry [57, 58]. In this way it is possible to measure dioxins and dioxin-like compounds in an inexpensive and simple-to-use way and it is not necessary cell culture or radioactivity. The lower detection limit of 1.0 pg and the high sensitivity permits to use these assays for the screening of large samples and also for quantitative analysis. The fact that the cross-reactivity of Ah-Immunoassay is very similar to TEFs indicates theoretical basis for a good relationship with WHO-TEQ [59, 60]. This method has some advantages as high selectivity, high sensitivity, and low cost, but the procedure is complicated and several hours are required for a single measurement.

DNA-binding assay in vitro

These technologies are based on DNA binding of the AhR when the receptor is in presence of suitable ligands. This system is used for studying important biological effects of active compounds at the AhR level because it represents one of the excellent methods for measuring the ability of a compound or extracts to stimulate AhR transformation. But it may be not suitable for the detection of synergistic effects of natural and environmental dioxin-like compounds [61]. For example the GRAB bioassay has been used for the detection of pharmacological agents that activate the AhR signalling system [62-64]. But all the quality control problems related to this technique did not permit to use this as a screening method for dioxin-like compounds.

For the detection of dioxins emerges also the need of new analytical, specific and low cost methods, that require short time for analysis and inexpensive equipments: a technique suitable for

rapid screening and for the analysis of a big number of samples. These are the objectives that were tried to reach in our research work with the development of nanobiosensors.

Biosensors for environmental toxins and foodborne pathogen detection

Introduction to biosensors

The methods commonly used for the detection of foodborne pathogens and environmental toxins are often time-consuming and complicated, for this reason it is useful to develop a new, reliable, sensitive, rapid, specific, simple, low cost technology that can be used for in situ real-time monitoring. In recent years, there have been many research activities in the area of biosensor development because it could be a promising method to conventional analytical techniques that combines the specificity and sensitivity of biological systems in small low cost devices. The design of a biosensor is a fusion between molecular biology and information technology that together give information about the interaction biomolecule-analyte. There are different reports about the development of biosensors for medical devices but there are not many real applications to monitor the food quality, for this reason our research was addressed towards this new field.

The purpose in the construction of our sensor is to have a device that recognises an event and responds to it by a signal that gives information about the food quality; the intention was to create a field-portable biosensor that can be used in real time for the identification of possible environmental toxins, microorganisms and food contaminants. The expected results provide to reduce the time required for food safety testing, to find a possible contamination, limiting foodborne illness and thus reducing the health risks and the medical costs.

Biosensors for food quality / safety control

Food quality control is essential in the food industry and an efficient quality assurance is becoming increasingly important. Consumers want an adequate quality of food product at a fair price, long shelf-life, and high product safety, while food inspectors require safe manufacturing practices,

adequate product labelling and compliance with the FDA regulations. Further, food producers are increasingly demanding efficient control methods particularly through on-line quality sensors to satisfy consumers and regulatory requirements and also to improve the feasibility of automatic food processing, product quality, and to reduce the production time and the final product cost. Also the wave of terrorist acts and foodborne disease outbreaks has stressed the importance of the food traceability and authentication [65]. Therefore a development of biosensors for food safety and quality control was encouraged by acquiring several new food safety and quality requirements: Hazard Analysis Critical Control Points (HACCP), Total Quality Management (TQM), ISO 9000 Certifications. Safety problems require intensive control, data logging, and data treatments and can be effectively controlled only with new generations of biodetection systems. All this tasks require in-time and on-line sensors for data analysis systems, warning systems, and check point for automated processing. To obtain these results, functionalized chips were constructed that can be immersed into food samples (e.g. Milk) at specific control points to detect and identify pathogenic microorganisms and environmental toxins, all in a continuous, real-time, field-portable instrument.

The next sections describe the structure of a biosensor focusing on the specific bioreceptors and transducer used in our work to understand the design of our devices.

Biosensor components and classification

A biosensor is an analytical device with two components: biological and electronic. The conversion of a biological response into an electrical signal is possible thanks to the presence of two main elements: a bioreceptor which recognizes the target compound and a transducer that converts the recognition in an electrical signal (Fig. 3).

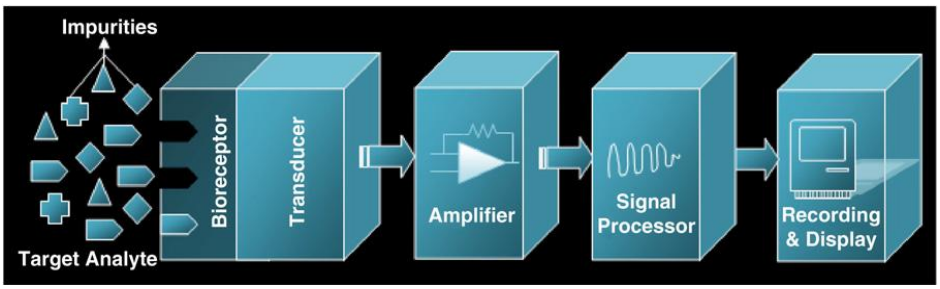

Fig.3 Schematic diagram of a biosensor. Reproduced by [22]

The **bioreceptor** used for molecular detection is composed of highly specialized macromolecules or complex systems with an appropriate selectivity and sensitivity. The **transducer**, which is in intimate contact with the bioreceptor can measure different properties or the optical activity of the substance. Since it is essential that the response of the sensor is detected, it is necessary to use an appropriate transduction mode that detects for example changes in fluorescence or absorbance after the interaction. In any case the signal is then transduced by passing into a circuit where it is digitized. The obtained digital information can be stored in a memory, displayed on a monitor, or made accessible via digital communication ports.

Biosensors can be classified by their bioreceptor or their transducer type (Fig. 4).

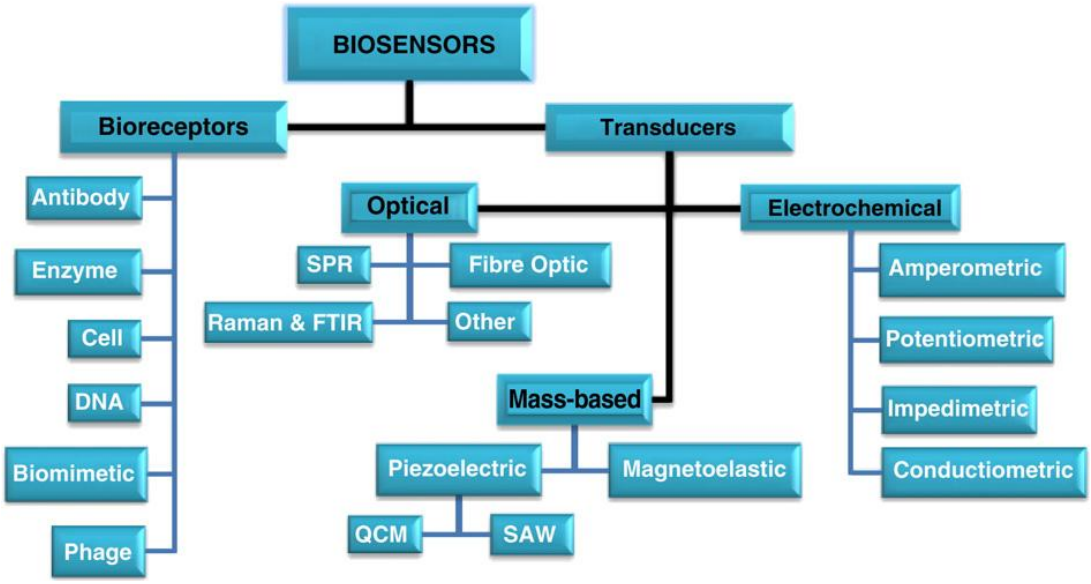

Fig. 4 Classification of biosensors. Reproduced by [22].

Bioreceptors

Bioreceptors are the elements that give specificity to the biosensor through a biochemical mechanism. Binding the analyte under investigation produces a physicochemical effect that can be detected by the transducer. The classification of bioreceptors includes five categories: enzymes, proteins, peptides, biomimetics and bacteriophages, antibody/antigen, cells, nucleic acids [22]. The most used bioreceptors are nucleic acids and enzymes. In particular, in our work, antibodies and peptides were used as bioreceptors and will be analyzed in detail.

Antibodies as bioreceptors

Antibodies are biological molecules made up of hundreds of individual aminoacids arranged in a highly ordered sequence that exibits selective binding capabilities for specific structures; they may be polyclonal, monoclonal or recombinant, depending on their properties and the way they are synthesized. Generally they are immobilized on a substrate, which can function as detector surface or a carrier [66]. The way in which antigen-specific antibodies interact is similar to a lock and key fit [67]. An antibody fits its unique antigen in a highly specific manner, so that the three-dimensional structures of antigen and antibody molecules match. The basic structure of an antibody and antigen–antibody lock and key fit is illustrated in figure 5. Immunosensors, for these properties, can be estimated a powerful tool for analyte recognition through the development of antibodies that can bind selectively different molecular species as biomolecules, microorganisms, toxins and chemicals. In this way an antibody works as a probe that binds the analyte of interest, also in small concentration.

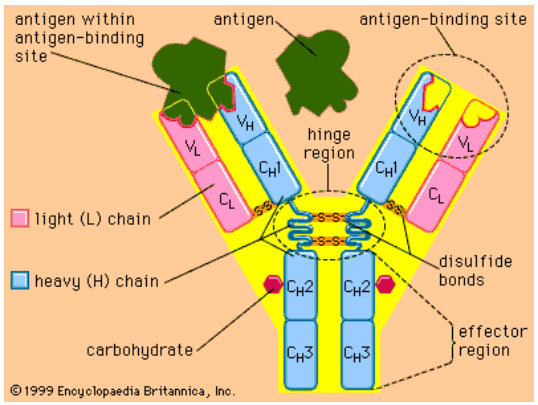

Fig. 5 The basic structure of an antibody with antigen–antibody lock and key fit.

Antibodies can be created for different purposes and there are recent reports that describe their use in foodborne pathogen detection for the construction of different types of biosensors: evanescent wave fiber-optic biosensors [68], surface plasmon resonance (SPR) [69, 70], self-excited PZT-glass micro cantilevers [71], nanowire labelled direct-charge transfer biosensor [72], magnetoelastic resonance sensors [73], and immunosensors [74]. Many of these methods use labelled antibodies with biotin, fluorophores, enzymes, and radioactive isotopes that give a clear signal in biological assays; in this way it is possible to combine the specificity of the antibody with a sensitive label useful for the detection [75, 76]. In our work, that provided the linking of the pathogen (E.coli) with the respective antibody, no labels were used, because we tried to have a

quick analysis and a direct fingerprint of the pathogen linked to the sensor without the use of any probe.

Polypeptides as bioreceptors

Polypeptides are structures that can be assembled artificially and can be used as receptors for the recognition of analytes, in biosensing and in systems for the screening of chemicals or microorganisms. In our case we used a synthetic pentapeptide for the recognition of environmental toxins (TCDD), that is a better bioelement then a natural antibody, for different reasons: the problems of denaturation in organic solvents that happens with the use of antibodies or natural peptides are avoided, better quality control procedures are possible, these bioreceptors can be regenerated and reused. These properties are very important because to extract dioxins by food samples and solubilise these lipophilic molecules are necessary big amounts of organic solvents that could destroy the antibodies. Polypeptides can be synthesized with well studied methods and can be created in short time with low cost and little effort. The amino acid sequence can be changed in relation to the binding domain structure to permit a specific site for recognition. Fluorophores, chromophores, or other biomolecules can also be linked to improve the interaction with the specific analyte. In detail, in our work, peptides have been linked to Fluorescein isothiocyanate (FITC) molecules, a fluorochrome commonly used for the high interaction with nucleophiles, including amino and sulfhydryl groups present in peptides and proteins, that has been used to monitor the presence of TCDD in solution and their quantification.

Immobilization of bioreceptors

To explain its function the bioelement have to be immobilized on a support in order to stabilize its structure ensuring a possible use for different time. The methods used in our work consider the physical and chemical entrapment of bioreceptors. The physical method is used to trap proteins, peptides or antibodies with big sizes or high molecular weights but it is not a technique that permits a long activity and stability, in opposite of chemical methods. In particular the chemical immobilization has used cross linkings to immobilize the bioelement, increasing the molecular weight of the immobilized species and ensuring their insolubility. In detail in our work linkers as

APTES (3-aminopropyltriethoxysilane) were used to create an amino-functionalized substrate and glutaraldehyde as cross-linking agent for its properties of bifunctional agent. GA (Glutaraldehyde) in fact has two terminal aldehydic groups that can react with the amino group of the peptide or antibody, and with the amino-group of the functionalized substrate, forming derivatives that are analogues of Shiff bases. In this way it should be possible to anchor antibodies and peptides to the substrates for the last detection step.

Transducers

Transducer plays an important role in the detection process because they prove that the reaction of the bioreceptor has occurred. Transduction can be accomplished with a great variety of methods. The choice of the transducer depends on the reaction type, on the substances liberated or consumed and on the application of the biosensor. If it has to be used in vivo, its size should be reduced and the form has to be studied to avoid any damage to the living tissues; while if it has to be used in a biological environment it has to be biocompatible, in particular with regard to the deposition of proteins, lipids or cells on its surface. Furthermore the possible release of toxic components should be considered when it works. Actually there is a big variety of transduction methods and the most common and popular are:

- optical
- electrochemical
- mass based

These classes include different subclasses and they can also be divided in label and non-labelled methods. The labelled methods are correlated with the detection of a label, while the label-free detection measures directly what is happening during the biochemical reaction on the transducer surface. In particular in our work optical based transducers were used and will be analysed in detail.

Optical-based transducers

Optical biosensors have been considered really interesting, for pathogen and environmental toxins detection, for their high selectivity and sensitivity. Optical- based methods include different subclasses that use various types of spectroscopy (infrared, Raman, SERS, reflection, refraction,

dispersion, absorption, fluorescence, chemiluminescence, and phosphorescence) and the spectrometer records different properties of the analyte. The most commonly employed techniques of optical detection are surface plasmon resonance and fluorescence due to their sensitivity but there are other interesting techniques that must be developed. In particular Raman or infrared adsorption spectroscopies measure the energy of the electromagnetic radiation, giving information about the local changes around the analyte as the formation of new energy levels or intermolecular atomic vibrations; these techniques are very useful for the detection and quantification of the analyte, for this reason we choose these new types of transducer for the construction of our biosensor together with fluorescence methods.

Raman, FTIR and Fluorescence transducers

Raman spectroscopy is a non-destructive analytical technique that provides spectra with spatial resolution of an optical microscope with almost no sample preparation. Raman spectroscopy is based on the measurement of the vibrational energy levels of chemical bonds by measuring the inelastically scattered light following excitation. Biologically associated molecules such as nucleic acids, protein, lipids, and carbohydrates all generate strong signals in Raman spectra. Therefore, the Raman spectroscopic method can be used to generate "whole-organism fingerprints" for the differentiation of biological samples or in analyzing the effect of nanoparticles interactions with biological cells or chemicals. Raman scattering techniques have elicited significant interest for biomolecule detection as they provide several advantages over other spectroscopic techniques. Unlike IR and NMR, Raman signals are not affected by the presence of water and Raman bands are much narrower than fluorescence bands. Raman-active molecules exhibit characteristic "fingerprint" spectra that can be used to definitively identify a molecule. Additionally, Raman responses are less susceptible to photobleaching than fluorescence responses, thus allowing longer signal collection times and improved signal averaging. Normal Raman signals are too weak to be of use in ultrasensitive detection methods, but surface-enhanced Raman spectroscopy (SERS) results in Raman signal enhancement factors as high as 10^{14} [77]. SERS is observed for molecules on or nearby the surface of metallic nanostructures, with a diameter of typically 20–100 nm, which can support localized surface Plasmon resonances (SERS substrate). SERS can tolerate water molecules and can generate more sharp and distinguishable bands of specific molecules. The surface enhancement effect allows the observation of Raman spectra of single molecules or cells excited at low incident powers and short data acquisition times [78, 79]. The high sensitivity of

SERS can be exploited either for the label-free detection of analytes or in targeted research with SERS labels. Currently, the label-free detection of an analyte is the most widely used approach: the identification is based on the characteristic SERS spectrum of the analyte when it is adsorbed onto the surface of the colloidal particle. In the second approach metallic nanoparticles are used in combination with Raman labels: the organic Raman reporter molecules are adsorbed on the surface, giving rise to the characteristic SERS signature which is necessary for the indirect identification of the target molecule. Enzymes, dyes (Rhodamine), molecular fluorophores and quantum dots are well known labelling agents for the selective detection of biomolecules [80, 81]. Advantages of SERS over existing labelling approaches include: the tremendous multiplexing capacity for simultaneous target detection due to the small line width of vibrational Raman bands; quantification using the characteristic SERS spectrum of the corresponding label; the need for only a single laser excitation wavelength; high photostability and optimal contrast by using red to near-infrared excitation in order to minimize the disturbing auto fluorescence of cells and tissues.
In our work this new technique was used in addition to new materials to try to reach better results in this field. A recent development of this technique allowed to detect pathogens of interest with specific biomolecules, as antibodies, absorbed on the device and a few label free techniques were developed [82-85]. It is clear as there is a great interest for the development of this technique that can lead to interesting results [86-99]; for this reason a part of our work was focused on these transduction methods. The other methods of transduction used are well known and for this reason they will be mentioned only briefly.

The other optical technique used in our work is the Fourier transform infrared (FT-IR) spectroscopy. It is a well known, low cost, simple and non-destructive technique. Actually the instruments are largely available and there are also some portable instruments that can be used for on-field analysis. Today there are only few applications on food pathogen detection because the previous instruments did not ensure a good signal to noise ratio to discriminate different pathogens. The first studies found in literature, using this technique, were about the quantification of eight different microorganisms including Salmonella [100-103]; this study allowed differentiating the microorganisms at a concentration of 10^3 colony-forming units (CFU)/ ml in apple juice. Other studies were reported but with worst detection limits [105-108]. Our purpose is to use new materials associated to this techniques to improve the simple detection of pathogens and food contaminants at lower concentrations.

The last technique is fluorescence that is a type of spectroscopy that can be used as transduction method for sample analysis. In general the biological sample with the fluorescent probe is excited by a beam of light which leads to the emission of light of a lower energy resulting in an emission spectrum which is used to interpret the reactions that happened [109]. In particular this transduction method was used in our work for the final detection of TCDD which proved to be a good optical technique with fast and rapid detection ability, high sensitivity and specificity.

Future perspectives

Although conventional detection methods are sensitive, they require long time for the analysis. However, the analytical techniques, like optical and electrochemical biosensors, have some disadvantages as sensitivity and cost; therefore, new rapid methods are necessary for better performances. Since foodborne pathogens and environmental toxins are mostly present in very low concentrations it is very difficult to detect them. In this way there are more chances for these contaminants to get lost during the detection. For this reason the new device should be able to detect contaminants in very low concentration and should be suitable for in situ real-time monitoring, obtaining a detection technique which would be reliable, rapid, accurate, simple, sensitive, selective and cost effective. Furthermore it should be able to detect different analytes, and capable of on-line analysis on real samples; the device should be simple and inexpensive to design and manufacture. Nanobiotechnology is claimed to satisfy these requirements.

Nanomaterials in biosensing

Nanotechnologies in agro-food field

Nanotechnology has the potential to be applied at the different parts of the food and agricultural system for example:

- ✓ Food security
- ✓ New tools for molecular and cellular biology
- ✓ New materials for pathogen detection
- ✓ Protection of the environment

Nanotechnology application in the food industry is also contributing to increase the consumer awareness of food safety. In recent years there have been some studies for the development of sensors for the detection of pathogenic microorganisms and environmental toxins. The need for rapid and sensitive assay methods to detect foodborne pathogens and environmental toxins has led to the incorporation of biosensor technology into microarray and other platforms (mimetics and aptamers). To improve the detection methods it has been necessary to follow new routes as nanotechnologies, to develop nanosensors placed in food production, food distribution facilities and in packaging, leading to the detection of any kind of traces of contaminants. Actually researchers are studying nanobiosensors to detect water contamination, food materials, agricultural pesticides, changes in food and crops genetically modified. For example, quantum dots have been used for the detection of E. coli and other pathogens [110], nanobarcodes for food traceability [111] and nanodevices to monitor parameters, as temperature, to which the food can be exposed, from the plant to the consumer. The possibility of combining biology and nanoscale technology into sensors and the incorporation of nanoelements in various procedures decreases the dimensions of the instruments and increases the automation, the sensitivity, and rapidity of results.

Introduction to nanoporous materials

In the last years, nanomaterials have been considered really interesting in the field of nanoscience, a new sector that is attracting investments and expectations. Various nanostructures have been studied as nanorods, nanotubes, nanoparticles, nanofibers, and thin films and used for different applications. Nanoporous materials, in particular, have unique properties for their capacity to adsorb or interact with molecules thanks to their large surface area enhanced by the pore surface. They are interesting because they have similar dimensions to biostructrures and for this reason a size-dependent interaction is possible. The fields of nanoporous materials as microelectronics, manufacturing, medicine, clean energy, environment are different; and various are the applications (separation, ion exchange, sensors, catalysis, e.g.). Constructing new structures at molecular level, as building blocks, leads to control the dimensions in the range between 1 and 100 nm, according to the properties and functionalities wanted. In particular molecular self-assembly, that mimics structures present in nature can be used to create porous materials. All the self-assembled structures and porous thin films are interesting for their use as substrates for the development of sensors because they can self assemble and organize in structures that can be useful for the entrapment of biomolecules as cells, proteins, tissues, enzymes, receptors, etc. The presence of

pores (holes) in a material can give properties missing in bulk materials. Pores can be connected with the surface or can not be connected, but this type is not useful for the absorption of biomolecules. Pores can have different shapes as cylindrical, spherical, hexagonal, cubic, etc. and can be straight, curved or tortuous [112]. To clarify the definition of nanopores size IUPAC refers to micropores if they are smaller than 2 nm in diameter, mesopores between 2 and 50 nm and macropores larger than 50 nm but normally there have not been found pores bigger than 100 nm for functional applications (Fig. 6).

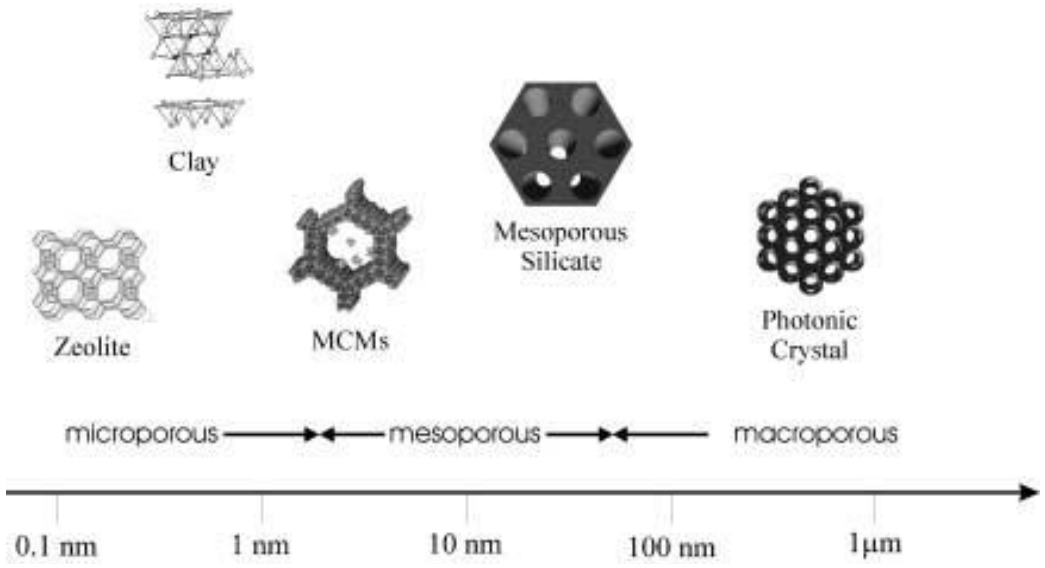

Fig.6 Typical length scales of three-dimensional porous structures. Reproduced by [113]

The composition of nanoporous materials often is based on oxides because they are chemically and thermally stable, inert and non toxic and due to these properties they find a good application in the biological world. Microporous zeolites have been the first materials with nanopores built but the too small dimensions (0.2 – 1.0 nm) have limited their applications; for this reason there has been a big interest to expand the pore dimensions to mesoporous range. Other traditional materials used have been silica gels, alumina, and activated carbons but having a broad pore size they did not guarantee selectivity. The invention in the early 1990's of MCM-41 and M41S by Mobil scientists has been advantageous for their use in separation, catalysis and biological applications. Mesoporous molecular sieves (M41S) (pore size 2-10 nm), were synthesized using long chain cationic surfactants as template and pore forming agents during the hydrothermal sol-gel process.

They have been created with a new approach using as templates self assembled aggregates instead of single molecules (as for zeolites). Depending on the starting materials and changing the synthesis conditions, different mesoporous silica oxide with ordered structure in the form of hexagonal (MCM-41) cubic (MCM-48) and lamellar (MCM-50) have been created. These mesoporous silicate materials, with well-defined pore sizes of 15-100 nm, have broken the past pore-size constraint <15 nm of microporous zeolites. The extremely high surface areas (>1000 m^2/g) and the precise tuning of pore sizes are among the many desirable properties that have made such materials the focus of great interest. For this reason we took these silica materials as reference for the construction of new one with better characteristics. Liquid-crystal templating (LCT) mechanism was proposed [114] as the common mechanism for their construction in which surfactant liquid crystal structure is used as organic template. The templating way to assemble nanoporous materials influences the final material. Today there are many pathways but the research is always advancing to improve the composition, the pores size, the chemical and thermal stability of each material. There are different models to describe the formation of mesoporous materials but all the synthesis routes have in common the presence of surfactants that, from the inorganic precursors, cooperate to the formation of the mesostructure. Surfactants have two extremities: a hydrophilic head and a hydrophobic tail that self-organize to minimize the contact between head and tail and the respective solvent. The different synthesis routes diverge on the mechanism of interaction between the inorganic precursor and the surfactant. Generally surfactants self-assemble in micelles to form an hexagonal array that is covered in solution by inorganic molecules (silicate in the first experiments) with an EISA process, then, after stabilization processes and thermal treatments is applied the final calcination step that removes completely the surfactant molecules, leaving pores in their place and produces an inorganic structure that reflects the previous hexagonal micellar array (Fig. 7).

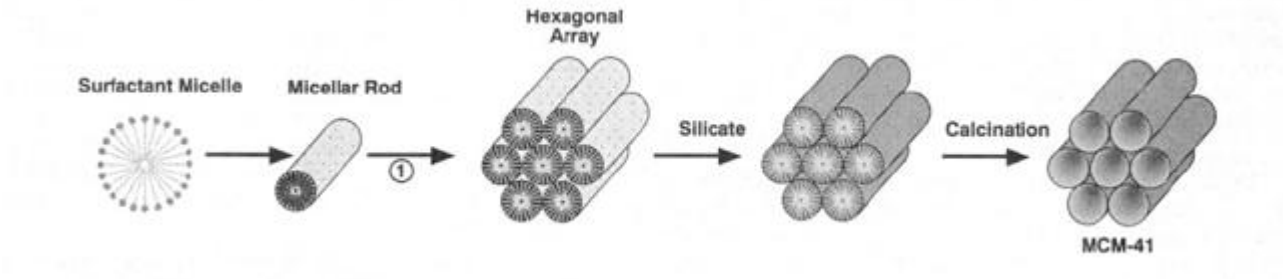

Fig. 7 Possible pathway for the formation of MCM-4. Reproduced by [114]

EISA Theory

The evaporation-induced self assembly (EISA) describes the formation of an ordered mesophase organic-inorganic after the evaporation of the solvent from a dilute solution, as described by Brinker et al [115], obtaining a Liquid Crystal phase.
In particular, mesoporous materials prepared by EISA require a definite composition of the initial solution (inorganic precursors, templating agents, and volatile media); the shape can be decided by selecting an evaporation method and the physicochemical and functional properties can be created by a thermal or chemical post-synthesis modification. For this reason a reproducible synthesis of mesoporous materials with EISA requires to control the chemical composition of the precursor solution, the deposition process and the post -treatments performed on the film. The EISA method for the formation of mesoporous materials has met a great interest for the possibility of obtaining porous arrays interconnected and with a definite size that can be used as nanoreactors, selective membranes or sensors. This route has been chosen in our work for the formation of mesoporous materials combining

- sol-gel chemistry
- self-assembly of an organic surfactant template

Sol-gel chemistry

A sol is a colloidal suspension of solid particles in a liquid in which the dispersed phase is very small (1-1000 nm). In a colloid the interactions are conducted by short range forces as surface charges and van der Waals attraction. The colloids include: sol (solid particles in a liquid), aerosol (solid particles in a gas), and emulsion (liquid droplets in another liquid). All of these can generate polymers or particles for the constitution of ceramic materials. In the sol-gel process the precursors are metal or metalloid elements surrounded by various ligands for the final preparation of a colloid. The latter is an alkoxide commonly used as precursor in sol-gel chemistry and, in metal alkoxides, the metal atom is linked to an organic ligand. Metal alkoxides have metal-oxygen-carbon linkages and the most studied is tetraethoxysilane (TEOS) $Si(OC_2H_5)_4$. The sol-gel process consists on different steps: Hydrolysis, condensation, gelation, ageing, drying, densification (Fig. 8) and according to the followed route are formed different materials with different properties.

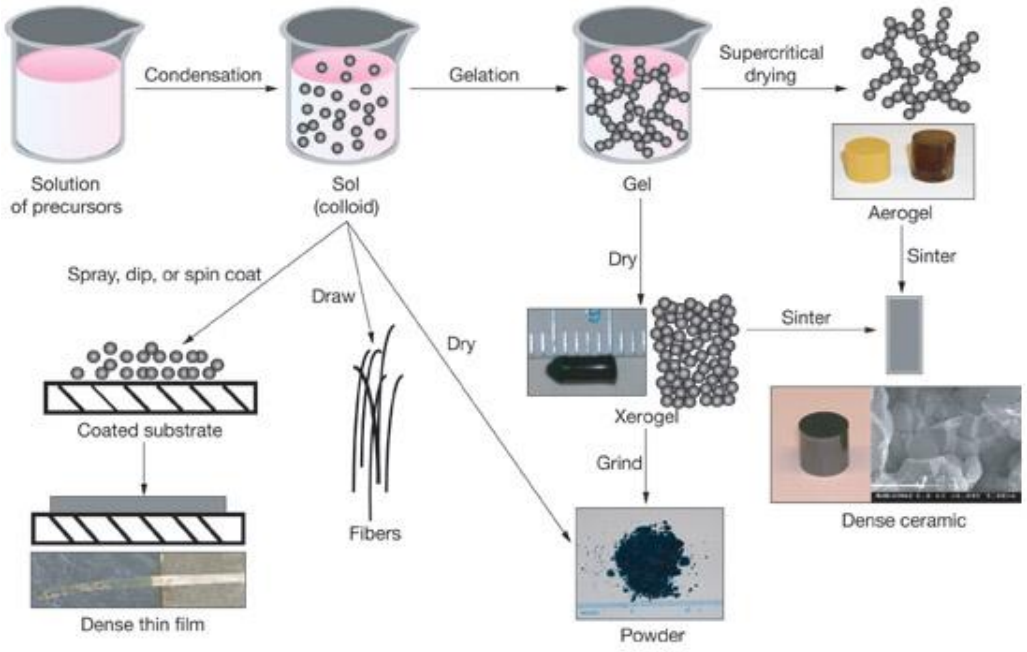

Fig.8 Sol-gel process. Reproduced by [116]

Sol-gel materials are very interesting for different reasons:

- ✓ The temperatures required for the process are low and frequently at room temperature, except for thermal treatments necessary in some cases for the removal of template; in this way the degradation of biological species entrapped is slight.
- ✓ Precursors such as metal alkoxides are frequently volatile and well purified leading to high-purity final products; they are also miscible and it is possible to control the doping.
- ✓ The chemical conditions used for the synthesis are mild, in fact, usually extreme pH conditions are avoided, especially when the two step method is used, in which acid catalysed hydrolysis is followed by rapid neutralisation of buffering. In this way pH sensitive organic species (e.g. dyes) and even biological species, including enzymes and whole cells, may be entrapped and can retain their functions.
- ✓ Porous and nanocrystalline materials can be prepared with this route.
- ✓ Controlling the reaction it is possible to monitor the speed of hydrolysis and condensation, the particle and pore size of the desired material.
- ✓ Using functionalized precursors it is possible to link organic and biological species with a covalent attachment to porous silicate structures.
- ✓ By controlling the ageing and drying conditions a control of pore size and mechanical strength may be achieved.

- ✓ The combination of organometallics with organic ligands leads to hybrid materials with an inorganic-organic polymer network.
- ✓ Entrapped organic species can be used as templates for creation of pores with controlled size and shape. Subsequent removal of these species (by heat or strong acid treatment) leaves molecular footprints with potential as catalytic sites.
- ✓ Since liquid precursors are used it is possible to cast ceramic materials in a range of complex shapes and produce thin films or fibres as monoliths, without the need for machining or melting.
- ✓ The optical quality of the materials is often good, leading to applications for optics.
- ✓ The low temperature of sol-gel processes is generally below the crystallization temperature for oxide materials and this allows the production of unusual amorphous materials [117].

The preparation of thin films is the most important use of sol-gel method that we developed in our work.

Self assembly of an organic surfactant template

To control the constitution of nanomaterials the physical chemistry of organized matter, that confide on the successful combination of sol–gel chemistry and self-assembly procedures, is fundamental. Self-assembly is based on the organization of building blocks in bigger structures with a "bottom up" approach that is possible with no covalent interactions as electrostatic, hydrophobic and hydrogen bonding [118, 119]. Self-assembly of nanomaterials is proving as one of the most interesting field of nanoscience because, through the manipulation of atoms, molecules, or clusters in nanostructures, it is possible to create new technologies and materials with different properties. In this way it is possible a fusion between materials science, that comes from the micrometer range, and biochemistry/chemistry that combines individual molecules, reaching unique physical and chemical properties as the quantum size effect, mini size effect, surface effect and macro quantum tunnel effect [120]. These features can reflect on sensitivity and on other analytical properties that are essential for the development of biosensors. For these reasons nanomaterials are a large promise for new biosensing and bio analytical systems through several biochemical modifications.

In particular it is possible to obtain these materials starting by hybrid networks template with surfactant (structure directing agents) [121-146]. The combination of inorganic materials with

organic templates has been estimated as the next generation of functional materials [147]. This mechanism is possible with the use of appropriate surfactants and among the most interesting there are block copolymers.

Block copolymers as templates

The first studies on the synthesis of mesoporous oxides have described the use of different types of ionic surfactants as the cationic alkyltrimethylammonium, anionic n-alkylsulfonates or alkyl phosphates as templates. For these synthesis the pH of the solutions to control the pore size, that unfortunately were too small to be used for different applications, was fundamental. To overcome this problem amphiphilic block copolymers has been proposed as templates for their properties of self-assembling in different solvents to give robust and regular structures on the nanometer scale as spherical, cylindrical or lamellar structures. The block copolymer self-assembly is probably the best mode to obtain new organized materials thanks to their characteristics of soluble-insoluble molecules, depending on the solvent used ("amphiphilic" polymers).

In our case, mesoporous thin films were synthesized using PEO–PPO–PEO (Polyethylene oxide-Polypropylene oxide- Polyethylene oxide, trade name Pluronic, BASF Corp. USA) as template (Scheme 1).

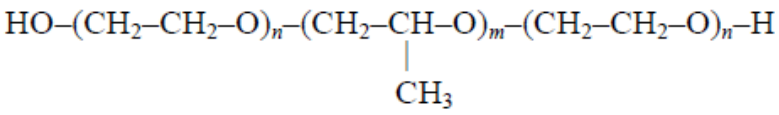

Scheme 1. Pluronic molecular structure

These amphiphilic polymers consist of an hydrophobic polypropylene oxide block (PPO) surrounded by two hydrophilic polyethylene oxide blocks (PEO), and can schematically be written (PEO)x–(PPO)y– (PEO)x. There are different Pluronics available, with different molecular weights and variations in the PEO/PPO ratio that can lead to different porous structures as hexagonal form, SBA-15 (*p6mm*), cubic (*Im3m*) form called SBA-16, and several other structures [148]. The broad variety of self-organizing structures of surfactants and block copolymers is shown in Fig. 9. As shown, it is possible to control the formation of different structures as spherical micelles with cubic packing (FCC, BCC), hexagonally packed cylindrical micelles (HEX), lamellar phases (LAM), and other phases as cubic bicontinuous structures such as the

gyroid. With the phase diagrams it is possible to choose the morphology of the materials wanted, choosing the block lengths and polymer concentration to prepare different nanostructured materials.

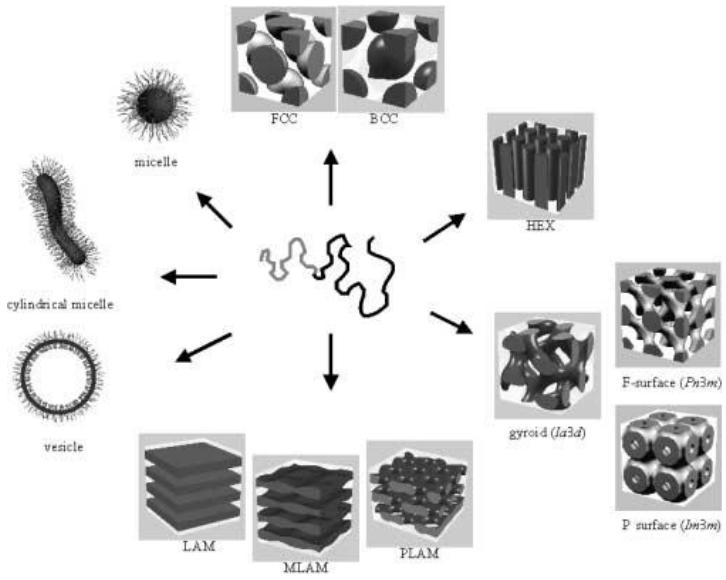

Fig. 9 Organization of block copolymers. Reproduced by [113]

The formation of micelles, in a block copolymer templating procedure (Fig. 10), occurs for the interaction of inorganic compounds with the organic micelles. This is possible with a replacement of the majority of the solvent with a metal or metal oxide precursor with similar polarity and the final condensation around the micelles. The final calcination process at high temperature removes the organic phase and the template, leaving the pores surrounded by the inorganic phase. A typical precursor used is hydrated silicic acid but it is also possible to use hydrolysable metal species or metal salts (metal chlorides, as in our case) to obtain different materials as metal oxides, metal chalcogenides, or even elemental metals [149-156].

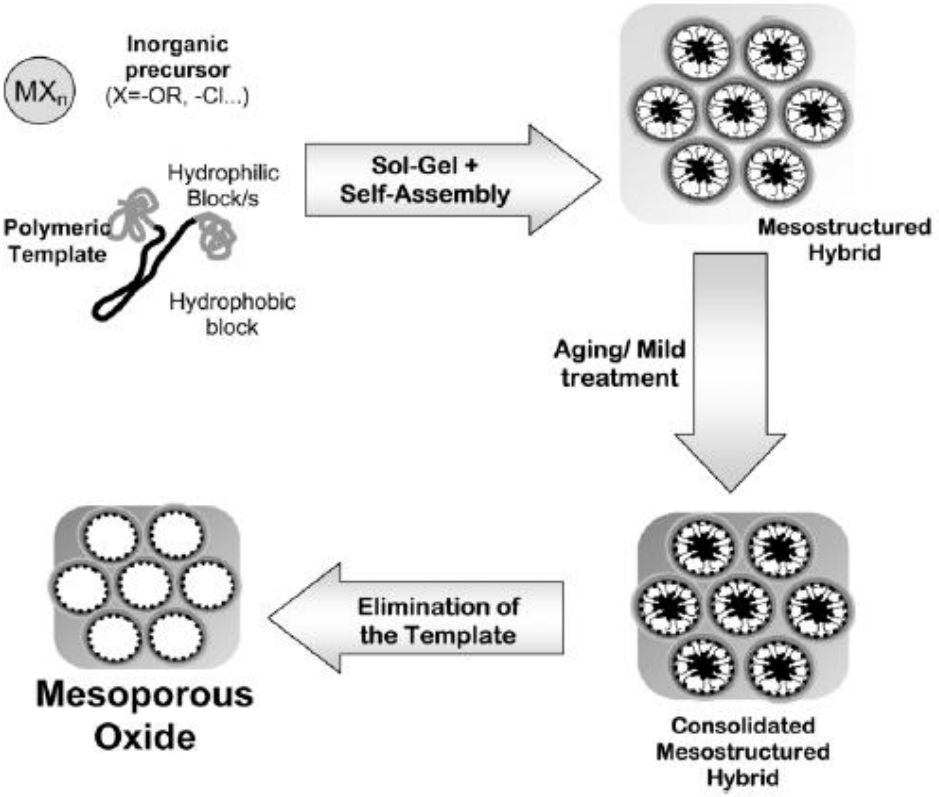

Fig. 10 Schematic view of the steps leading from a solution to a mesoporous oxide network. Reproduced by [150].

Aims of the research work

The aim of the present research work is to develop new detection methods to prevent the diffusion of contaminated food with, in particular, environmental toxins (e.g. dioxins) and pathogens (e.g. E.coli). These compounds were chosen for the frequent food complaints related to these contaminants that produce huge problems related to human health and safety. In fact these compounds are mostly present in very low concentration and it is very difficult to detect them because they may get lost during the detection.

Today there are several conventional methods for the detection and identification of contaminants based on chemical, microbiological and biochemical identification, but they are mostly time-consuming, expensive, complicated, require expertise in molecular biology and they require skilled workers to use them.

For this reason our idea was to create new devices able to detect contaminants in very low concentration, suitable for in situ real-time monitoring, obtaining a detection technique which would be reliable, rapid, accurate, simple, sensitive, selective, cost effective and that does not require skilled workers. Furthermore it should be able to detect different analytes, capable of on-line analysis on real samples.

To meet these needs the aim was to create field-portable biosensors that can be used in real time for the identification of possible environmental toxins, microorganisms and food contaminants. The expected results provided to reduce the time required for food safety testing to find a possible contamination, limiting foodborne illness and thus reducing the health risks and the medical costs.

To obtain these results simple, low cost, functionalized chips were constructed, that can be immersed into the samples (e.g. Milk) at specific control points, able to detect and identify microorganisms and environmental toxins that might be present, with a continuous, real-time, field-portable instrument, preventing the diffusion of dangerous food. In this way the analysis of a big number of samples for a fast screening should be possible, giving an immediate response, and, in case of contamination, the on-time production process could be stopped.

In detail peptides and antibodies can be used as recognising bio-elements to link to a silicon chip. With this transparent material in fact it is possible to use optical techniques as Fluorescence, FTIR and Raman as detection methods. These transduction techniques were chosen for the possible

availability, in a laboratory of a food factory, between simple, low cost, portable instruments that do not require skilled workers.

To immobilize the bioelement on the surface of silicon wafers the aim was to deposit a thin film on this substrate and, new ways to improve the features of the recognition and transduction were considered. The purpose has been to develop elements with higher sensitivity or selectivity, with more rapid response characteristics, broader working ranges, and improved reusability. To achieve these desirable traits it could be useful to improve the interface between the material and the target. To join this objective mesoporous thin films were developed, in fact with these materials there is the possibility to immobilize probes or nanoparticles into the pores or the materials can be used directly to stabilize the bioelement.

Another objective was to study if it was possible to have an enhanced concentration of the probe immobilized on these materials. In fact, thanks to a large surface area, in theory it should be possible to have the diffusion of the analyte into the pores, reducing the time to have a response. The pores should be used also as selective membranes that choose the analytes based on different sizes and solubility.

Final objective was to try new porous materials, (instead of silica synthesized and used in this work only as reference) for the construction of the substrate, to optimize the synthesis process, to study the stability of these materials in biological solutions, to select the most efficient functionalization techniques and the most suitable nanostructured material to obtain a biosensor with the desired features.

The possibility of combining biology and nanoscale technology into sensors and the incorporation of nanoelements in various procedures should decrease the dimension of the instrument and increase the automation, sensitivity, and rapidity of results. This is what we have tried to obtain.

Experimental Section

Materials and Methods

Chemicals. All commercially available solvents and reagents were used without further purification. $TiCl_4$ (reagent grade >98%), anhydrous ethanol (EtOH, reagent grade >99,9%), bidistilled water, acetone (reagent grade >99,8%), hydrofluoric acid (reagent grade 50%) and toluene (reagent grade >99,5%), were purchased from Carlo Erba. $ZrCl_4$ (reagent grade >99.5%), $HfCl_4$ (reagent grade 98%), triethoxysilane (TEOS, reagent grade 95%) pluronic F-127 (cell culture test), phosphate buffered saline (PBS powder, pH 7.4), 3-(aminopropyl)trimethoxysilane (APTMS, reagent grade 97%), 3-(aminopropyl) triethoxysilane (APTES, reagent grade > 98%), silver nitrate (reagent grade > 99%), glutaraldehyde (GA Grade I, 50% in H_2O, specially purified for use as an electron microscopy fixative or other sophisticated use), 2,3,7,8-Tetrachlorodibenzo-p-dioxin (TCDD, solution 10 μg/ml in toluene, ampoule of 1 ml Supelco), cytochrome c (from bovine heart), rhodamine B isothiocyanate (mixed isomers, BioReagent, suitable for protein labelling), dimethyl sulfoxide (reagent grade ≥ 99.5% GC, plant cell culture tested), N,N´-Dimethylformamide (DMF pure p.a., > 99.8%), 1-methyl-2- pyrrolidone (NMP for peptide synthesis > 99.8%), dichloromethane (DCM, reagent grade > 99.5%), 2-propanol (reagent grade > 99.5%), trifluoroacetic acid (TFA, reagent grade > 98%), piperidine (reagent grade > 98%), triisopropylsilane (TIS, 99%), N-Ethyldiisopropylamine (DIPEA 99%) and N,N,N′,N′-Tetramethyl-O-(7-azabenzotriazol-1-yl)uranium hexafluorophosphate (HATU, 99%) were purchased from Sigma Aldrich. Fmoc-Pal-Peg resin (substitution 0.21 $mmol \cdot g^{-1}$) was obtained from Applied Biosystems (Applied Biosystems Inc, USA). The Fmoc-amino acids and 1-hydroxybenzotriazole hydrate (HOBt) were purchased from Novabiochem (Novabiochem, Switzerland), α-cyano-4-hydroxycynnamic acid from Fluka was used as matrix for MALDI TOF experiments. All solvents used in the chromatography section were of the gradient grade for HPLC and were purchased from Merck-VWR (D-Darmstadt, Germany). Fluorescein isothiocyanate (FITC), isomer I (90 % purity) was purchased from ACROS organics and used without further purification. E. coli O157:H7 and E. coli K12 were obtained from Purdue University (Bindley Discovery Park, IN). BHI agar and LB were purchased from Teknova, Hollister, CA. Bac-trace Affinity purified antibodies goat anti-E.coli O157:H7 were purchased from Kirkegaard and Perry laboratories. Silicon Wafer (Test grade, P-type boron doped, diameter 4", thickness 475-575 micron, 100 oriented, one side polished and on side etched were obtained from Jocam.

Synthesis of mesoporous hybrid thin films

Solution preparation of transition metal oxides (TiO_2, HfO_2 and ZrO_2)

TiO_2, HfO_2 and ZrO_2 solutions were prepared with the following procedure and using three different flasks. 1.34 g Pluronic were dissolved in 46.64 ml of EtOH with the aid of the sonicator. The solutions were stirred for two hours at 25°C in a closed vessel. After the immersion of the flasks in an ice bath 2.2 ml of $TiCl_4$ (yellow liquid) were added to the first solution, 6.4 g $HfCl_4$ to the second and 1.66 ml $ZrCl_4$ to the third. After 20 minutes of stirring at room temperature 3.6 ml of H_2O were added to the $TiCl_4$ solution and 7.2 ml to the solutions containing $HfCl_4$ and $ZrCl_4$. These solutions were left to react for 3 hours at 25°C under stirring in a closed vessel. The addition of water caused the hydrolysis of MCl_4 (M=Ti, Hf, Zr) producing EtOH and HCl, responsible of the high stability of the sols that, for their high acidity are stable for several months at 25°C (Fig. 11). The molar ratios in solution were $TiCl_4$: Pluronic F127 : H_2O : EtOH = 1 : 0.005 : 10 : 40 for the first solution and $HfCl_4$/ $ZrCl_4$: Pluronic F127 : H_2O : EtOH = 1 : 0.005 : 20 : 40 for the second and third solution.

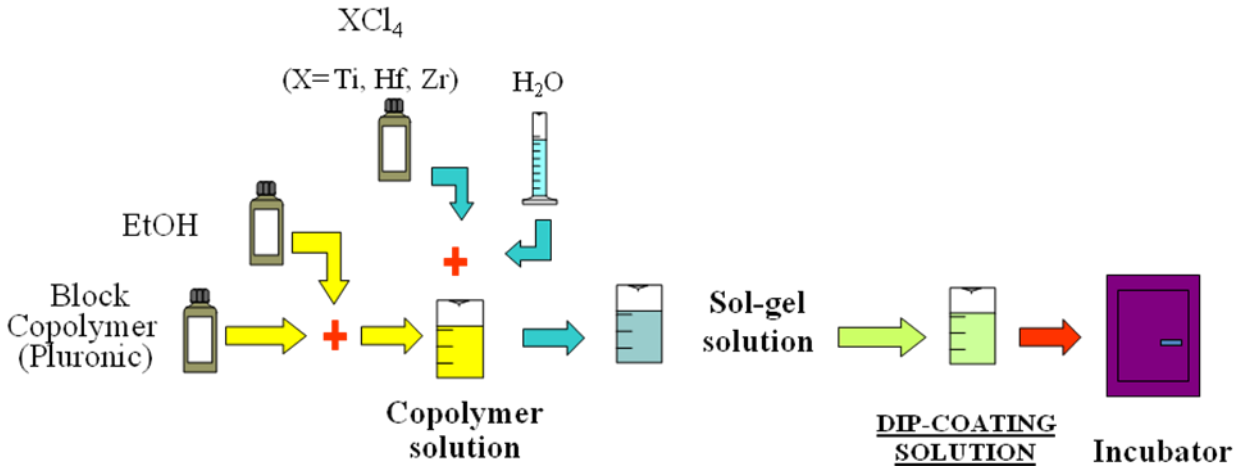

Fig. 11 Solution preparation of transition metal oxides (TMO)

Solution preparation of SiO_2

This solution was prepared in two steps: in the first one were mixed 3.08 ml of EtOH with 4.26 ml of tetraethoxysilane (TEOS) and water and, after the addition of 0.355 ml of HCl 0.768 M, the solution was left under stirring for 60 minutes. The second step provided the addition of the templating solution obtained by mixing 15 ml of EtOH with 1.3 g of Pluronic F127 and 1.5 ml of HCl 0.057 M (Fig. 12). The final molar ratios were TEOS : Pluronic F127 : H_2O : HCl : EtOH 1: 0.005 : 5.4 : 0.02 : 16.4

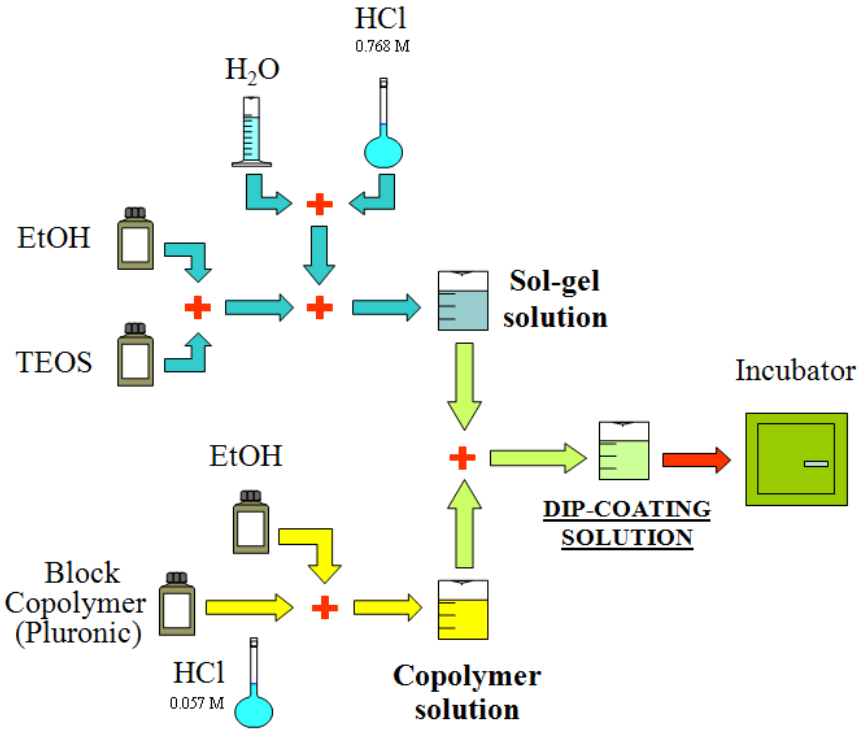

Fig. 12 Solution preparation of silica

Film deposition

Thin films were deposited dipping the wafers into the solutions described above. Before the deposition with the dip-coater, silicon wafers were washed with acetone and ethanol while quartz wafers were activated with HF and washed with water, EtOH and acetone. There were different parameters that have been important to consider and to change in the deposition steps during all the experiments. The first experiments were carried out in this way: thin films were deposited with a RH (relative humidity) 18-21% within the dip-coater and with a RH 33% outside the dip coater, the speed deposition was 15cm·min^{-1}. HfO_2 and ZrO_2 films as deposited became opaque outside

the chamber of deposition, for this reason they were exposed to water vapour for 5 sec that made them transparent. This treatment was not necessary for SiO_2 and TiO_2 films that, after the deposition, had a good optical quality. Then the films were placed in a chamber with controlled humidity (saturated solution $Ca(NO_3)_2$ 98% RH) and left there for 24h. Thermal treatments were carried out heating the films in an oven at 100°C for 24 hours, after that the back of the films was removed with a solution of HF (2%), acetone and EtOH; finally the films were put for 60 hours into a furnace at 350°C where the calcination (removal of the template) was performed.

During different trials the deposition conditions were changed to improve the film quality. The deposition was carried out by dip-coating silicon wafers into the precursor solution at 25°C and at a withdrawal rate of 15cm·min^{-1}. The relative humidity (RH) inside the dip-coater chamber was maintained between 18-25% to obtain good optical quality and a high structural order of the films. Such deposited films were aged at room temperature RH 50% for 24 hours. To increase the inorganic polycondensation and stabilize the mesophase the films were submitted to different firing steps at 60°C, 120°C and 200°C for 24 hours at each temperature in an oven with heating rate of 10°C·min^{-1}. This treatment has been important to allow the formation of highly organised and high surface area mesoporous coatings, exhibiting crystalline frameworks. The final calcination process to remove the organic template of these stabilized coatings was done at 350°C for 3.5 h in air under static conditions with a heating rate of 10°C·min^{-1}. The final thin films were characterized with FT-IR measures.

Stability of mesoporous thin films in PBS (1x)

The stability of mesoporous thin films of TiO_2, HfO_2, ZrO_2, SiO_2 was studied in a buffer solution of Phosphate buffered saline (PBS) 1x. Two types of experiments were carried out; in the first one different films of the same material were immersed in a PBS solution 1x under stirring for 6, 12, 18, 24, 36 and 48 hours and the changes in thickness, refractive index and in Fourier Transform Infrared (FT-IR) spectra were studied. In the other experiment a mesoporous film of each type was taken and dipped in a PBS solution, under stirring, for the first step of 2h; after that the film was dried in an oven at 100°C for 30 min and FTIR and ellipsometric measures of thickness and refractive index were carried out. Finally the film was incubated in PBS solution for the following steps of 4, 6, 8, 10, 12, 18, 24, 36, 48h, and for each step the measures were done as previously described for each film type.

Functionalization of mesoporous materials

One pot synthesis of TiO_2 thin films with APTES

0.67g of Pluronic (F127) were dissolved and sonicated in a flask containing 23.32 ml of EtOH and were left under stirring for 2h. After placing the flask in an ice bath, 0.86 ml of $TiCl_4$ were added to the solution. After about 20 minutes, 1.8 ml of water and 0.47 ml of 3–Aminopropyl triethoxysilane (APTES) were added to the mixture at room temperature. After 3 h of stirring, the solution was used for the deposition on silicon wafers. The deposition conditions were RH 18-21% into the deposition chamber and 33% outdoor, and the temperature of deposition was of 22°C with a deposition rate of $15cm \cdot min^{-1}$. The molar ratios were $TiCl_4$: APTES : Pluronic F127 : H_2O : EtOH = 0.8 : 0.2 : 0.005 : 10 : 40.

After the deposition, the films were placed in a chamber with a RH = 99% (Magnesium Acetate) for 24h and then were treated at 60°C for 24h and 100°C for additional 24 h. Then the films were cleaned one-side with a solution of acetone-ethanol 1:2 and FTIR measurements were carried out. Finally, the films were put into the oven at 150°C for 65h, to remove as much as possible template without destroy the APTES, and FTIR and ellipsometric measures were carried out.

To assess the stability in biological solutions of mesoporous TiO_2 films functionalized with one-pot methods, a sample was immersed in a PBS (1x) solution at room temperature for different times (2, 4, 6, 8, 10, 12, 18, 24, 36 and 48 hours). The variations in thickness and refractive index were studied and FTIR measurements were performed.

One pot synthesis of SiO_2 thin films with APTES

In a flask were added 8.3 ml of EtOH at 3.38 ml of TEOS and 0.355 ml of HCl 0.768M. The solution was stirred for 60 minutes to facilitate the hydrolysis. At the same time was prepared another solution with 15 ml of EtOH, 1.3 g of Pluronic F127 and 1.5 ml of HCl 0.05M and was left under stirring for 1h. Then the two solutions were mixed and left under stirring for another hour. Finally 0.33 ml of HCl 11.37M (37%) and 0.886 ml of APTES were added dropwise to this solution and, after a few minutes the mixture was used for film preparation. The deposition conditions were RH 18% in the deposition chamber, RH 31% outdoor, the deposition temperature

in the chamber was 22°C with a deposition rate of 15cm·min^{-1}. The molar ratios were TEOS : APTES : Pluronic F127 : H_2O : HCl : EtOH 0.8 : 0.2 : 0.005: 6 : 0.02 : 16.4

After the deposition process the samples were stabilized at 60°C for about 18h and 100°C for 24h. To remove the template, thin films were put in a flask with EtOH under reflux for 6 hours. Finally the films were washed with fresh EtOH and dried in an oven at 100°C before FTIR and ellipsometric characterization.

To assess the stability in biological solutions of mesoporous SiO_2 films synthesized with the one-pot method, a sample was immersed in a solution of PBS (1x) at room temperature for different times (2, 4 , 6, 12, 18, 24, 36 and 48 h). Film variations in thickness and refractive index were studied and FTIR measurements were performed.

Post grafting synthesis of TiO_2 thin films with APTES

The precursor solution was prepared as previously described. Pluronic F127 was dissolved in ethanol; the solution was stirred for two hours at 25°C in a closed vessel. $TiCl_4$ was slowly added to the ethanolic solution of Pluronic F127, under stirring for 20 min in an ice bath. Finally water was added to this mixture that was left to react under stirring for 3 hours at 25°C in a closed vessel. The addition of water causes the hydrolysis of $TiCl_4$ producing EtOH and HCl, responsible of the high stability of the sol that is stable for several months at 25°C. The molar ratios in solution were: TiCl4 : Pluronic F127 : H2O : EtOH = 1 : 0.005 : 10 : 40.
Titania thin films were deposited by dip-coating silicon wafers into the precursor solution at 25°C and at a withdrawal rate of 15 cm·min^{-1}. The relative humidity (RH) inside the dip-coater chamber was maintained between 18-25%. The as deposited films were aged at room temperature (RH = 50%) for 24 hours. Then the films were submitted to different firing steps: 60, 120 and 200°C for 24 hours at each temperature in an oven with a heating rate of 10°C·min^{-1}. The final calcination process was carried out at 350°C for 3.5h in an oven with a heating rate of 10°C· min^{-1}.

The functionalization process was studied in different solvents (EtOH, toluene), at different temperatures (20-80°C), under reflux, for different concentration of APTES (0.002-0.2M) and for different times (1-24 h), to avoid the formation of an opacity on the film surface. The optimization of the functionalization with amino-groups was obtained by immersing the calcined film in a solution 0.2 M of APTES in toluene for 24h, under stirring at 25°C. The amino grafted films were

carefully washed with toluene for several washing cycles and finally dried in air. Titania thin films were characterized with spectroscopic ellipsometry and FT-IR.

Post grafting synthesis of SiO_2, TiO_2, HfO_2, ZrO_2 thin films with APTMS

Mesoporous thin films of SiO_2, TiO_2, HfO_2, and ZrO_2 were synthesized as previously described in the section "Synthesis of mesoporous hybrid thin films". Mesoporous thin films were immersed in 10 ml of a solution 20 mM of 3-Aminopropyltrimethoxysilane (APTMS) in toluene and left 24h. Subsequently, the samples were washed with EtOH and dried at room temperature. The film surface, after functionalization, appeared highly opaque also after a long treatment in EtOH. The films obtained were characterized with ellipsometry and FT-IR techniques.

To assess the stability in biological solutions of mesoporous thin films synthesized with post grafting methods, a sample was immersed in a solution of PBS (1x) at room temperature for 2h, washed with water and dried in a oven, then the same sample was put into the solution for increasing times (4, 6, 8, 10, 12, 18, 24, 36 and 48 hours). Finally the film variation in thickness and refractive index were studied and FTIR measures were performed.

Synthesis of titania dense films

To compare the different films, TiO_2 dense films (non porous) were synthesized with the same materials and methods, and variations in stability and in the functionalization process were studied.

TiO_2 one pot dense films

These films were synthesized following the previous method used for one-pot mesoporous films with the only difference that, in this case, the template (Pluronic) was not used. The molar ratios were $TiCl_4$: APTES: EtOH: H_2O 0.8 : 0.2 : 40 : 10. The applied treatment was the same of mesoporous films with the only difference that once deposited the film was not subjected to water vapour and was not put in a chamber with high humidity because organic – inorganic phases were not present. After the conclusion of the thermal treatments ellipsometric and FT-IR measurements were carried out.

TiO_2 post grafting dense films

These films were synthesized following the previous method used for mesoporous thin films with the only difference that in this case it was not used Pluronic as template. The molar ratios used were $TiCl_4$: EtOH : H_2O 1 : 40 : 10. The applied treatments were the same of mesoporous films with the only difference that once deposited the films were not exposed to water vapour and were not put in a chamber with high humidity. The functionalization with APTES was carried out immersing the films in a solution 0.2M of APTES for 24h, under stirring, at room temperature and followed by washing in toluene and drying at RT.

TiO_2 dense films synthesized with one-pot and post grafting methods were immersed in PBS 1x for 2, 4, 6, 8, 10, 12, 18, 24, 36 and 48 hours and the variations in thickness, refractive index and in FTIR spectra were studied.

Part 1 Detection of dioxins using mesoporous titania thin films and pentapentides

For the detection of dioxins three pentapeptides were synthesized, that, as reported in recent literature [157, 158], were chosen from a combinatorial pentapeptide library and were found to be able to bind dioxin molecules and in particular 2,3,7,8-tetrachlorodibenzodioxin (TCDD).

Optimized Microwave-Assisted Solid-Phase Peptide Synthesis

The peptide synthesis and characterization was carried out thanks to a collaboration with Dr. A.M. Roggio and Porto Conte Ricerche. Three different linear pentapeptides were synthesized in our laboratories H-Ile-Gln-Asp-Leu-Phe-COOH, H-Val-Gln-Asp-Leu-Phe-COOH and Fmoc-Phg-Gln-Asp-Leu-Phe-COOH with the following procedure. 0.1 mmol (500 mg, loading 0.21 mmol/ g) of Fmoc-PAL-PEG resin was transferred to a 10 ml bottom-filtration reaction vessel, which was swollen in 4 ml of DCM/ DMF (1:1) for 30 min. After that, 2 ml of piperidine 30% in DMF was added to the resin. The reaction vessel was placed into the microwave cavity and irradiated for 30s at 75°C (SPS mode, maximum power 20W, ΔT 3 °C). The resin was subsequently washed with 4 ml of DMF and 2 ml of piperidine 30% in DMF were added to the sample and irradiated for additional 2.5 min at 75 °C (SPS mode, maximum power 20W, ΔT 3°C). The suspension was then washed for five times with DMF and DCM (4 ml each). In separate vials the corresponding

Fmoc-amino acid (0.2 mmol), HATU (0.5 mmol), DIPEA (0.5 mmol) and HOBt (0.2 mmol) were prepared and were sequentially added to the reaction vessel. The coupling cocktail was added to the resin after 2 min and the reaction mixture was irradiated at 75°C for 10 min using the SPS program (maximum power 10W, ΔT 3°C). After the last deprotection step, the peptidyl resin was dried under reduced pressure.

Final Cleavage from the Resin. The peptide was cleaved from the solid support with a cleavage cocktail (5 ml) of TFA / triisopropylsilane / water (95 : 2.5 : 2.5 v/v) at room temperature for 3 h. The resin was filtered and washed with a small amount of cleavage cocktail. The residual product was precipitated with ice-cold diethyl ether and the peptide was collected by filtration, dissolved in deionised water, and lyophilized.

Peptide Purification. The linear pentapeptide H-Ile-Gln-Asp-Leu-Phe-COOH was purified by semi preparative Jupiter column (RP C18-5 *ί*m , 250 mm-10 mm) using acetonitrile 95% (0.07% TFA) in H_2O (0.1% TFA), with a 20% - 95% linear gradient over 25 min. A flow rate of 4.0 $ml \cdot min^{-1}$ was used, and the detection was at 220 nm. The purity of the final peptide was checked with analytical HPLC (Discovery C18-10 *ί*m column, 250 mm-4.6 mm) using the same gradient program.

Peptide immobilization

There have been different trials to immobilize the pentapeptides on the surface of functionalized mesoporous TiO_2, directly on the film, on the film with APTES, on the film with APTES and Glutharaldheyde and with the method used for the peptide synthesis. The linking was followed with FTIR, AFM and spectroscopic ellipsometry to study the best method, solvent and concentration to link the pentapeptides to TiO_2-APTES thin films.

Reaction with HATU and DIPEA. The usual method for peptide synthesis was tried to attach the pentapeptides to the amino- groups of the substrates. In particular 1eq of peptide was solubilised in 2ml of DMF with 2eq HATU under stirring for 10 minutes, after that 3.5eq DIPEA and 3ml of DMF were added and left under stirring for 3h. Then a TiO_2 mesoporous thin film functionalized with APTES was immersed in this solution and left under stirring for 48h. The sample was washed with water and dried at room temperature.

Optimized procedure. TiO_2 thin films were immersed in a solution 0.1 $mg \cdot ml^{-1}$ of peptides in toluene and left under stirring for 24h at 25°C. After that thin films were washed different times with toluene, dried at room temperature and the linking was monitored with FTIR measures. For the detection of dioxins some fluorophore was linked to the peptides, that could be sensitive to the presence of TCDD. For this reason a study of the best fluorophore has been essential.

Identification of the fluorescent probe that is sensitive to dioxins

Stock solutions of Fluorescein and Rhodamine were prepared dissolving these probes (1 mg) in 100 µl of DMF. From these stock solutions progressive dilution (1:500, 1:250, 1: 125 etc.) were prepared starting from 1 ml of stock and adding 500 µl of buffer (Tris-HCl pH8). At this point UV measurements (λ = 200-800 nm using the buffer solution as a blank) were carried out and the solution concentration was studied in order to have an absorbance maximum of 0.1. For the following measures were chosen the solutions that presented an absorbance A = 0.09 and a λ_{max} = 490 nm for Fluorescein and an absorbance A = 0.11 with a λ_{max} = 550 nm for Rhodamine. The experiment was tried also with another fluorophore, the ANS (1-anilino-naphthalene-8-sulfonic acid) preparing the stock solution by dissolving about 1 mg of ANS in 200 µl of DMF. Then 10 µl were taken from this solution and solutions with progressive dilutions were prepared by adding different rates of DMF. From UV-vis measures appeared that the ANS probe had an A=0.1 at a λ_{max} = 370 nm.

Then the fluorescence measurements were performed using for Fluorescein a λ (wavelength) excitation of 490nm and an emission λ between 500-700 nm with a 20V lamp and a slight = 1, obtaining a λ_{max} of emission at 520nm. The measures were repeated several times in order to exclude the phenomenon of photobleaching. The same conditions for the measurement of rhodamine were used varying only the slight (equal to 2) and recording the emission spectrum with a λ range 550-700 nm for rhodamine and an emission with a λ_{max} at 470 nm for ANS.

To monitor the possible changes in fluorescence due to the presence of dioxin in solution and their interaction with the probes 1 µl of a solution of dioxin ((TCDD 10 µg/1ml of toluene) was added to the solutions of fluorescein, rhodamine and ANS and UV-vis and fluorescence measures were carried out. It was noted that only with the fluorescein there was a considerable variation in the emission peak due to the addition of dioxin, for this reason this probe was chosen for the following detection steps.

Detection of TCDD

For the final detection of TCDD it was tried to link fluorescein directly to mesoporous titania thin films obtaining a low fluorescence; for this reason it was tried to link FITC to peptides. This linking was tried after the immobilization of peptides on the films but this procedure was difficult; for this reason the following procedure was tried for the reaction FITC-peptide and the subsequent linking with TiO_2-APTES mesoporous films.

A solution of fluorescein isothiocyanate (FITC) in dimethyl sulfoxide (DMSO) was prepared at the concentration of 5 $mg \cdot ml^{-1}$. Then 1 mg of peptide were dissolved in 1 ml of toluene and 20 µL of FITC in DMSO were added to this solution. The Peptide-FITC solution was left under stirring for 3 hours, then diluted by adding 20 ml of toluene and used to immerse the titania films functionalized with APTES. Different measures were also tried on these solutions before immersing the films, to study the variation of fluorescence due to solvent, peptide and FITC. Then the samples were immersed and left into the solution, under stirring, for 24 hours in the dark. Finally the films were washed with toluene, dried in air and the fluorescence measures were carried out. Carbonate buffer 0.1 M and sodium carbonate 0.1 M solutions were also tested as possible solvents instead of toluene but the samples immersed in these solutions were not able to give fluorescence and were not further used. The same experiment was also carried out linking GA glutaraldehyde to the titania films functionalized with APTES. This step was possible by dipping the films in a solution of GA 50% in water for 15h followed by washing with water. Then the films were dipped in a solution of Peptide-FITC in toluene for 24h in the dark, washed with toluene, dried and, finally, fluorescence measures were made.

For the final detection of TCDD titania, films functionalized with APTES-Peptide-FITC and APTES-GA-Peptide-FITC were dipped in different solutions of TCDD in toluene at a concentration $3 \cdot 10^{-6}$ M, $3 \cdot 10^{-8}$ M, $3 \cdot 10^{-10}$ M, $3 \cdot 10^{-12}$ M for 1h, after that the samples were washed with toluene, dried at room temperature and the fluorescence measures were carried out.

Part 2 Detection of E.coli using mesoporous titania thin films and antibodies

Linking of antibodies to titania thin films

The second part of the work was based on the detection of pathogens and in particular E.coli using antibodies linked to titania thin films alone or functionalized with APTES and GA. The functionalization of TiO_2-APTES films with GA was obtained immersing the films in GA 50% in

water for 24h, washing with water and EtOH and drying at room temperature. Different experiments were carried out for the immobilization of antibodies on titania thin films directly on the films, on the films functionalized with APTES and on the films functionalized with APTES and GA. Antibodies solutions were prepared dissolving 200µl of anti E.coli O157:H7 in 800µl PBS with a final concentration of 50 µg/ml, then the films were covered with this solution for 15h at 4°C. Finally the films were washed with PBS and water, dried at room temperature and FTIR measures were done to monitor the presence of antibodies on the films. The detector was cooled with liquid nitrogen for 60min before data collection and also during the measures.

Bacteria preparation

E. coli O157:H7 and E. coli K12 were cultured on agar plates for 24 h, then a single colony of each species was transferred into 10 culture tubes containing 5 ml each of LB (Luria-Bertani Medium) and put into the incubator at 37 °C, under shaking for 18 h at 120 rpm. After that the tubes were centrifuged at 3500 rpm for 10 min, obtaining a pellet. Then the LB was removed from the tube and the cells were first washed three times with sterile PBS to remove residual medium and resuspended in 3ml PBS for binding experiments. Serial dilutions of bacteria were prepared for the detection step.

Determination of the Detection Limits of E.coli O157:H7

Titania thin films alone or functionalized were incubated with anti-E.coli O157:H7 antibodies covering the films with 1 ml of E.coli O157:H7 at concentrations ranging between 10^8 and 10 CFU/ ml for 90 min to allow the binding. Then these films were washed and left 15min in PBS solution, washed with PBS and water, dried in air at room temperature and finally analyzed by FT-IR spectrometry to determine the sensitivity of the methodology. Some trials with E.coli K12 were also carried out to study the selectivity of the method.

Part 3 Development of SERS substrates with mesoporous titania thin films

To create devices able to detect analytes in very low concentration, mesoporous TiO_2 thin films were modified to obtain new substrate for SERS, using them as host matrix for the grown of Ag nanoparticles. TiO_2 films were synthesized as described in the section “synthesis of mesoporous hybrid thin films”.

Grown of silver nanoparticles

Titania thin films were immersed in a solution 1M $AgNO_3$ in H_2O : EtOH = 1 : 1 (v/v) and left in the dark, under stirring, to optimize the impregnation process. Different times were tried for this step, from 20 minutes to 24 h. The films were then placed in a petri dish and were completely covered by the $AgNO_3$ solution. Finally the Petri with the films was placed under a UV lamp (Spectroline, 4W, at a wavelength of 356 nm) and exposed for different times (10 minutes, 1, 3, 5 and 6 hours) to UV light. After the exposition the samples were washed with ethanol and water and dried at room temperature.

Detection of Rhodamine B isothiocyanate and Cytochrome C with Raman spectroscopy

To evaluate the SERS effect of the titania mesoporous films containing the silver nanoparticles, different samples were impregnated with solutions of Rhodamine B isothiocyanate or Cytochrome C. The films were dipped into an aqueous solution of rhodamine B isothiocyanate (RhBITC) or cytochrome C (Cyt C) at different concentrations ($1\cdot10^{-3}$, $1\cdot10^{-6}$, $1\cdot10^{-8}$, $1\cdot10^{-10}$, $1\cdot10^{-12}$, $1\cdot10^{-14}$, $1\cdot10^{-16}$ M for RhBITC and $1\cdot10^{-4}$, $1\cdot10^{-6}$, $1\cdot10^{-8}$, $1\cdot10^{-10}$, $1\cdot10^{-12}$, $1\cdot10^{-14}$, $1\cdot10^{-16}$ M for CytC) and left at 25°C for 1 hour; after that the films were washed with water and dried in an oven at a temperature of 37°C. Finally the Raman measures were carried out for the detection of RhBITC and CytC.

Characterization techniques

Film characterization

Fourier Transform Infrared (FTIR) analysis was performed using a Bruker Vertex 70v spectrophotometer. The optical bench and the sample compartment were kept in vacuum during the measurement at pressure lower than 0.5 hPa. The measurements in the middle infrared (MIR) region were performed using a Globar source, a KBr beamsplitter, and a RT-DLaTGS detector averaging 256 scans with 4 cm^{-1} of resolution. The measurements in the far infrared range were done using a Globar source, a Si beamsplitter, and a RT-DTGS-FIR detector. The spectra were recorded in transmission, in the 600-100 cm^{-1} range by averaging 32 scans with 4 cm^{-1} of resolution. A silicon wafer was used as the substrate to measure the background; the baseline was calculated by a rubber band algorithm (OPUS 7 software).

The organization of the porous structure was investigated by 2D grazing incidence small angle X-ray scattering (GISAXS) at the Austrian SAXS beam line of ELETTRA synchrotron facility (Trieste, Italy). An incident energy of 8 keV (wavelength 1.54 Å) was used; the instrumental glancing angle between the incident radiation and the sample was set slightly above the critical angle (grazing incidence). A two-dimensional CCD detector (Photonic Science, U.K.) was used to acquire the scattering patterns; each measurement consisted typically on the average of 10 acquisitions with integration time of 6 s.

Pore arrangements were also studied by transmission electron microscopy (TEM). TEM micrographs were obtained in bright field mode on a JEOL 200CX microscope equipped with a tungsten cathode operating at 200 kV. Finely ground films scratched from the substrate were dispersed in n-octane by sonication, and then they were dropped on a carbon-coated copper grid and dried for TEM observations. Centre-to-centre interpore distance was evaluated by line profile analysis on a set of representative TEM images as the average FWHM of the intensity distribution along a line passing through the pore centres.

Film thicknesses and refractive indexes were measured by spectroscopic ellipsometry using a α-SE^{TM} instrument (J.A.Woollam, U.S.A.) working in the 400-850 nm range.

For the characterization of functionalized films with peptides of the Part 1 was used the FTIR and spectroscopic ellipsometry described above.

Fluorescence analysis was done using a FluoroMax-3 Horiba Jobin Yvon spectrofluorometer. The probing beam was set to impinge on one side of the sample (silicon substrate, incidence angle of 2-3°) so that the sample acted as a waveguide for the incident light wave, while the luminescence was collected at 90° with respect to the incident beam. This configuration enhanced the signal-to-noise ratio and avoided reflection effects. Each acquisition is the average of 3 different accumulations. An excitation wavelength of λ_{ex}= 490 nm was used for acquiring the emission spectra.

Atomic force microscopy (AFM) images were taken using a NT-MDT Ntegra AFM; surfaces were measured at 0.5–1 Hz scan speed in semi-contact mode, using a silicon tip with nominal resonance frequency of 150 kHz, 5 $N \cdot m^{-1}$ force constant, and 10 nm typical curvature radius.

For the second part of the work mesoporous titania thin films were characterized with a FTIR Nicolet Nexus spectrophotometer equipped with a KBr-DTGS detector and a KBr beam splitter. The measure was carried out in the range 4000-700 cm^{-1} with 256 scans and 4cm^{-1} of resolution.

The spectra were recorded in transmission, under an N_2 flow, on films deposited on silicon wafers. The background was recorded using a silicon substrate.

For the third part of the work titania thin films with silver NPs were characterized as follows.
UV-visible absorption spectra were obtained using a Nicolet Evolution 300 spectrophotometer. The measures of mesoporous titania thin films on silica slides, with or without AgNPs, were done from 200 to 800 nm; a silica glass slide was used for the background.

Fourier Transform Infrared (FTIR) analysis was performed using a Bruker Vertex 70 spectrophotometer. The spectra were recorded in transmission, in the 4000-400 cm^{-1} range by averaging 128 scans with 4 cm^{-1} of resolution. A silicon wafer was used as substrate to measure the background; the baseline was calculated by a rubber band algorithm (OPUS 7 software).

X-ray diffraction (XRD) patterns were collected in the angular range $10<2\theta<80$, using a Bruker Discovery 8 instrument with a copper tube CuK_α ($\lambda = 1.54056$ Å); the X-ray generator worked at a power of 40 kV and 40 mA. The scan type used was the Detector scan, starting at 10° and ending at 80°. The step size was 0.02° and the time per step was of 0.5s repeated until a good signal to noise ratio was obtained.

Atomic force microscopy (AFM) measures were taken with an Asylum Research 3-D AFM in contact mode.

Raman measures were taken using a Bruker Senterra confocal Raman microscope using two excitation wavelengths at 532 and 633 nm, an objective of 50X, with a power of 0.2 mW for RhITC and a power of 2 mW for CytC. The integration time for the RhITC was varied from 0.2 sec for the measures at 532 nm and two acquisitions of 1 sec for the measures at 633 nm, while for the measures of CytC an integration time of 10 s was used for the measures at 532 nm and two acquisitions of 1s for the measures at 633 nm. The Raman measurements were performed to assess any SERS effect of the Ag-doped titania mesoporous films with the dye. The measures were done on the titania mesoporous film, on the titania mesoporous film with AgNPs and on the titania mesoporous film impregnated with RhBITC or CytC.

Results and Discussion

Preparation of mesoporous hybrid thin films, functionalization and choice of the best material for biosensor development

Solution preparation

Different chemical and physical conditions were essential to obtain organized mesoporous thin films as the type of inorganic material used, the type of precursors, the hydrolysis-condensation kinetics, the type and concentration of surfactants, pH, additives, solvents, temperature, synthesis time and order of introduction of the compounds. In particular with our synthesis method mesoporous hybrid thin films were produced starting from a solution containing an alkoxide (TEOS) or metal chlorides ($TiCl_4$, $HfCl_4$, $ZrCl_4$) as inorganic precursors, an organic template (Pluronic) and additives as HCl to control the pH (except when metal chlorides were used as inorganic precursors) all in a volatile solvent (EtOH).
The reactions that occurred were the following:

$Si(OR)_4 + H_2O \rightarrow (RO)_3Si\text{-}OH + ROH$ (1)
$(RO)_3Si\text{-}OH + HO\text{-}Si(OR)_3 \rightarrow (RO)_3Si\text{-}O\text{-}Si(OR)_3 + H_2O$ (2)
$(RO)_3Si\text{-}OR + HO\text{-}Si(OR)_3 \rightarrow (RO)_3Si\text{-}O\text{-}Si(OR)_3 + ROH$ (3)
$R=CH_3CH_2$ with $Si(OR)_4$ =TEOS

For silica preparation the hydrolysis reaction (eq.1) started with the addition of water that replaced the alkoxide groups (RO) with the formation of hydroxyl (OH) groups and alcohol. Then the condensation reactions started (eq. 2 and 3) involving the silanol groups (Si-OH) and creating siloxane bonds (Si-O-Si) and water or alcohol. Usually the condensation process starts before the hydrolysis is complete, for this reason it was very important to control the pH and the molar ratio H_2O/Si to complete the hydrolysis before condensation begins. The reagents used for this reaction were water, ethanol and HCl. Water was essential for the hydrolysis process, while EtOH was used because water and alkoxides are immiscible and in this way the hydrolysis is facilitated; finally HCl was added, because under acidic conditions the alkoxide group is protonated quickly making it more electrophilic and more available for water attack. In the final condensation process, the

increasing number of siloxane bonds lead to the aggregation of the molecules in the sol that became gel.

For the preparation of transition metal oxides the reaction of hydrolysis and condensation were the same but in this case HCl was not added because it was developed in the reaction as shown below:

$MCl_4 + 2ROH \rightarrow MCl_2(OR)_2 + 2\ HCl$

$MCl_2(OR)_2 \xrightarrow{m H_2O} [\ M(OH)_2(H_2O)_n(Z)_x]^{(2-x)} + (2-xHCl) + (2-xEtOH)$

Z=OH, Cl, OEt; m>4; x<2

M=Ti, Hf, Zr R= CH_3CH_2

Different parameters have been considered in the synthesis step as the aging of the sol before the deposition, in fact with a short aging time cubic mesostructured films were obtained (Fig. 13). Also the ratio between water and ethanol was important to obtain a well-aligned phase avoiding that the condensation of the inorganic precursors disturbed the organization of the amphiphilic molecules. The presence of water and acid (added or developed) helped the folding of the template giving more ordered phases.

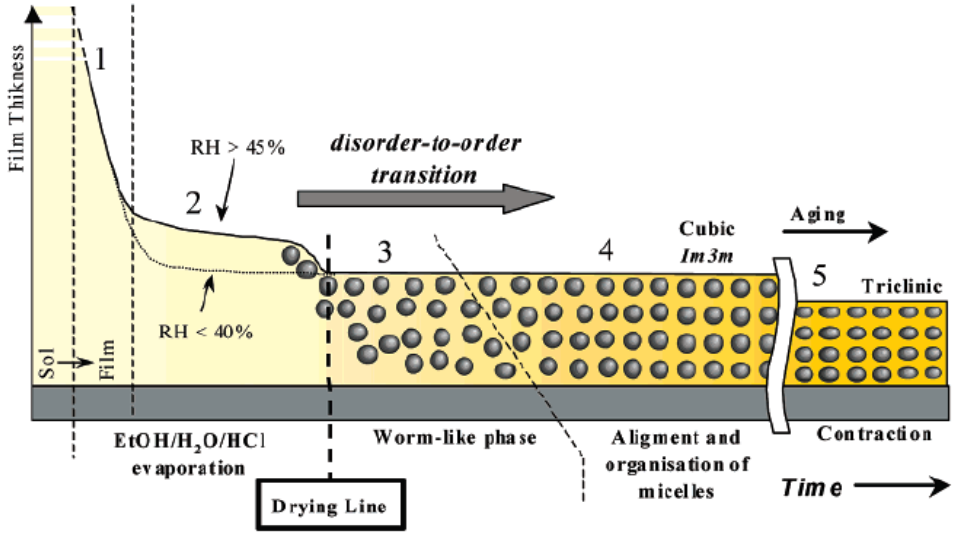

Fig. 13 Formation of the hybrid organic-inorganic structure. Reproduced by [125]

Film deposition

For the deposition of the sols on the substrates it was used the dip coating method (Fig. 14, 15).

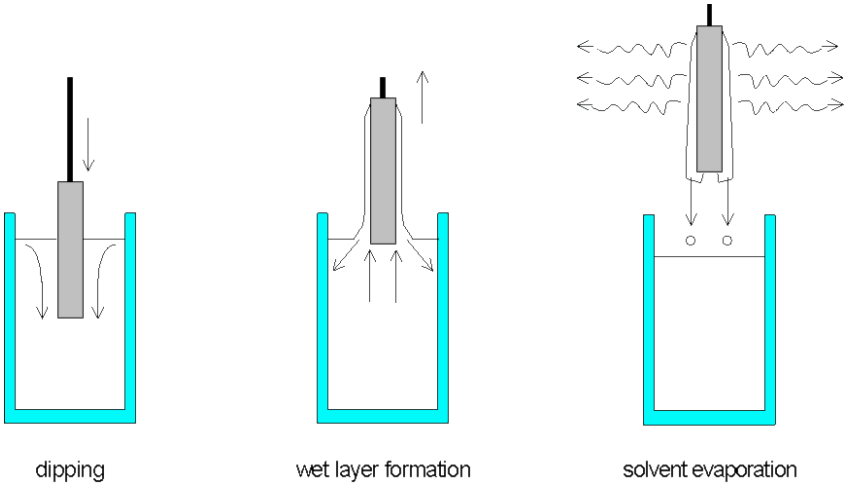

Fig. 14 Dip coating process. Reproduced by [136].

Dip coating was realized dipping silicon and quartz wafer of size 1cm x 3cm into the precursor solution and extracting the substrate with a well-defined speed, under controlled humidity, temperature and atmospheric conditions. The final film thickness, in the deposition step, was influenced by the withdrawal speed, the solvent used and the viscosity of the solution.

Fig. 15 Picture of the home made dip-coater used in the present work (left), and the deposited thin film on Si (right) .

Evaporation process

After the immersion and extraction of the silicon or quartz wafer into the micellar solution, the evaporation process of the volatile species (EtOH and HCl) started leading to the self assembly of the surfactant (Pluronic) with the inorganic species, according to a process called EISA (Evaporation induced self assembly). To obtain the self organization it was important to use a definite molar ratio between the template and the inorganic compounds allowing the electrostatic interactions among the surfactant head groups and the inorganic molecules.

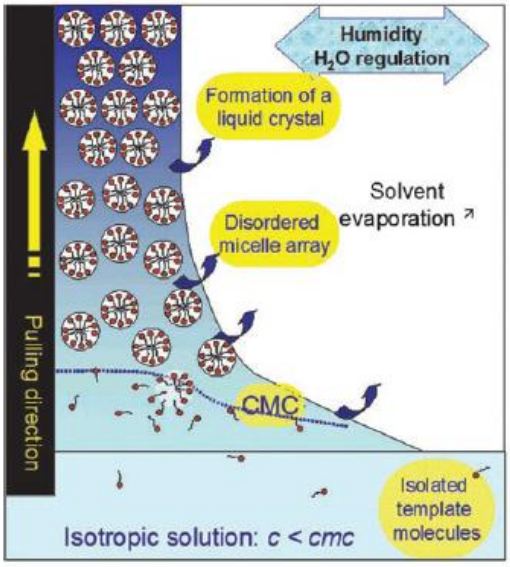

Fig. 16 Evaporation induced self assembly process. Reproduced by [139].

As shown in Fig. 16 the evaporation of water and ethanol produced an increase in the concentration of the surfactant, of the acid and of the inorganic precursor, starting the evaporation from a micellar concentration C_0 ($C_0 << C_{mc}$) and arriving to a surfactant concentration that exceeds the critical micelle concentration (C_{mc}), leading to the development of the mesophase. In this step to obtain ordered structures it was indispensable to control the temperature and RH that influenced the evaporation of the solvent and the reactions occurring in the sol.

Post treatments

To assembly the network in the desired mesostructure, it was necessary to age the film for at least 24 h at high humidity, after that, it was stable enough to be calcined. Different values of humidity were tried because this parameter affected the final aspect of the film. In fact films deposited at

high RH were transparent, but with an inhomogeneous thickness for the slow drying process due to the absorption of water during the formation of the layer, while films deposited with RH < 45% were homogeneous but became opaque when exposed to the external humidity. To obtain films with high optical quality and excellent organization it was carried out the deposition at low RH and a post-processing at high RH. This post-treatment has been more efficient if applied quickly, to avoid the condensation of the inorganic framework that could stop the intermediate disordered structure. The film thickness was also influenced by the temperature because the increasement of temperature led to a fast evaporation and condensation rate that is negative for the formation of organized films. The best results were obtained using temperature from 20 to 30 °C during the dip coating process for combining good optical qualities and film organization. Also the post deposition treatments have been considered because they were determinant for organization, degree of contraction, and thermal stability of the final film. The thermal treatments were used to eliminate the volatile species, to increase the condensation of the inorganic species and to remove the template. It was found that to obtain highly organized films with high surface area it was better to use a set of aging treatments (from 60 to 120 °C and 200°C) under controlled RH and a slow heating process (10°C/ min) then a quick step at high temperatures. The template removal was obtained with a calcinations process at 350 °C. The final heating led to a further condensation, which stabilized the structure and caused a contraction.

Film formation and template removal were followed by FTIR measures, as shown in the next section.

Characterization of mesoporous SiO_2 thin films with FTIR

FTIR spectra of silica thin films were carried out in the 4000- 450 cm^{-1} range (Fig. 17). As shown in the spectrum there are two regions corresponding to different vibration modes attributed to hydroxyl species (3800 - 3000 cm^{-1}) and silica species (1800 - 400 cm^{-1}).

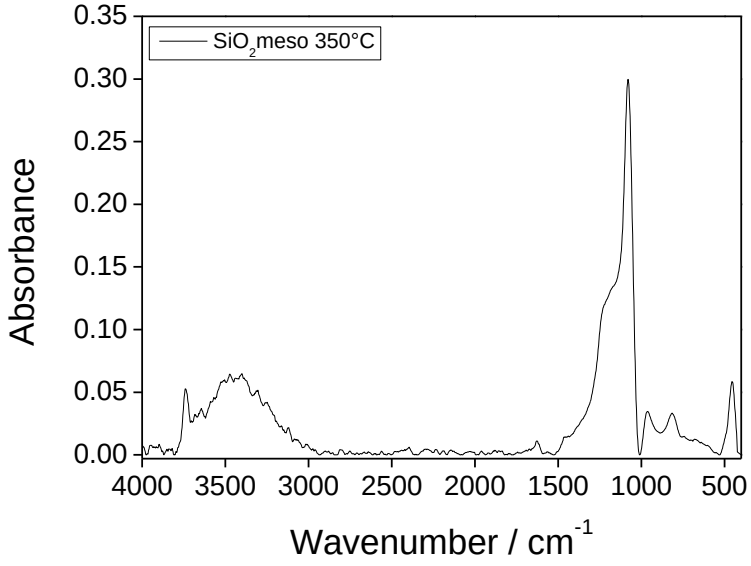

Fig. 17 FTIR of mesoporous silica films in the range 4000-450 cm^{-1}

In the region related to hydroxyl species (3800 - 3000 cm^{-1}) can be observed (Fig.18A) different vibration modes.

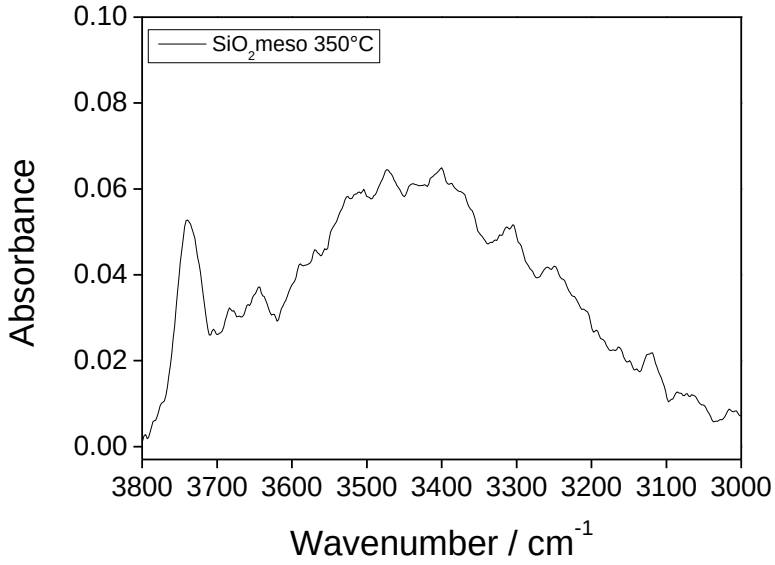

Fig. 18 A FTIR of mesoporous silica films in the range 3800-3000 cm^{-1}

In the region ~3800-3650 cm^{-1} can be seen the stretching modes of OH groups not involved or slightly involved in H-bonds, while in the region ~3650-3200 cm^{-1} can be observed the stretching modes due to H-bonds. In the region around ~3740 cm^{-1} can be noted a sharp narrow peak that is assigned to isolated silanol groups and, in the same region (~3700-3600 cm^{-1}) can be observed other peaks due to terminal silanols. Also a broad band in the ~3700- 3200 cm^{-1} region can be

observed for the H-bonds of silanol groups (Si-OH stretching). Finally the adsorbed water shows an intense band around 3300 - 3500 cm^{-1} due to O-H stretching and H-bonds.

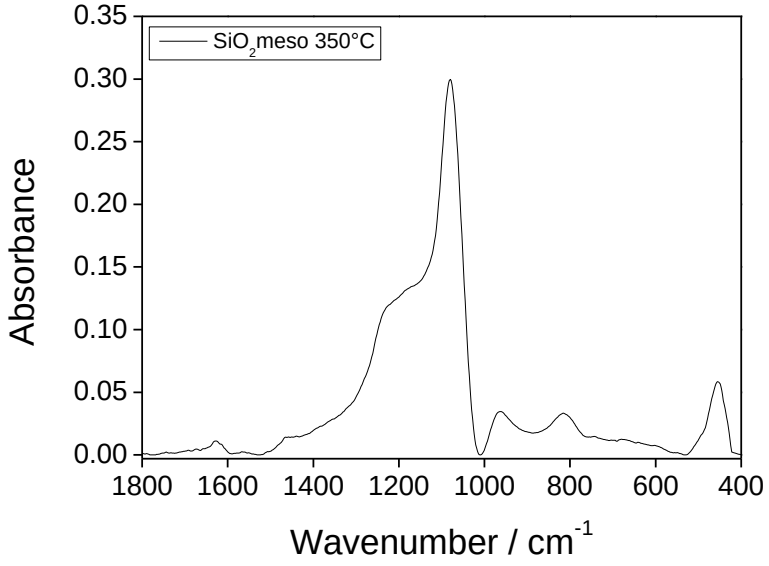

Fig. 18 B FTIR of mesoporous silica films in the range 1800-400 cm^{-1}

In the part of the spectrum (1800 - 400 cm^{-1}) related to silica species (Fig. 18B) can be noted a low band at 1645 cm^{-1} due to the bending H-O-H vibrations of water. Other significant bands can be observed in the region around 1070 cm^{-1} (Si-O-Si asymmetric stretching), 800 cm^{-1} (Si-O-Si symmetric stretching), and 460 cm^{-1} (Si-O-Si rocking), due to Si-O-Si vibrational modes. The attribution of these bands is well known and represents the silica fingerprint.

Characterization of TiO_2, HfO_2, ZrO_2 mesoporous thin films with FTIR

FTIR spectra of thin films of TiO_2, HfO_2, ZrO_2 were collected. These spectra show a broad band in the range 3800-3000 cm^{-1}, region of hydroxyl groups. It was observed a shift in the absorption maximum of the OH group that was induced by the thermal treatment. In fact, after thermal treatment at 100°C (Fig. 19), a broad main peak was noted around 3400 cm^{-1} for HfO_2 and ZrO_2 thin film due to M-OH stretching (M=Zr ,Hf); instead for TiO_2 thin films the band centred around 3300 cm^{-1} was observed.

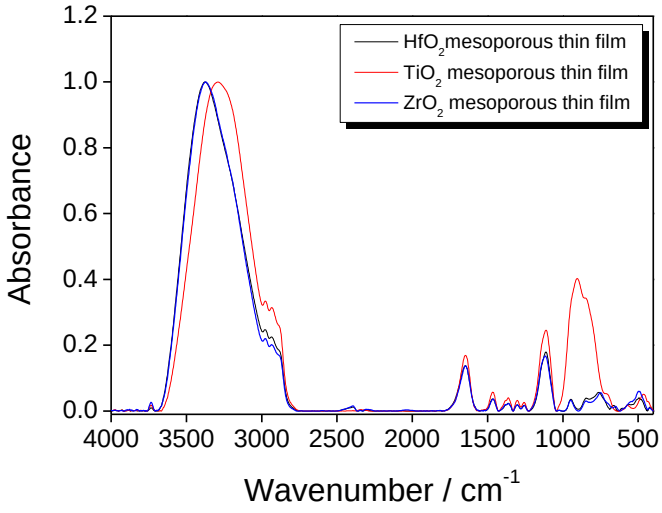

Fig. 19 FTIR of HfO_2, TiO_2, ZrO_2 films after treatment at 100°C in the range 4000-400 cm^{-1}

Furthermore the spectra changes due to the thermal treatment and the consequent template removal (Pluronic) due to the calcination process were studied. To simplify the exposure only the titania spectra were reported because the behaviour of ZrO_2 and HfO_2 thin film was the same.

The elimination of template (Pluronic) and of all the organic molecules with FTIR spectra was evaluated (Fig. 20).

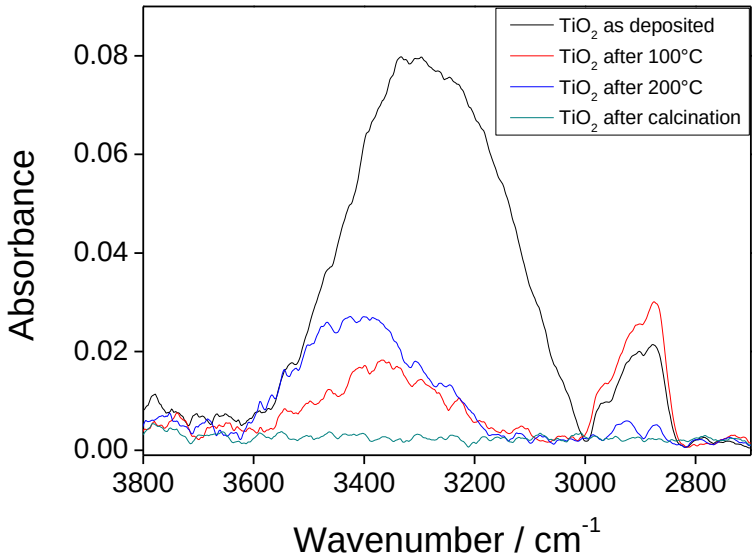

Fig. 20 FTIR of TiO_2 thin films after different thermal treatments in the range 3800-2700 cm^{-1}

It was noted that with the thermal treatments the band related to Pluronic, two intense peaks at 2930-2850 cm^{-1}, due to C-H stretching, decreased and, with the calcination process, they

disappeared; the same happened for the band around 3600-3200 cm^{-1} due to O-H stretching. The progressive removal of template can also be observed in the range 1500-1200 cm^{-1} (Fig.21); in fact the peaks due to methylene wagging around 1300 cm^{-1}, twisting at 1250 cm^{-1} and stretching of C-O-C around 1100 cm^{-1} disappeared.

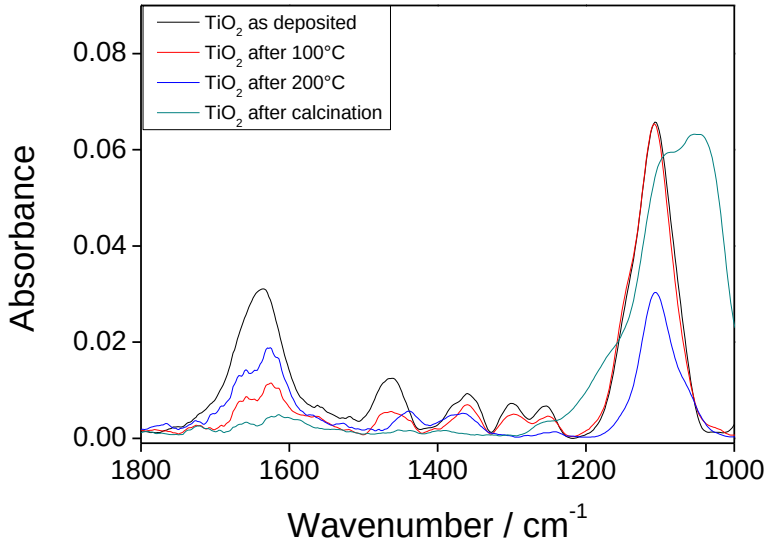

Fig. 21 FTIR of TiO_2 thin films after different thermal treatments in the range 1500-1200 cm^{-1}

For this reason, it can be concluded, that the desired films with the characteristic peaks were obtained and that all the organic compounds were removed from TiO_2, ZrO_2, HfO_2, SiO_2 thin films with a calcination process at 350 °C, producing mesoporous inorganic materials ready for the subsequent functionalization process.

Study of stability in PBS

The stability of mesoporous thin films was studied at 25°C after their immersion in PBS (phosphate buffer solution) pH 7.4 used to mimic biological environments. After the film immersion in this solution for different times (2, 4, 6, 8, 10, 12, 24, and 48 h), FTIR measures were carried out but without significant changes (not reported for this reason). Ellipsometric analysis were also carried out to study thickness and refractive index variations of these films after immersion, to obtain qualitative information about their possible dissolution.

In the next figures (Fig. 22, 23, 24, 25) are shown the results obtained for TiO_2, HfO_2, ZrO_2 and SiO_2 mesoporous thin films. For all the samples an increase in refractive index (1.79 to 1.83 for TiO_2, 1.57 to 1.64 for HfO_2, 1.67 to 1.79 for ZrO_2, 1.30 to 1.52 for SiO_2) can be noted after 48 h in buffer solution that can be due to water adsorption into the pores. A minimum increase in thickness was observed after 48 h of immersion of TiO_2 (213-216 nm) and HfO_2 (184-187 nm)

films, instead a decrease in thickness was observed for ZrO_2 (198-191 nm) and a strong one for SiO_2 (445-10 nm).

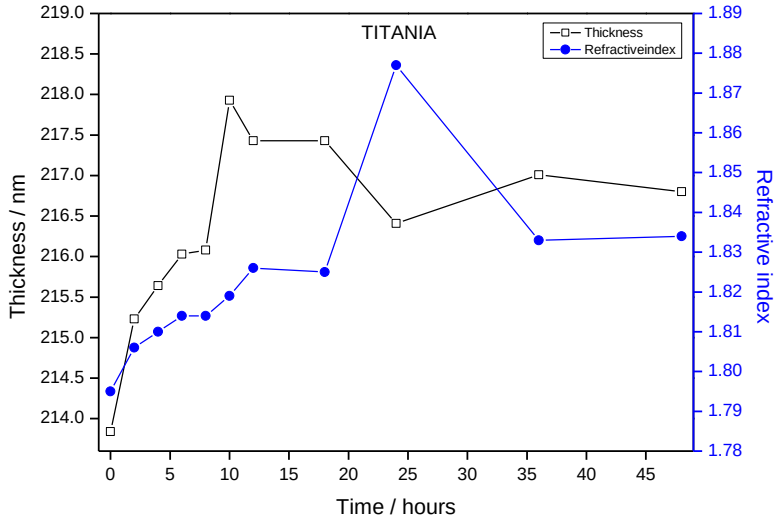

Fig. 22 Ellipsometric measures of TiO_2 thin films after immersion in PBS for 2-48h. Changes in thickness and refractive index were reported.

Time (hours)	*Thickness (nm)*	*n(refractive index)*	*MSE (mean square error)*
0	213.84	1.795	61.58
2	215.23	1.806	61.52
4	215.64	1.81	62.53
6	216.03	1.814	62.53
8	216.08	1.814	62.16
10	217.93	1.819	62.34
12	217.43	1.826	61.20
18	217.43	1.825	61.12
24	216.41	1.877	60.74
36	217.01	1.833	63.32
48	216.80	1.834	62.9

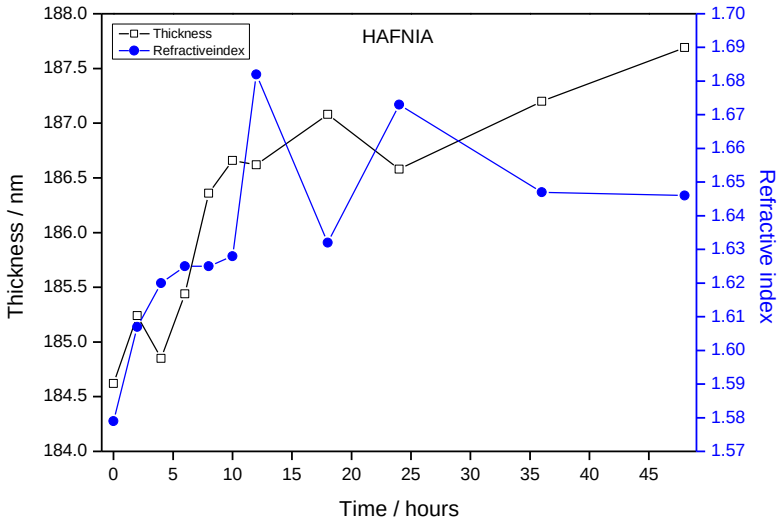

Fig. 23 Ellipsometric measures of HfO_2 thin films after immersion in PBS for 2-48h. Changes in thickness and refractive index were reported.

Time (hours)	*Thickness (nm)*	*n(Refractive index)*	*MSE (mean square error)*
0	184.62	1.579	14.28
2	185.24	1.607	12.6
4	184.85	1.62	15.17
6	185.44	1.625	15.09
8	186.36	1.625	14.97
10	186.66	1.628	15.06
12	186.62	1.682	14.99
18	187.08	1.632	15.89
24	186.58	1.673	12.47
36	187.20	1.647	16.18
48	187.69	1.646	15.92

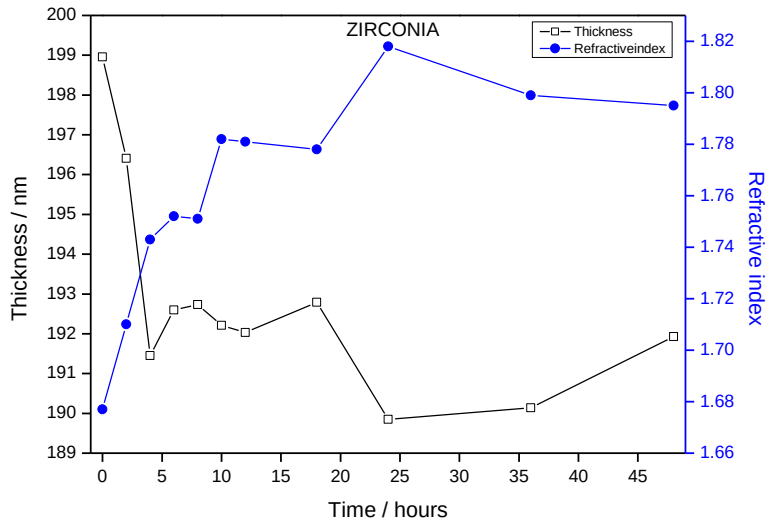

Time (hours)	*Thickness (nm)*	*n(Refractive index)*	*MSE (mean square error)*
0	198.96	1.677	35.7
2	196.41	1.71	34.9
4	191.45	1.743	37.06
6	192.6	1.752	35.36
8	192.73	1.751	35.63
10	192.21	1.782	31.17
12	192.03	1.781	32.3
18	192.79	1.778	32.77
24	189.85	1.818	30.45
36	190.14	1.799	34.19
48	191.93	1.795	32.25

Fig. 24 Ellipsometric measures of ZrO_2 thin films after immersion in PBS for 2-48h. Changes in thickness and refractive index were reported.

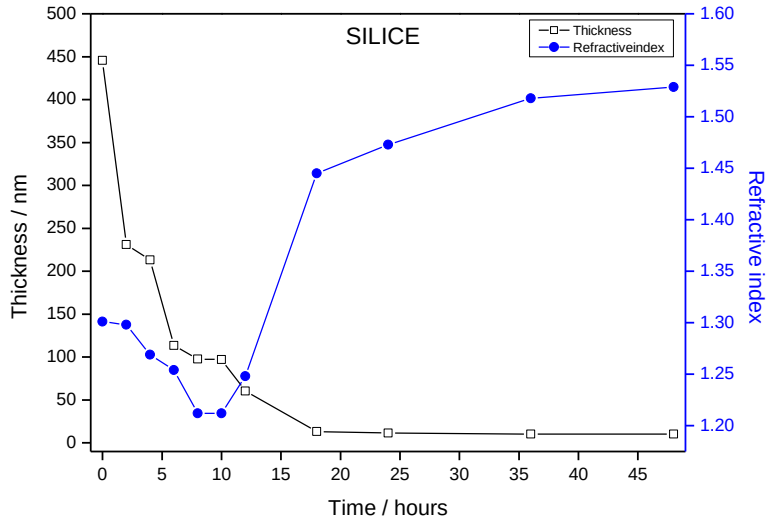

Time (hours)	*Thickness (nm)*	*n(Refractive index)*	*MSE (mean square error)*
0	445.72	1.301	60.29
2	230.99	1.298	105.60
4	213.3	1.269	196.26
6	113.58	1.254	43.09
8	97.82	1.212	27.93
10	97.08	1.212	47.6
12	60.46	1.248	39.58
18	13.40	1.445	1.79
24	11.47	1.473	1.87
36	10.28	1.518	2.02
48	10.21	1.529	2.67

Fig. 25 Ellipsometric measures of SiO_2 thin films after immersion in PBS for 2-48h. Changes in thickness and refractive index were reported.

In the case of SiO_2 thin films it was observed that only after 2h the film thickness halved and, after 18h, the hydrolysis was complete. At the same time it was observed a decrease of refractive index until 10h of treatment; after that the film was so thin that the refractive index value was due only to Si wafer. It is clear as SiO_2 thin films are not appropriate substrates for the development of biosensors because of their low stability in solution.

Comparing the other films (Fig. 26) it was observed a similar trend for TiO_2 and HfO_2 thin films that presented an increase in thickness of 3 nm after 48h of treatment. These values can be due to the measure that is not so sensitive to distinguish between few nanometres of difference. In conclusion we can confirm that there was no variation in film thickness for TiO_2 and HfO_2 thin films after 48h of treatment. In the case of ZrO_2 a decrease in thickness (around 10 nm) can be noted during the treatments with a partial hydrolysis that is not desirable for the construction of the final device.

In conclusion the following order of stability was found for the mesoporous thin film synthesized: HfO_2 ~ TiO_2 > ZrO_2 >>>> SiO_2.

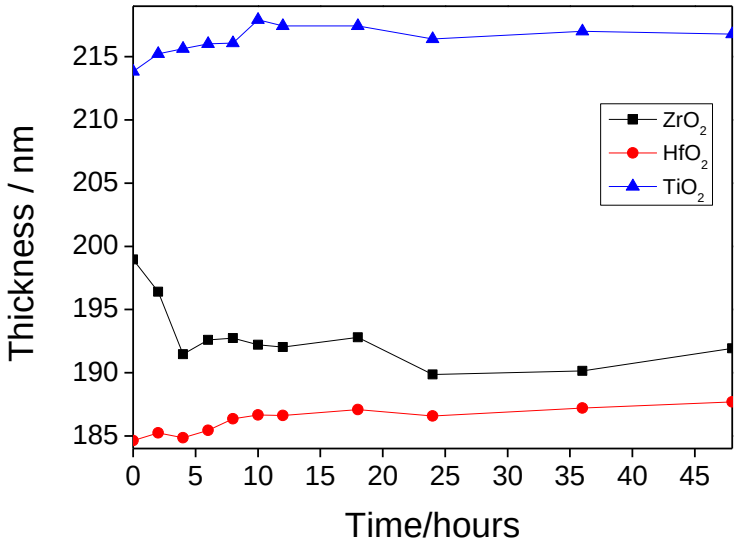

Fig. 26 Thickness measures of ZrO_2, HfO_2, TiO_2 thin films after immersion in PBS for 2-48h.

Functionalization process

Mesoporous thin films, obtained as previously described, presented large surface area and were rich in Si-OH or other M-OH (M= Ti, Hf Zr) groups that were available for a possible functionalization. The basic idea to link organic and inorganic chemistry with biological species led us to include appropriate molecules into the mesoporous thin films to obtain multifunctional materials. In this way it was possible to immobilize a molecule into the pores in an inorganic framework able to protect the immobilized species. Combining mesoporous thin films of SiO_2 or transition metal oxides (TiO_2, HfO_2, ZrO_2) with organosilica precursors it was possible to create inorganic films with an organic function. The organic functions (organosilanes as APTMS or APTES) were included in the precursor solution with the templates (***"one-pot"*** method) or added after the calcination process of the films with a post synthesis treatment (***"post grafting"*** method) as shown in figure 27.

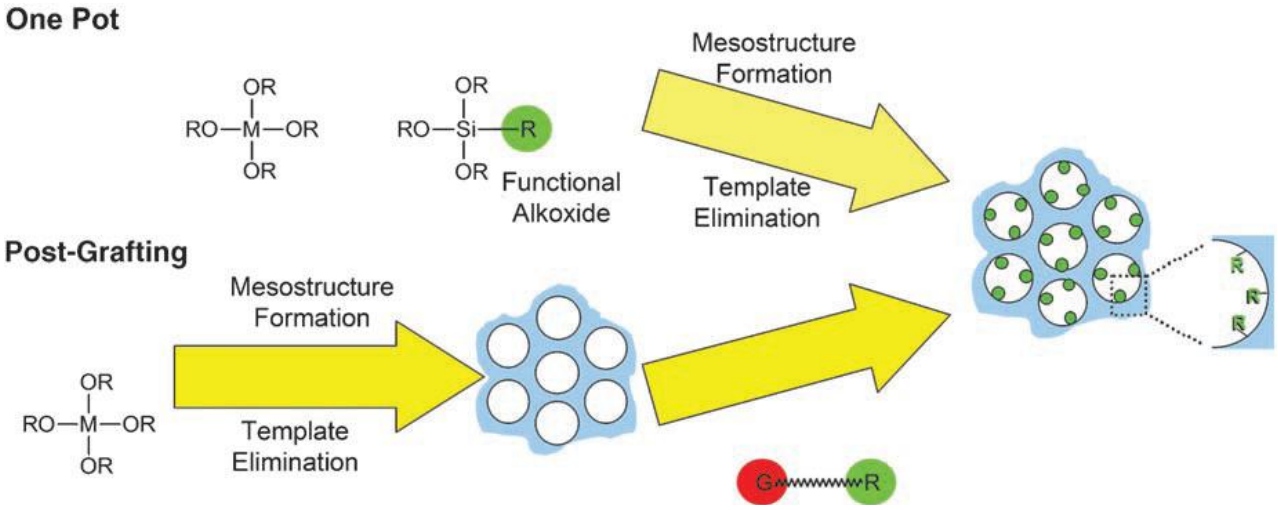

Fig.27 The main routes towards functionalized mesoporous hybrid thin films. Reproduced by [139].

With the "One pot" technique the final films have the organic molecule included inside the material and on the pore surface, with the disadvantage that during the thermal treatments it is not possible to use high temperatures to remove the template completely because it can destroy the functionalizing organic molecule. At the same time, with this method, the homogeneity of the organic function incorporation can be highly controlled and the pore blockage that can happen with the post grafting process can be avoided.

On the other hand, with the post-functionalisation method, the functional organic molecules on the pore surface can be grafted. With this route the template can be removed in a previous step, allowing linking a new function on the pores surface.

In detail using the one pot method TiO_2 and SiO_2 mesoporous thin films were functionalized, while the second method was used for TiO_2, HfO_2, ZrO_2 and SiO_2 films.

One Pot

SiO_2 One pot

SiO_2-APTES mesoporous thin films were synthesized with the one pot method and on these films FTIR and ellipsometric measures were carried out before and after the exposition to a PBS solution for different time.

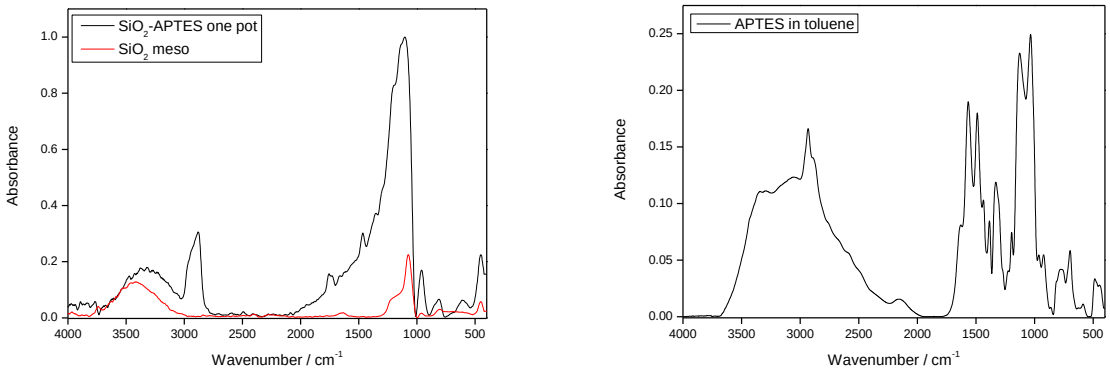

Fig.28 FTIR of SiO_2 mesoporous films synthesized with one pot method (black spectrum) and of silica films without APTES (red spectrum). As reference on the right was reported the APTES spectrum.

In particular in figure 28 it was reported the FTIR spectrum of SiO_2 mesoporous thin film with the spectrum of the same film with APTES obtained with one pot method. The reference spectrum of APTES in toluene was shown with the characteristic peaks: N-H stretching at 3300 cm^{-1}, N-CH_2 stretching around 2800 cm^{-1}, NH_2 scissoring and N-H bending at 1615 cm^{-1}, aliphatic C-N stretching at 1020-1220 cm^{-1}, NH_2 wagging and twisting at 850-750 cm^{-1} and N-H wagging at 715 cm^{-1}. From the comparison of these peaks with the SiO_2 – APTES spectrum it can be concluded that the functionalization occurred. It was also noted the presence of the bands related to Pluronic (2930-2850 cm^{-1} C-H stretching, 1300 cm^{-1} methylene wagging, 1250 cm^{-1} twisting and stretching of C-O-C at 1100 cm^{-1}) due to the incomplete removal of template.

The stability of these functionalized films was also studied in PBS as shown in the following fig. 29.

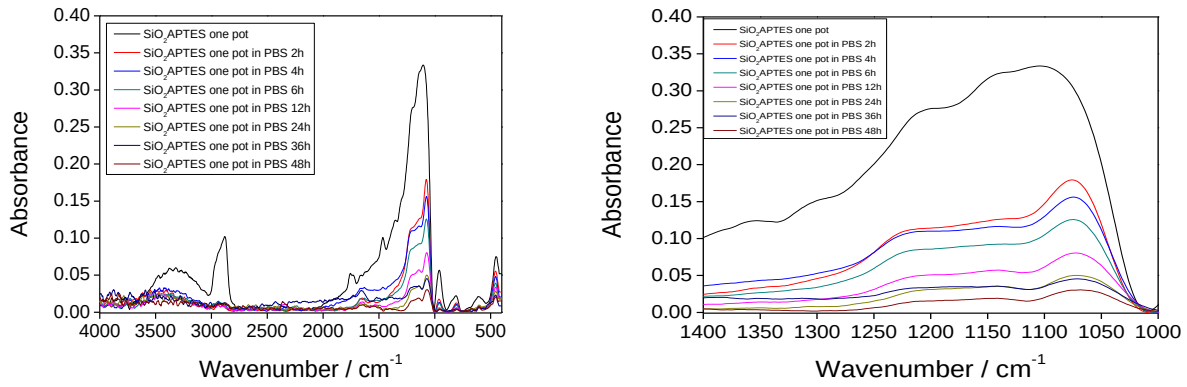

Fig. 29 FTIR of SiO_2-APTES mesoporous films synthesized with one pot method after immersion in PBS for 2-48h.

The FTIR spectra show how during the immersion of the films in PBS solution there was a proportional decrease of the peaks related to SiO_2 and APTES. This was evident in particular in the range 1300-1000 cm^{-1} related to C-N stretching and Si-CH_2 stretching of the aminopropyl chain and at 1070 cm^{-1} related to Si-O-Si bonds .

This behaviour was confirmed by ellipsometric measures (Fig. 30) that reported a strong decrease of film thickness from 550 to 100 nm after immersion due to the hydrolysis of the framework.

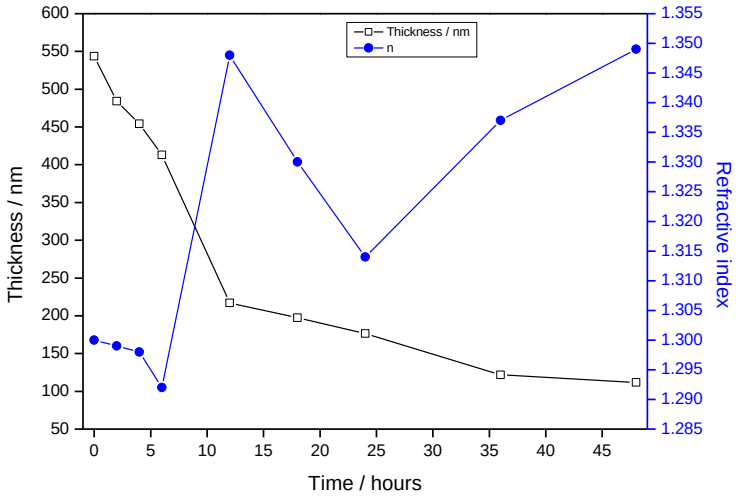

Fig. 30 Ellipsometric measures of SiO_2-APTES thin films after immersion in PBS for 2-48h. Changes in thickness and refractive index were reported.

TiO_2 one pot

TiO_2 mesoporous thin films with APTES, using the one pot method, were synthesized. To characterize the films was used the FTIR. In particular in fig. 31 it can be noted the TiO_2 spectra of mesoporous films and of TiO_2 films with APTES. Also in this case the functionalization was carried out as shown by the peaks related to APTES (N-H stretching at 3300 cm-1, N-CH^2 stretching around 2800 cm-1, NH_2 scissoring and N-H bending at 1615 cm-1, aliphatic C-N stretching at 1020-1220 cm^{-1}, NH_2 wagging and twisting at 850-750 cm^{-1} and N-H wagging at 715 cm^{-1}). It could be also noted the presence of the bands related to Pluronic (2930-2850 cm^{-1} C-H stretching, 1300 cm^{-1} methylene wagging, 1250 cm^{-1} twisting and stretching of C-O-C at 1100 cm^{-1}) due to the incomplete removal of template.

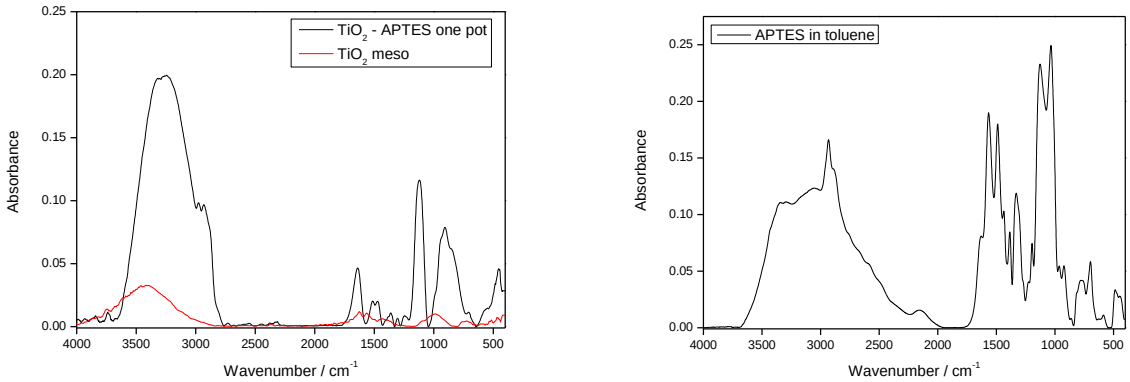

Fig.31 FTIR of TiO_2 mesoporous films synthesized with one pot method (black spectrum) and of titania films without APTES (red spectrum). As reference, on the right, the APTES spectrum is shown.

The stability of these functionalized films in PBS was also studied. In particular FTIR measures (not reported) were carried out; they did not show a consistent modification in the spectra before and after the immersion of the films in PBS solutions. While, from ellipsometric measures (Fig. 32), a decrease in film thickness was noted after 48h of immersion for totals 50 nm.

In this experiment a strong increase of refractive index can also be noted with the time, probably due to the pores filling with water or phosphate groups that remained trapped inside the pores.

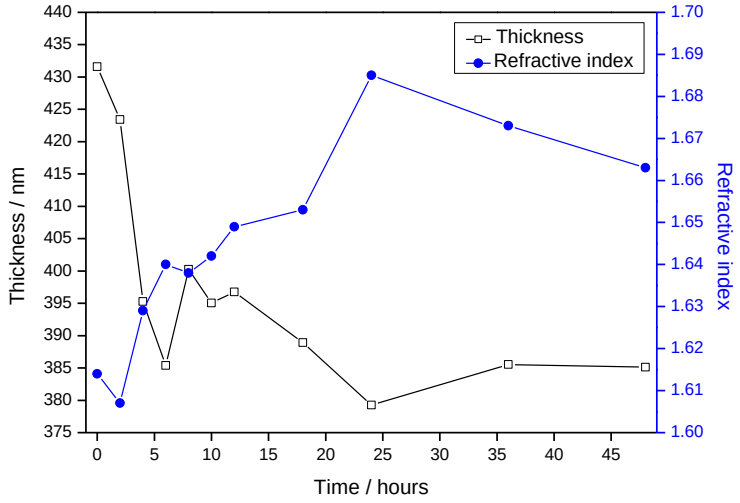

Fig. 32 Ellipsometric measures of TiO_2-APTES thin films after immersion in PBS for 2-48h. Changes in thickness and refractive index were reported.

The results obtained with the one pot method revealed that the functionalization occurred for both SiO_2 and TiO_2 thin films and that in both cases were present all the organic molecules: Pluronic and APTES. In the case of silica there was a considerable decrease in thickness, also if minor than in not functionalized films. Also in the case of titania films there was a decrease in thickness after only 6h of immersion. This low stability did not allow using these materials as substrates for the following steps.

Post grafting

Post grafting with APTMS of TiO_2, HfO_2, ZrO_2, SiO_2 mesoporous thin films

Post grafting method was carried out linking APTMS (3-Aminoprpyltrimethoxysilane) to TiO_2, HfO_2, ZrO_2 and SiO_2 mesoporous thin films. The monitoring of the quality of post grafting was very important because it was necessary for the following linking of biological molecules and for the construction of the final biosensor. This step was evaluated by FTIR analysis (Fig. 33).

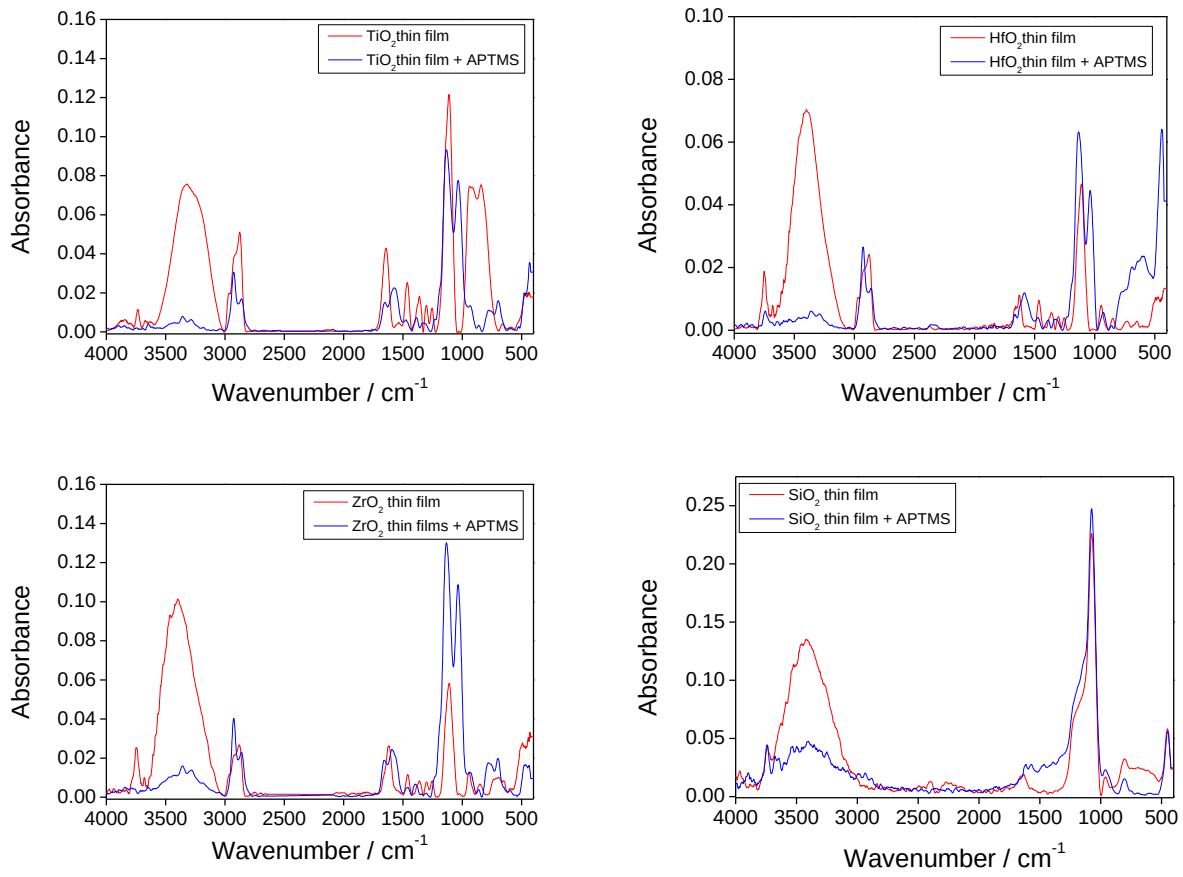

Fig.33 FTIR of TiO_2, HfO_2, ZrO_2, SiO_2 mesoporous films synthesized with post grafting method before (red spectrum) and after the functionalization with APTMS (blue spectrum).

In FTIR spectra the peaks related to amino groups on the mesoporous surface were identified. The spectra before the functionalization (red spectra) were compared with the spectra after the functionalization (blue spectra) and a new peak was seen around 3400 cm^{-1}, due to symmetric stretching of N-H (seen as a doublet for primary amines) that is partially covered with the –OH peaks. In the region between 3000-2700 cm^{-1} the presence of the propyl chain of APTMS was evident. Around 1600 cm^{-1} the peak due to N-H bending and NH_2 scissoring was present. In the range 1000-1200 cm^{-1} there could be observed the C-N stretching vibrations. In the same region the peaks can be overlapped with other Si-O-Si peaks due to the linking between APTMS molecules; but the peak due to amino group was clearly distinguishable. Finally in the range 700-850 cm^{-1} the peaks due to NH_2 wagging and twisting and N-H wagging were clear. As clearly shown by the spectra above, all these characteristic peaks were present in TiO_2, HfO_2, ZrO_2 films that confirmed the occurred functionalization, while in the SiO_2 films it did not occur a good functionalization. In fact, to functionalize thin films was not simple, because there are different parameters to consider such as the variety of ways that the primary amines can interact with the environment.

The stability of these functionalized films was also studied in PBS and the same results seen previously with the films not functionalized were obtained. In particular TiO_2 films were the most stable after 24h of immersion in PBS solution and for this reason this material was chosen for the final construction of the biosensor.

Results

Mesoporous thin films were synthesized and two methods were used to functionalize the films. The functionalization was carried out with a "One- pot" and "Post grafting" method with different results for each material. The strength of the bond was studied immersing the films in PBS solutions for different time and the result was that titania films are the most stable in both methods. In fact it should be stressed that in silica films it was not simple to control the surface silanols that can form different species reacting in several ways. Comparing with silicon oxides, the transition metal oxides were preferred for their properties of higher reactivity toward the hydrolysis and condensation step, for the possibility to functionalize the surface in a homogeneous way and for their feature to crystallize when heated, forming an ordered network.

For materials composed of metal oxides the one pot method was less effective because the alkoxides in solution can react in different ways and the self assembly method can modify the formation of pores. Furthermore there were not applied high temperatures to remove the template because it was taken into account the thermal degradation of the organic groups, obtaining in those way only a partial porous material. As shown in figure 34 the post grafting method was more effective to provide more functional groups available on the pores surface, than in the oxide framework, essential for the next grafting step and, for this reason, it was chosen as the most appropriate method.

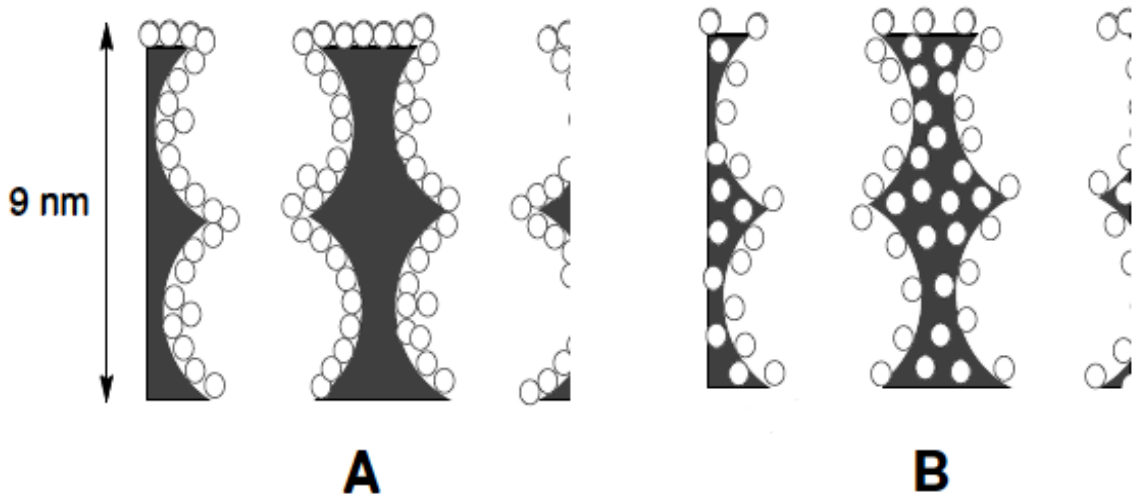

Fig. 34 Simplified model of pores in films synthesized by post-grafting (A) and by co-condensation (B) methods after thermal treatment. The empty circles represent the amine function. Reproduced by [161]

Titania thin films as synthesized were chosen as the best material because of their high hydrolytic stability in comparison with mesoporous silica samples and the other transition metal oxides which have a severe limit for applications in biosensors technologies due to their very low stability in water and physiological solutions.
Once chosen, it was carried out the detailed characterization of the material.

Characterization of mesoporous titania thin film

Mesoporous titania thin films were synthesized obtaining organized mesostructures after the removal of the templating micelles via thermal calcination; after firing, the films still presented high organization, excellent optical quality and hydrolytic stability.

The organization of the porous structures on films was studied by GISAXS (Fig. 35) showing the typical pattern of an ordered mesoporous titania film after thermal treatment at 350°C.

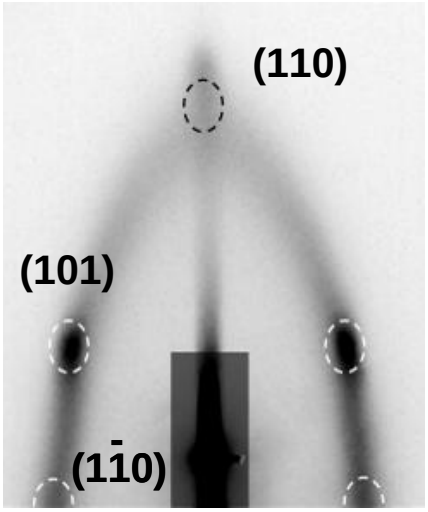

Fig. 35 GISAXS pattern of an ordered mesoporous titania film treated at 350°C.

The pattern appears composed of three peaks that can be indexed as (110), (101), and (1$\bar{1}$0) reflections of a body centred cubic ($Im\bar{3}m$ in the space group) structure with domains preferentially oriented with the [110] direction normal to the surface, and allowed by the circular permutation. The lower intensity of the (110) peak is due to the incident angle that reduces the quantity of domains having their in-plane diffraction in the Bragg conditions. As a consequence of the thermal treatment, the cubic unit cell is contracted in the out-of-plane [110] direction (normal to the substrate), which will be referred to as d_{110}, whereas the in-plane (parallel to the substrate) cell constant will be referred to as $d_{1\bar{1}0}$. Following this attribution, the lattice parameters were calculated to be $d_{1\bar{1}0}$ = 7.0 ± 0.1 nm and d_{110} = 3.1 ± 0.1 nm. The synthesis protocol has shown to be very robust and highly reproducible; in fact systematic GISAXS analysis were performed on different batches of samples (more than 20 samples have been analyzed by GISAXS) prepared in various times and it was always observed a cubic organization of the porous structure.

A direct observation of the pore arrangement was obtained by transmission electron microscopy to support the information provided by SAXS data. Bright field TEM images were collected for samples fired at 350°C. Figure 36 shows representative direct images of the deposited films showing some projections of a slightly distorted cubic structure.

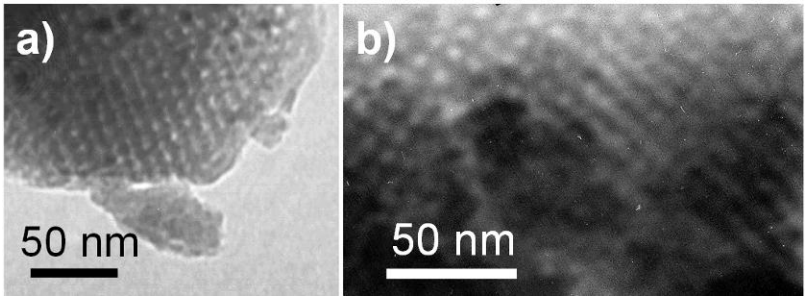

Fig. 36 Bright-field TEM images of mesoporous titania films treated at 350 °C

Even if an unambiguous identification would require cross-sectional TEM, according to the literature, we have attributed this images to the (110) projection. Under these conditions, in fact, the {110} face appears as a sequence of channels because the depth of field of the electron microscopy merges several spherical pore planes. Starting from this consideration, the distance among pores was calculated by a line profile analysis on representative TEM images. The centre-to-centre interpore distance was estimated to be 8.5 ± 1 nm.

Fig. 37 shows the FTIR absorption spectra in the 4000–2500 cm^{-1} interval of as deposited (black line) and calcined (blue line) mesostructured titania films; calcination was done in air at 350°C.

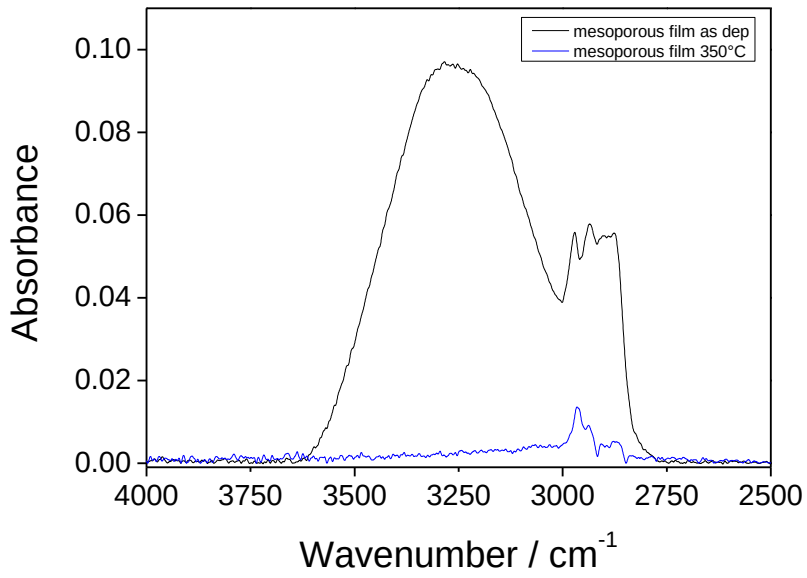

Fig. 37 FTIR absorption spectra in the 4000 – 2500 cm^{-1} interval of as deposited (black line) and calcined (blue line) mesostructured titania films; calcination was done in air at 350°C.

The spectra of the as deposited film show the presence of a wide intense band peaking around 3250 cm^{-1}, which was assigned to O-H stretching mode, due to Ti-OH species and absorbed water (overlapped band around 3200 cm^{-1}). The presence of the organic template in the as deposited film was indicated by the C-H stretching bands in the 3000-2800 cm^{-1} interval. After calcination of the film at 350°C the spectrum appears as a flat curve with only a very small signal around 2900 cm^{-1}; this indicates that the thermal treatment removed almost completely the surfactant and at the same time promoted the densification of the titania network, through condensation reactions of Ti-OH species.

The effect of the thermal treatment was also checked on the structure of the titania pore walls; in the as deposited films the titania was in the amorphous state and the analysis performed by glancing incidence XRD did not show the formation of titania crystalline phase even after calcination. However a more sensitive analysis by FT-FIR absorption spectroscopy was done on the 350°C calcined titania films. Fig. 38 shows the absorption spectra in the 600-100 cm^{-1} interval of a titania mesostructured film after calcination at 350°C.

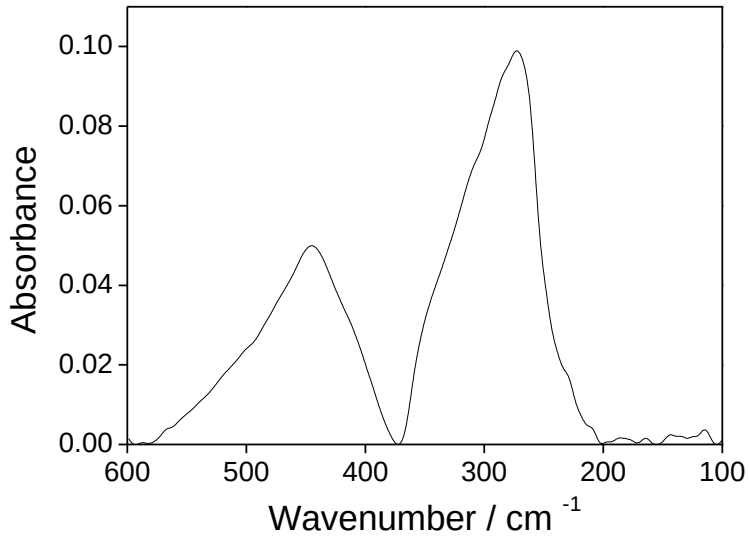

Fig. 38 FT-FIR absorption spectra in the 600-100 cm^{-1} interval of a titania mesostructured film after calcination at 350°C.

The spectrum shows two intense and well defined absorption bands peaking around 442 and 272 cm^{-1}. These bands were assigned to transverse optical (TO) E_u phonons in tetragonal anatase with two TiO_2 units per primitive cell. The spectrum indicates, therefore, that the titania is partially crystallized into the anatase phase, as small crystallites in an amorphous matrix; the dimension of the crystallites is likely very small because it is under the detection limit by X-ray diffraction.

Characterization of functionalized films with APTES

The calcined mesoporous titania films were modified with APTES in order to introduce the amino-function on the titania walls. 3-aminopropyltriethoxysilane (APTES) is a coupling agent that was commonly used for the modification of silica surfaces to promote protein adhesion, cell growth, to attach metal nanoparticles to silica substrates, for biological implants and in lab on chip applications. In our work the objective was to link to this agent peptides and antibodies. The reaction that occurs is a hydrolysis and condensation of silanes that drives the bonding of APTES to the substrate with the formation of siloxane bonds on the surface. In particular in titania materials the functionalization via APTES was realized by condensation of Ti-OH with Si-OH to form mixed Ti–O–Si bonds (Fig. 39).

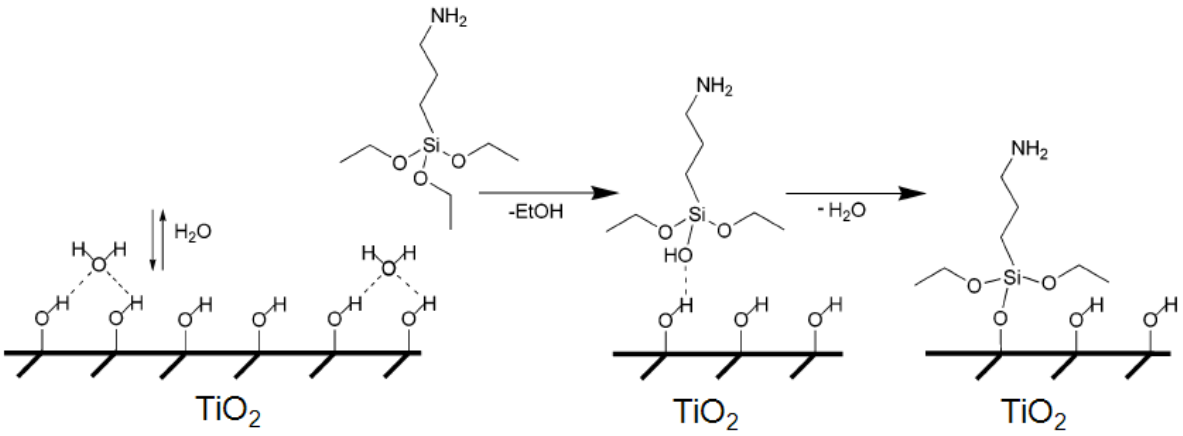

Fig. 39 APTES hydrolysis followed by condensation at hydrated titania surface. Reproduced by [162].

The initial hydrolysis step can occur either in solution or at the substrate surface depending on the amount of water present in the system. An overabundance of water will result in excessive polycondensation in the solvent phase (Fig. 40), while a deficiency of water will result in the formation of an incomplete monolayer. Solvent, concentration, reaction time, and reaction temperature are other parameters that affect the grafting kinetics.

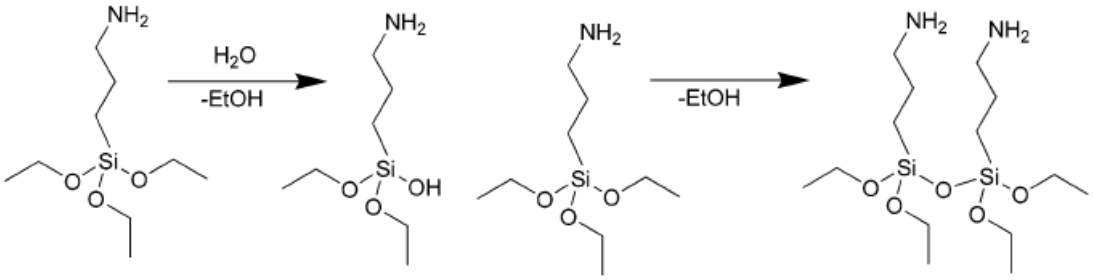

Fig. 40 APTES hydrolysis followed by condensation reaction in solution. Reproduced by [162]

In fact a control of all these parameters was of paramount importance to avoid the uncontrolled formation of multilayers.

In our research all these conditions were monitored and in particular the functionalization was tried with different methods, temperatures (25°C under stirring, at 80°C in a oven, at 80°C under reflux) and in different solvents (EtOH and toluene) but the best results, reported below, were found at room temperature and in toluene solution. In fact it was concluded that the toluene had the potential to extract water absorbed from the titania surface into the solution improving the silane deposition. Furthermore it was noted that at high temperature the kinetics of the APTES was accelerated, for an increased mobility of APTES in toluene that produced a quick reaction of silanization, forming thick layers and opacities; for this reason room temperature was preferred.

To monitor also the loading of APTES were synthesized and functionalized, as reference, dense films (non porous) (Fig. 41). As shown below the best functionalization was obtained with mesoporous thin films that allowed a major amino loading.

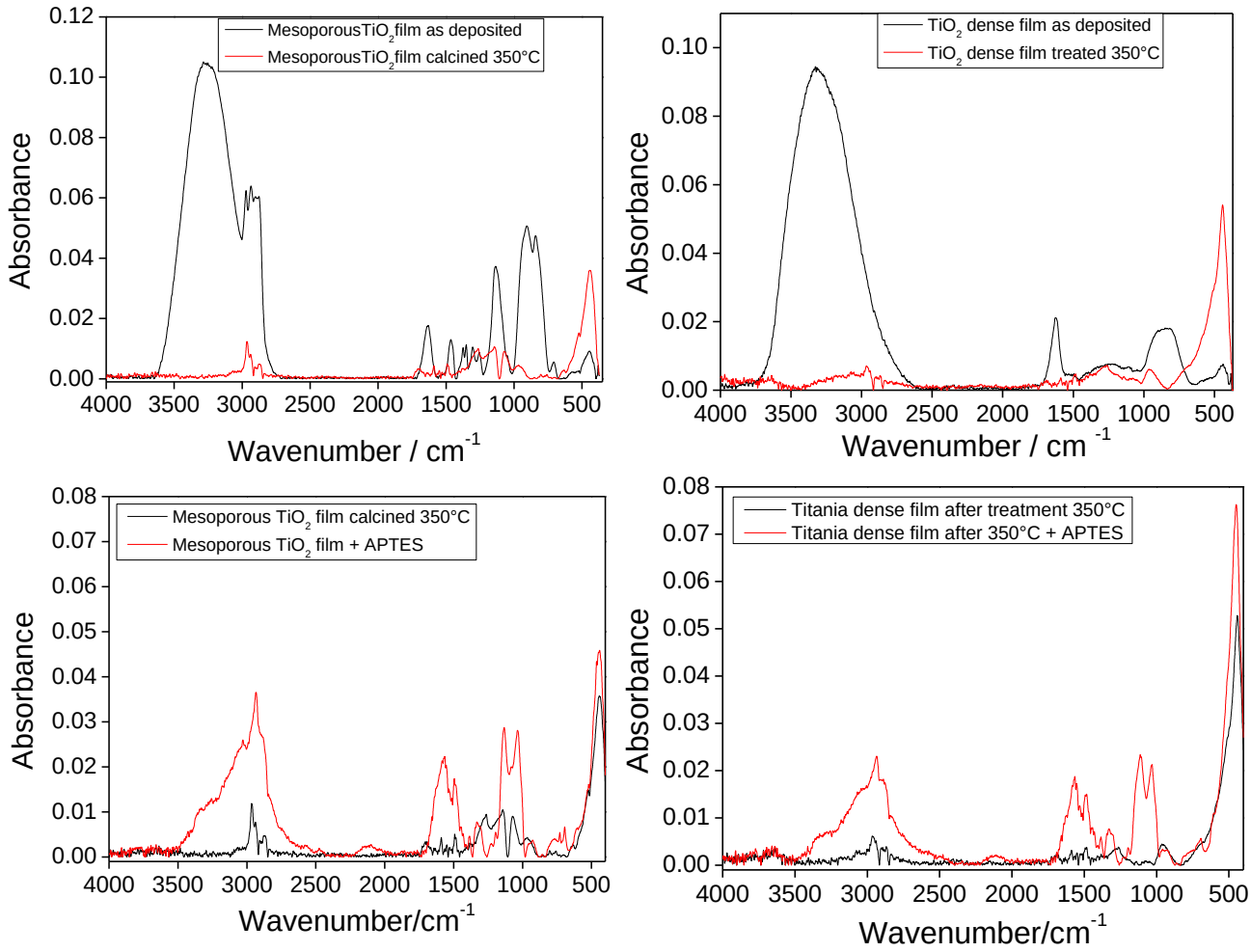

Fig. 41 FTIR spectra of (at the top) TiO_2 thin films before (black) and after (red) the thermal treatment at 350°C for mesoporous (left) and dense (right) films. Below the titania films were represented before (black) and after (red) the functionalization process with APTES for mesoporous (left) and dense (right) films.

It was also considered that an incomplete coverage of the films can be problematic and for this reason the functionalization to obtain a homogenous layer was monitored with FTIR (Fig.42) and AFM (Fig.43).

From FTIR measures was evident how with the time exposition to APTES there was an increase of the characteristic peaks until 24h of reaction.

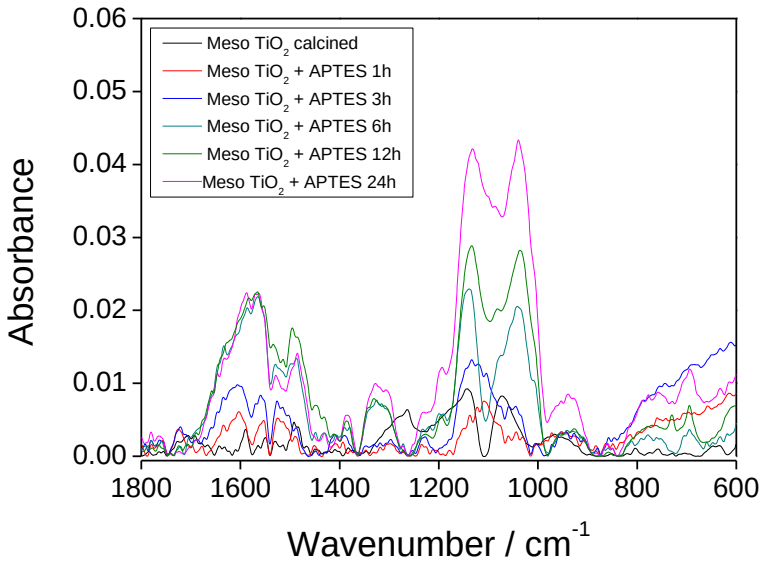

Fig. 42 FTIR spectra in the range 1800-600cm^{-1} of mesoporous titania calcined at 350°C and after the reaction in APTES solution for different time (1, 3, 6, 12, 24h).

In particular the best amino loading was reached after 24h of exposition. After this time, films left in solution for more than 24 h presented an opacity due to the formation of multilayers visible from AFM (Fig. 43 right). The presence of APTES with dimensions around 200 nm was noted in the top part of the figure, but increasing the time of exposition it could be noted the formation of aggregates and multilayers (Fig.44) until the dimension of 1µm and more.

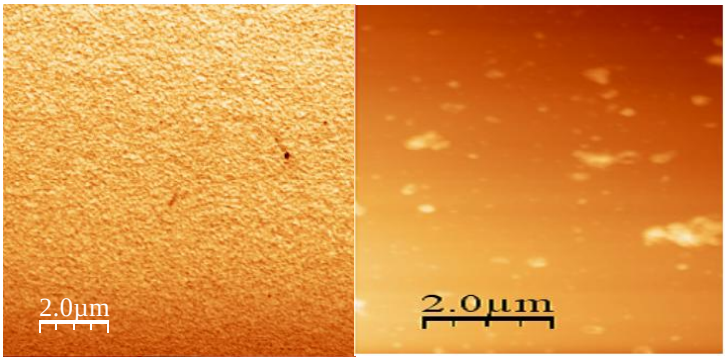

Fig. 43 AFM images of mesoporous titania thin films before (left) and after (right) the functionalization with APTES

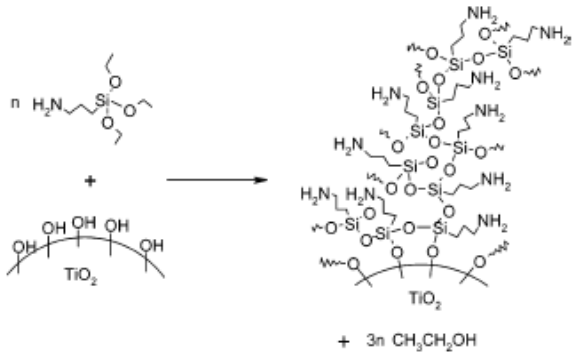

Fig. 44 Reproduction of the formation of APTES multilayer on titania surface

In this way the best conditions (solvent and time) for an efficient functionalization were found and, the final spectrum of the best functionalized mesoporous titania thin film was reported in fig. 45. It shows the FTIR absorption spectra of the film in the 1800-600 cm^{-1} range after calcination at 350°C (black line, a) and after functionalization with APTES (red line, b); the reference spectrum of APTES (liquid film) is represented by the blue curve c. The full spectra (right) were also reported.

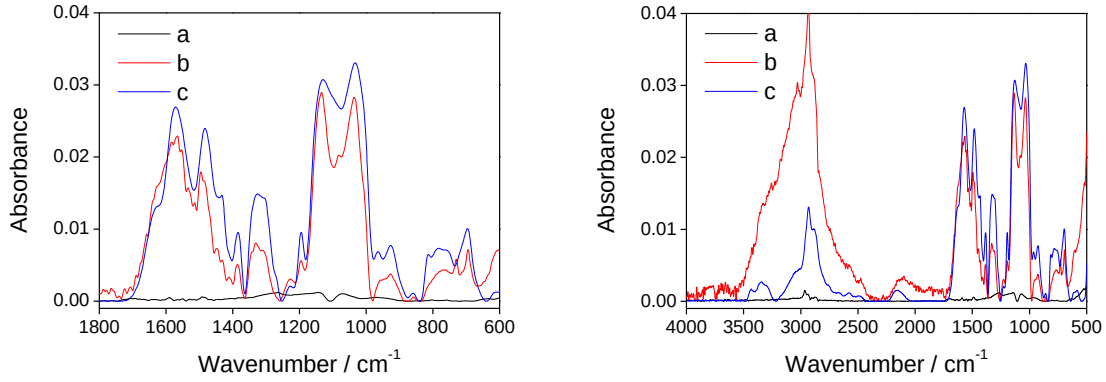

Fig. 45 FTIR absorption spectra of a mesoporous titania film in the 1800-600 cm^{-1} range, after firing at 350°C (black, a) and functionalization with APTES (red line, b). The reference spectrum of APTES is the blue line, c.

The spectrum of the functionalized titania film clearly shows the signature of APTES, which can be easily detected because the spectrum of calcined titania film has no absorption bands in the middle infrared range.

This material was then used as the host matrix for a further grafting step to bond specific peptides and antibodies.

Part 1 Detection of dioxins using mesoporous titania thin films and pentapentides

In this part of our work mesoporous titania thin films were used for the incorporation of selective pentapeptides for the detection of dioxins to create a biosensor. These materials were interesting for the incorporation of biomolecules because a good interaction between peptides and mesopores was possible thanks to an interaction of the amino groups of the functionalized titania with the different parts of the peptides. But the main advantage was to use these materials because of their large surface area that leads to immobilize a bigger amount of peptides into their internal channels and on their surfaces, in comparison with non porous materials. This linking was effective if the dimension of the peptides or of the linking part was minor than the pore diameter. The linking of peptides with the support was studied with FTIR, spectroscopic ellipsometry, AFM and fluorescence spectroscopy. In particular different routes were tried for peptide immobilization, by physical and chemical methods (using ligands as APTES and GA).

The first immobilization method followed different steps: peptide diffusion into the pores and on the surface of materials, absorption on the surface, structural rearrangement. But to have a stronger linking and avoid the leaching process it was necessary to use the covalent method for the interaction of peptides with the amino terminal groups (APTES) or aldheyde groups (GA) of the linking agents. All these methods of immobilization were tried and the best one was chosen to obtain stable chips with the immobilized peptides.

Peptide Synthesis

The purpose of this part of work was to develop a new detection method using a short peptide instead of an immunoantibody (method actually applied as screening). In fact the use of antibodies is not suitable because of their easy denaturation in organic solvents that are necessary to dissolve and extract dioxins from food samples, while using a lower concentration of organic solvents leads to an incomplete extraction of dioxins with a wrong detection of the quantity of dioxin present in a sample. For this reason oligopeptides were synthesized instead of antibodies to overcome the problem of denaturation in organic solvents. In this way, in fact, quality control procedures that are easier than for natural biomolecules, and a regeneration and reuse of the device, are possible. From recent literature [157, 158] three peptides that have a high affinity for the detection of dioxins were discovered. In particular they have the major affinity for TCDD. Their design was screened by a combinatorial library that led to the choice of three pentapeptides that have four amminoacids in

common (Gln-Asp-Leu-Phe) and differ for the N terminal amino acid (Ile, Val or Phg). It seems that the central aminoacids (Gln-Asp-Leu) are essential to recognize the dioxins but for the correct linking at least other two amminoacids are necessary.

This design was based for the similarity of sequence that is present in the binding pocket of aryl hydrocarbon receptor (the cytosolic cellular receptor responsible of the linking of dioxins) and of specific CDR domains (complementarity determining region) present in monoclonal anti-dioxin antibody. The sequence (Gln-Asp-Leu) was thought to contribute to the binding to dioxins thanks to their acidic (Asp) and amidic (Gln) residues and, in particular, the Gln could form H bonds between side chain and ligand, or side chain and main chain of peptides. Furthermore it was thought that the amine of the side chain (Gln) can form an H-bond with the chlorine atom or with the oxygen of dioxins.

Following these studies three pentapentides represented in Fig. 46 were synthesized, that, as shown in literature, have an high affinity to dioxins and in particular for TCDD.

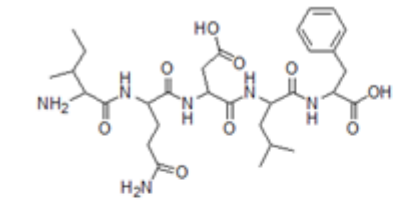

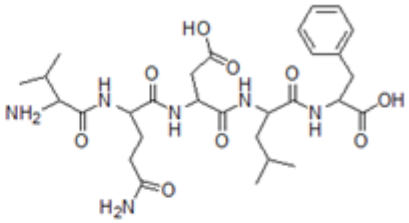

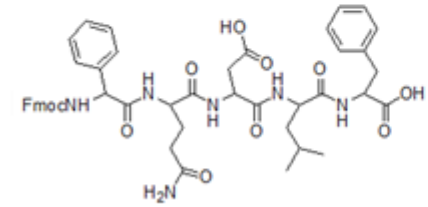

Fig. 46 Molecular structures of the synthesized pentapeptides.

To assemble the targeted three component collection of pentapeptides 1-3 it was planned to realize linear peptides. The synthesis was performed on a CEM Liberty microwave peptide synthesiser on a 0.1 mmol scale. Three pentapeptides of general formula H-X-Gln-Asp-Leu-Phe-OH were synthesized on solid phase, utilizing a conventional polystyrene-based PAL-PEG resin (Scheme 2).

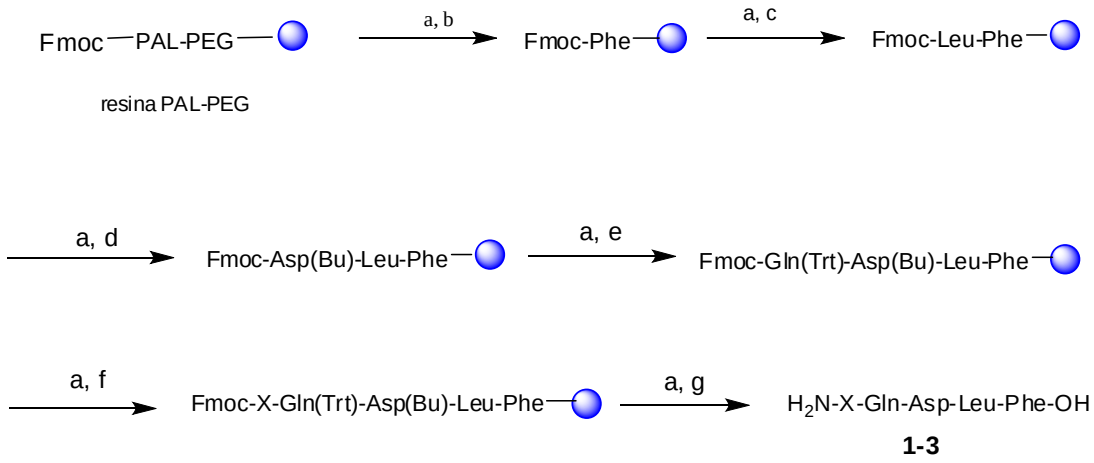

a Reagents:(a) piperidine/DMF 20%; (b) Fmoc-Phe-OH, TBTU/HOBt, DIEA, NMP; (c) Fmoc-Leu-OH, TBTU/HOBt, DIEA, NMP; (d) Fmoc-Asp(But)-OH, TBTU/HOBt, DIEA, NMP; (e) Fmoc-Gln(Trt)-OH, TBTU/HOBt, DIEA, NMP; (f) Fmoc-X-OH (X=Ile (**1**); Val (**2**); Phg (**3**)), TBTU/HOBt, DIEA, NMP; (g) TFA, TIS/H_2O (95:2:5:2.5) (53-76%, five steps).

Scheme 2 Synthesis of Pentapeptides 1-3

Although this type of linker is acid labile, its stability towards bases makes it ideal for the various coupling base promoters, as well as for the resident Gln and Asp protecting groups using the Fmoc strategy. After deprotection of the resin (20% piperidine in DMF), the condensation of the Fmoc-Phe-OH residue was attained using the TBTU-HOBt system in the presence of DIPEA. Next, the second aminogroup within the resin-bound amino acid Fmoc-Phe-Pal-Peg was liberated, as described in the experimental section, and the Fmoc-Leu-OH residue, Fmoc-Asp(tBu)-OH and Fmoc-Gln(Trt)-OH were then connected and the amino group liberated to afford a resin-bound tetrapeptide, which was connected with an X platform chosen among the three amino acids of this study (Fig. 47). The as synthesized pentapeptides finally had a common part (Gln-Asp-Leu-Phe) and a different amino acid X that gives them different properties.

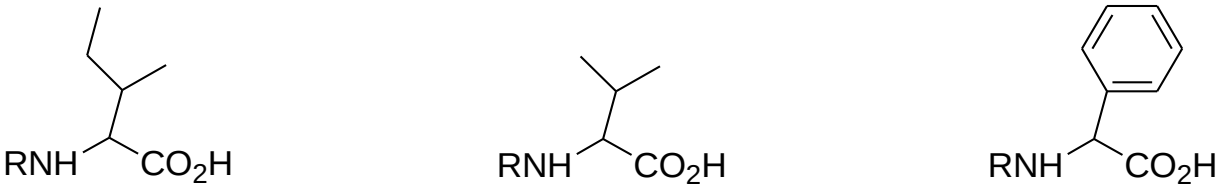

Fig. 47 Amino Acid Building Blocks X

The cleavage of the targeted products from the resin and the side-chain deprotection was carried out under acidic conditions in the presence of scavengers, with the reagent system TFA, TIS, H_2O. The crude linear peptides were thus obtained in yields ranging from 53% to 76% for the entire solid-phase sequence. Only the resulting compound 1 was first purified by preparative reversed-phase HPLC and finally his purity was checked by RP-HPLC analyses and judged to be 99.8%. All linear pentapeptides were characterized by MALDI-TOF mass spectrometry.

Characterization of peptide 1 H-Ile-Gln-Asp-Leu-Phe-OH

HPLC and MS analysis (Fig. 48 and 49)

Resin Loading: 0.21 mmol/g. Overall yield: 76.3%. A white solid. HPLC purity: 99.8% ; HPLC tR= 13.9 min; $[M+H]^+$= 635.55 $[M+Na]^+$=657.40 $[M+K]^+$=673.28.

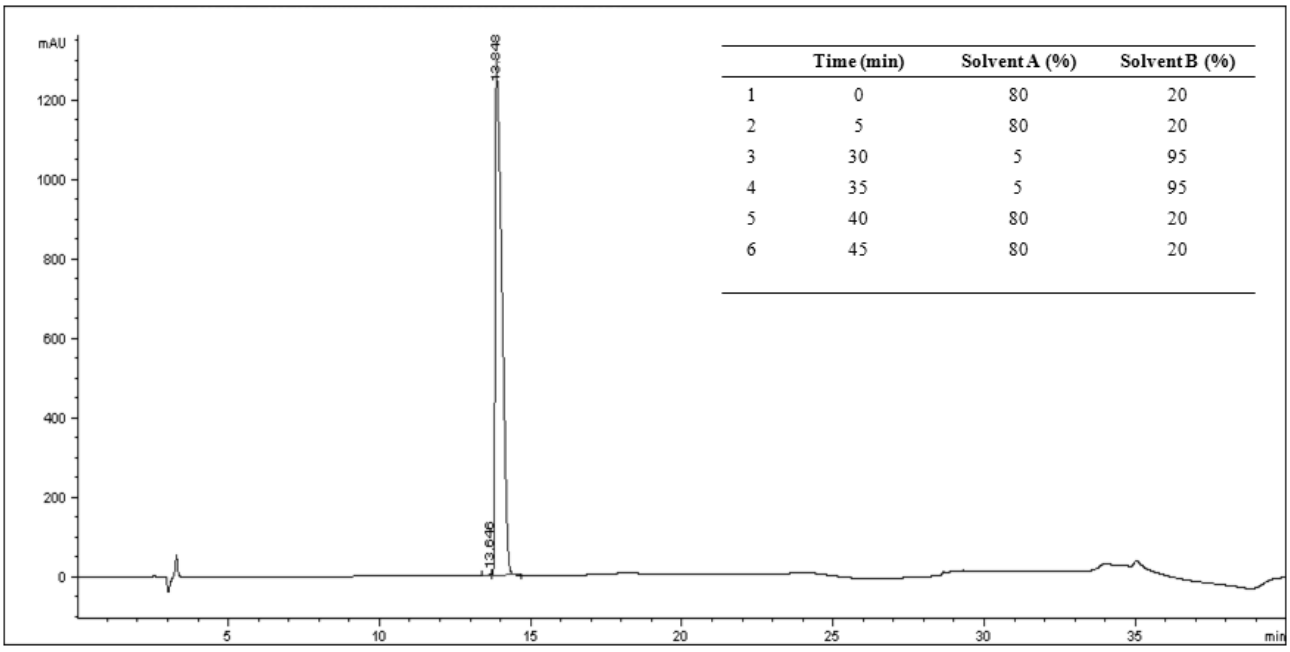

	Time (min)	Solvent A (%)	Solvent B (%)
1	0	80	20
2	5	80	20
3	30	5	95
4	35	5	95
5	40	80	20
6	45	80	20

Fig. 48 Peptide purity (HPLC chromatogram, UV absorbance at 220 nm) of Ile-Gln-Asp-Leu-Phe-OH.

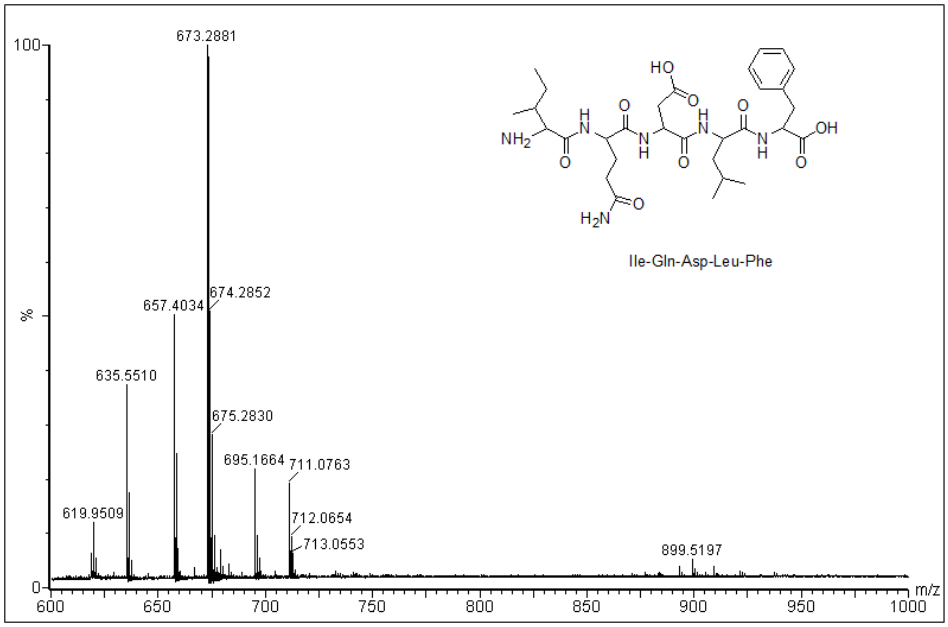

Fig. 49 Identification of Ile-Gln-Asp-Leu-Phe via MALDI-TOF MS.

The peptide 1 was synthesized (visible from the mass characteristic peaks) and purified, obtaining a purity of 99.8%.

Characterization of peptide 2 H-Val-Gln-Asp-Leu-Phe-OH

HPLC and MS analysis (Fig. 50, 51)

Resin Loading:0.21 mmol/g. Overall yield: 70.6%. A white solid. HPLC purity: 51,8% ; HPLC tR= 36.8 min; HRMS: $[M+H]^+$= 621.58 $[M+Na]^+$= 643.43 $[M+K]^+$= 659.32.

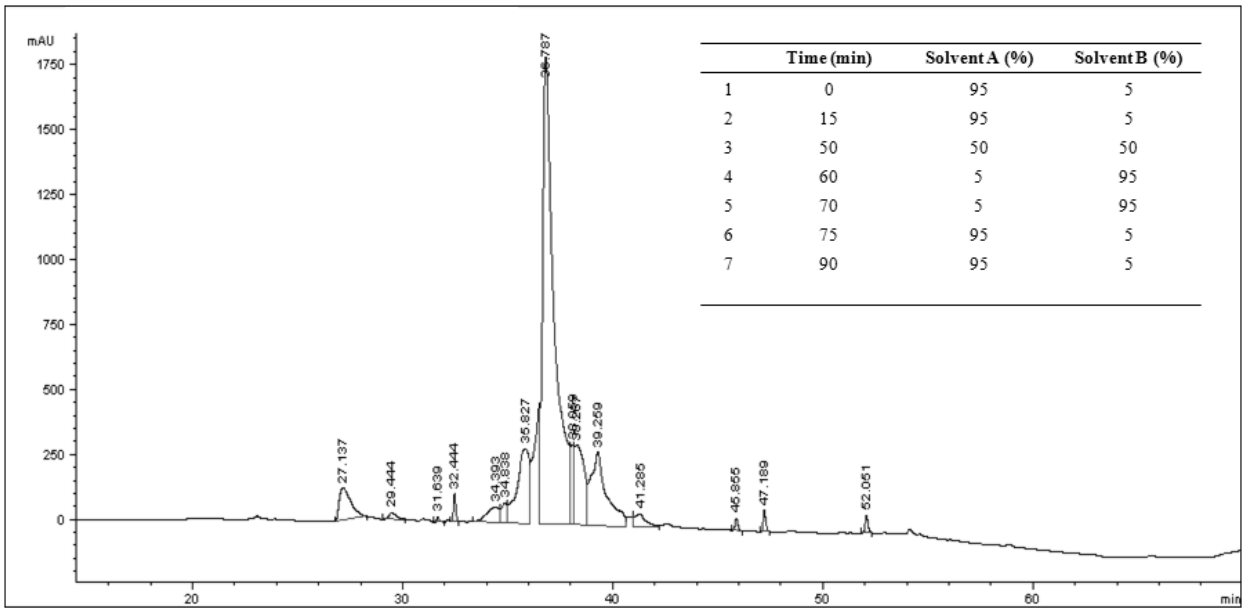

	Time (min)	Solvent A (%)	Solvent B (%)
1	0	95	5
2	15	95	5
3	50	50	50
4	60	5	95
5	70	5	95
6	75	95	5
7	90	95	5

Fig. 50 Peptide purity (HPLC chromatogram, UV absorbance at 220 nm) of Val-Gln-Asp-Leu-Phe-OH.

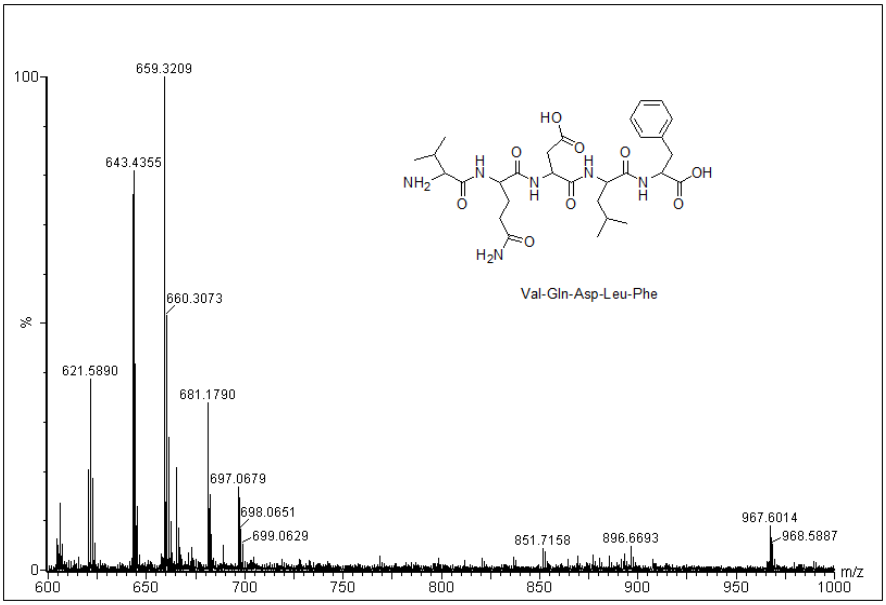

Fig. 51 Identification of Val-Gln-Asp-Leu-Phe and deletion sequences via MALDI-TOF MS.

The peptide 2 was synthesized (visible from the mass characteristic peaks) and purified, obtaining a purity of 70.6%.

Characterization of peptide 3 Fmoc-Phg-Gln-Asp-Leu-Phe-OH

HPLC and MS analysis (Fig. 52, 53).

Resin Loading:0.21 mmol/g. Overall yield: 81.8%. A white solid. HPLC purity: 53.5% ; HPLC tR= 56.4 min; HRMS: $[M+H]^+$= 898.58, $[M+K]^+$=936.48.

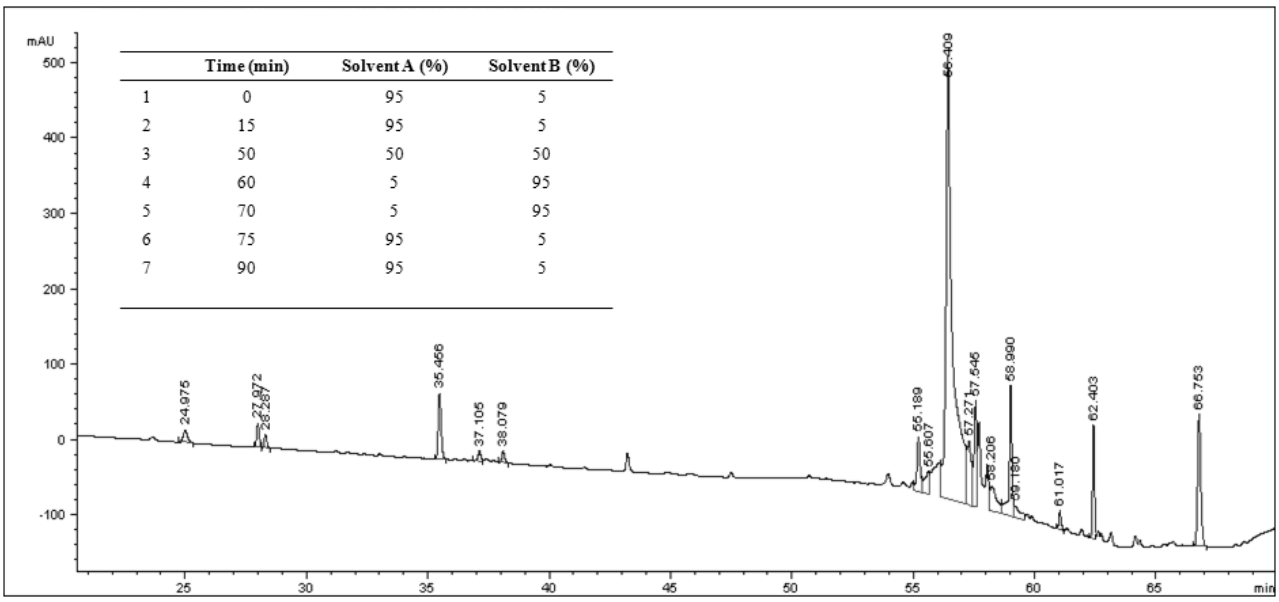

	Time (min)	Solvent A (%)	Solvent B (%)
1	0	95	5
2	15	95	5
3	50	50	50
4	60	5	95
5	70	5	95
6	75	95	5
7	90	95	5

Fig. 52 Peptide purity (HPLC chromatogram, UV absorbance at 220 nm) of FmocPhg-Gln-Asp-Leu-Phe-OH.

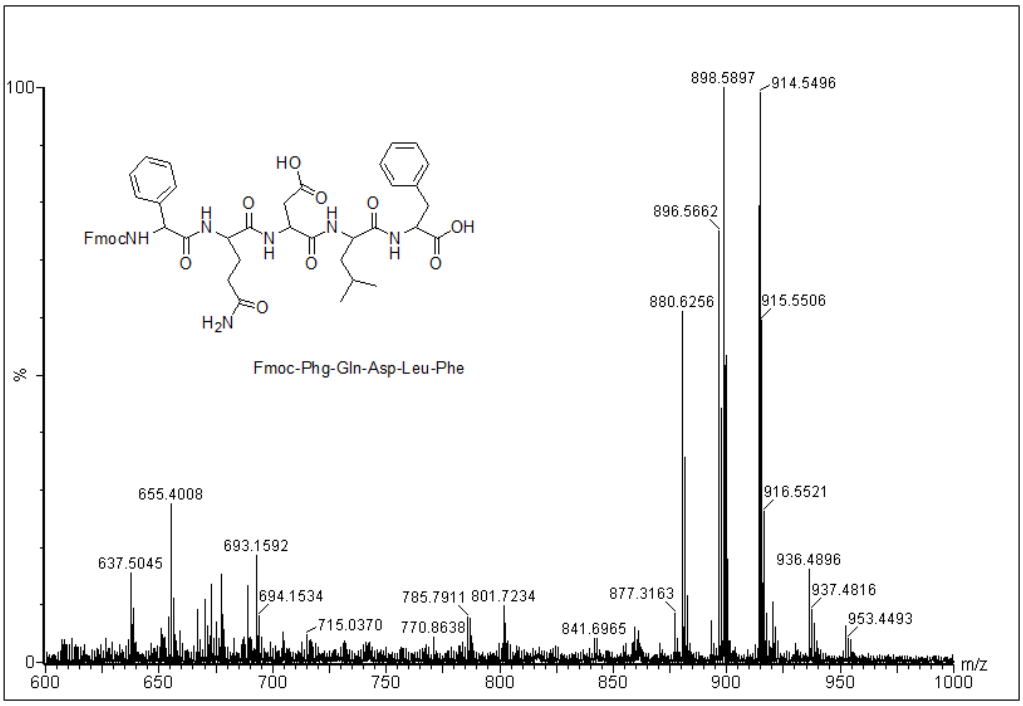

Fig. 53 Identification of FmocPhg-Gln-Asp-Leu-Phe via MALDI-TOF MS.

The peptide 3 was synthesized (visible from the mass characteristic peaks) and purified, obtaining a purity of 81.8%.

Peptide immobilization

Different ways to immobilize the peptides were tried, as previously described, on titania thin films. First of all it was tried to adsorb the peptides in PBS solutions directly on the films with a physical method but without positive results.

For the chemical absorption a similar method was tried using for the peptide synthesis DIPEA and HATU but even this time without positive results. Then it was tried to link a cross linker, glutharaldehyde (GA), to the TiO_2-APTES mesoporous films, that is commonly used as bifunctional cross-linking reagent, to covalently couple proteins with various surfaces. In particular it was tried to link, with the formation of imines, the titania- APTES film to GA and the terminal free aldehydic group of GA to the amino terminal group of peptide Fig. 54.

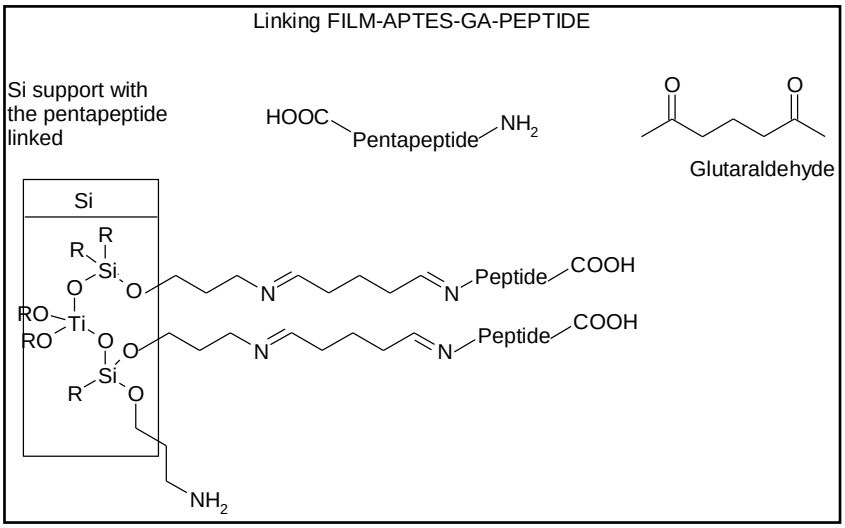

Fig. 54 Linking film-APTES-GA-Peptide

Different reactions, concentration of GA and different pH were tried. The GA was linked to TiO_2-APTES films but a good linking between GA-Peptides did not occur (Fig.55).

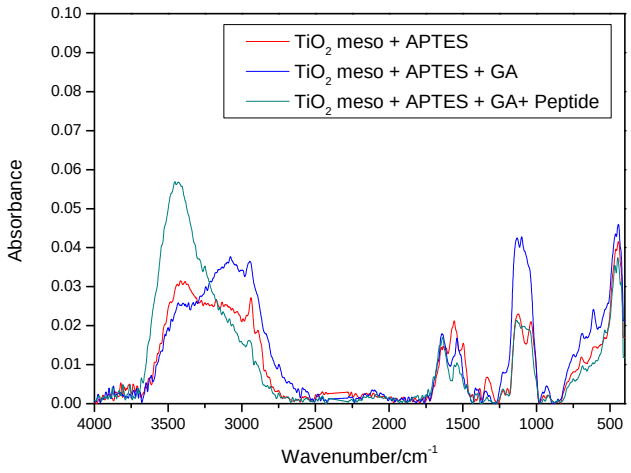

Fig.55 FTIR spectrum that shows the functionalization of titania films with APTES (red spectrum) and GA (blue spectrum) followed by the linking of peptide (light blue spectrum).

The best results were obtained immobilizing the peptides with a more simple method also used to attach proteins to surfaces without multiple steps. Different times (1-60h) solvents (PBS, toluene, ethanol) and methods of linking (for the reaction of the group APTES-Peptide with TiO_2 films or TiO_2-APTES films and after linking with Peptides) were tried. The best linking of peptides was obtained immersing the peptides dissolved in toluene for 24h, under shaking at room temperature.

The binding was followed by different washing steps with toluene and drying in air. It was thought that APTES reacted with the hydroxyl groups of the peptide supporting the formation of a monolayer of peptide under controlled conditions.

The best result was obtained with the peptide purified H-Ile-Gln-Asp-Leu-Phe-COOH and with the peptide H-Val-Gln-Asp-Leu-Phe-COOH (Fig. 56); while with the peptide Fmoc-Phg-Gln-Asp-Leu-Phe-COOH the solubilization was inefficient and the linking of the peptide to the substrate was limited (perhaps for the great molecular weight of the protector group FMOC it was impossible for this peptide to penetrate into the mesopores). Because of the small amount of the Peptide 1 available, the major part of the experiments was carried out with the peptide 2.

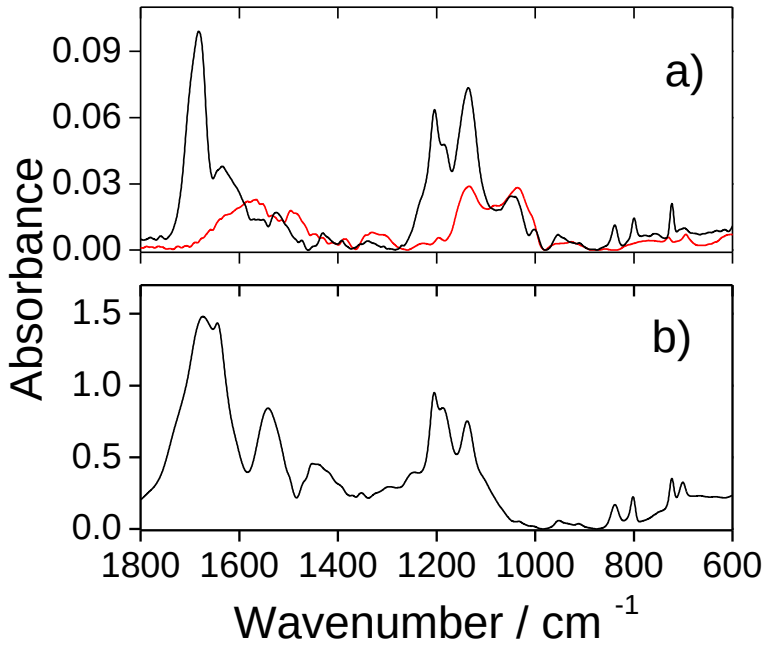

Fig. 56 FTIR absorption spectra of a mesoporous titania film: a) after calcination at 350°C and functionalization by APTES (red line) and after binding with the peptide (black line). The reference spectrum of the H-Val-Gln-Asp-Leu-Phe-COOH peptide is reported in the graph b).

The FTIR spectra show that the absorption of the peptide at the end of the grafting process is very effective; the signature of the peptide can be clearly observed in the titania-APTES mesoporous films even after a careful washing of the sample.

To monitor if there was an advantage to use mesoporous films the same experiment was carried out also on titania dense films as reported in fig. 57.

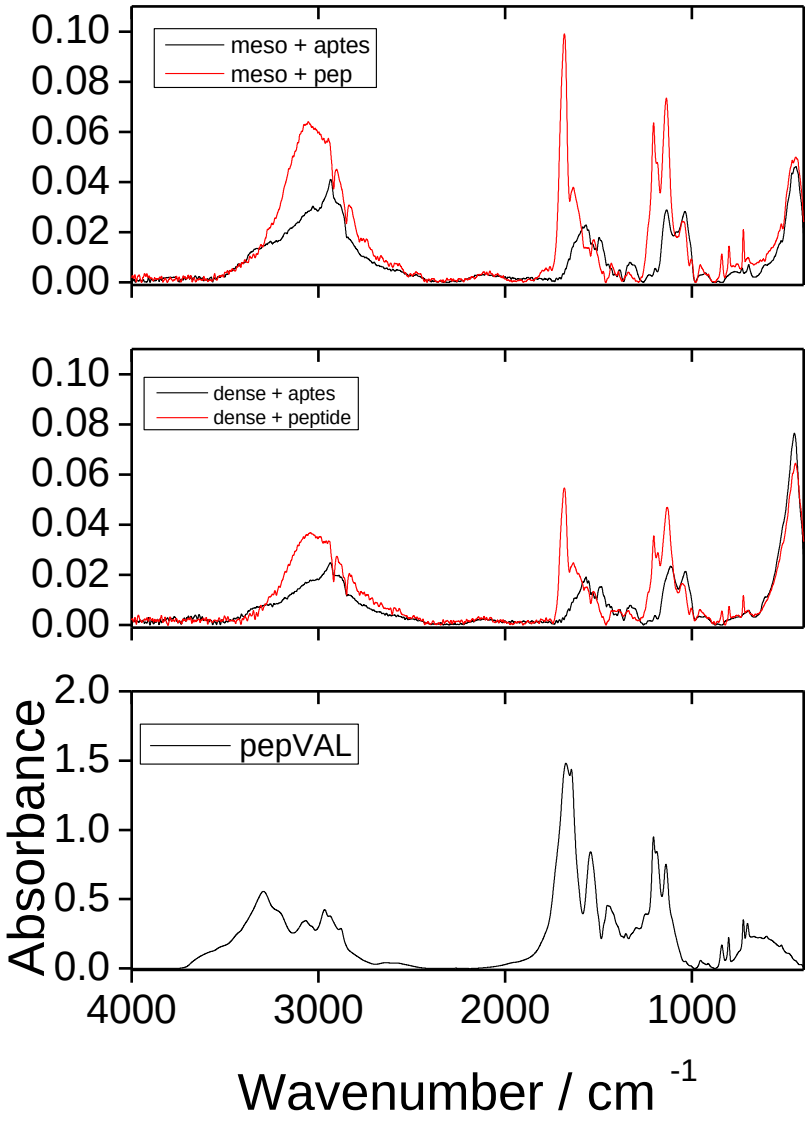

Fig. 57 FTIR absorption spectra, at the top of a mesoporous titania film after calcination at 350°C and functionalization by APTES (black line) and after binding with the peptide (red line) . At the centre titania dense film functionalized with APTES (black line) and after binding with the peptide (red line). The reference spectrum of the H-Val-Gln-Asp-Leu-Phe-COOH peptide is reported in the graph at the bottom.

This experiment proofs that films synthesized in the same way and with the same material had different filling properties depending on their porosity. In fact it was clear that mesoporous materials with incorporated peptides had much more intense peaks than non porous (dense) materials. In particular the intensity of the peaks due to the peptide was almost double. The presence of immobilized peptides was evident also from AFM measures (Fig. 58) in which was

noted the immobilization of peptides with dimensions around 300-400 nm but also bigger aggregates with dimension around 1µm. For this reason in the following measures of fluorescence a careful dissolution of the peptide was necessary to obtain homogeneous film coverage.

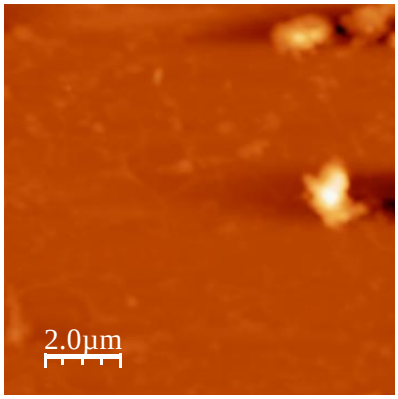

Fig. 58 AFM image of a TiO_2 mesoporous thin film functionalized with APTES and with the immobilized Peptide 2.

The effect of the film functionalization was also followed by spectroscopic ellipsometry (Tab 1). Data were obtained assuming a fitting model based on the assumption of transparent films on silicon (Cauchy dispersion relation). After calcination at 350 °C in air the titania films show an average thickness of 180 ± 5 nm with a refractive index of 1.72 measured at λ = 632.8 nm. After functionalization with APTES the film thickness increases to a value of around 270 ± 37 nm with significant changes of the refractive index to a value of 1.90. Finally, after peptide binding, the films reach a thickness of around 350 ± 30 nm with an average refractive index of 1.79. This value, which is lower than that measured on the amino-functionalized films, can be attributed to the formation of over layers with a low refractive index made of peptides bonded to mesoporous film surface.

Sample	Thickness / nm	Refractive index
TiO_2	180	1.72
TiO_2 +APTES	270	1.90
TiO_2 +APTES+ Peptide	350	1.79

Tab. 1 Ellipsometric measures of TiO_2 mesoporous films, of TiO_2 functionalized with APTES and of TiO_2 with APTES and Peptide 2.

Detection of TCDD

Fluorescence spectroscopy was used to get a better insight of the functionalization process and of dioxins detection. This approach was based on using a fluorescent marker, such as fluorescein isothiocyanate (FITC), which after reacting with amines shows an intense fluorescent emission revealing the presence of the peptides. Figure 59 shows the emission fluorescence spectra (λ_{ex} = 490 nm) of solutions of toluene (black line), toluene - H-Val-Gln-Asp-Leu-Phe-COOH peptide (red line), toluene – FITC (blue line), toluene – FITC - Val-Gln-Asp-Leu-Phe-COOH peptide (green line). The fluorescence of toluene and H-Val-Gln-Asp-Leu-Phe-COOH peptide in toluene is zero with the exception of a small band of very weak intensity peaking around 570 nm; the two spectra are completely overlapped which reveals that H-Val-Gln-Asp-Leu-Phe-COOH peptide in toluene is not fluorescent. The fluorescence spectrum of FITC in toluene shows a wide band of low intensity around 530 nm; after binding with the peptide the intensity of this band is highly enhanced, an intense emission band peaking around 530 is, in fact, detected (green line).

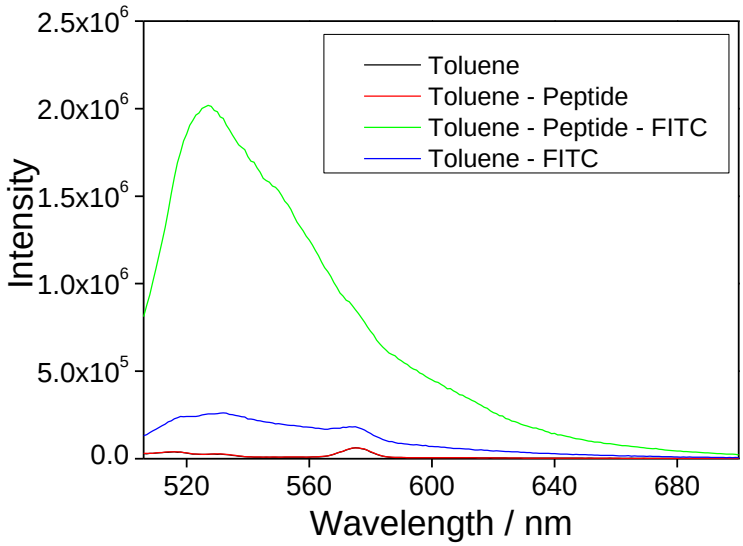

Fig. 59 Fluorescence emission spectra (λ_{ex}= 490 nm) of toluene (black line), toluene - H-Val-Gln-Asp-Leu-Phe-COOH peptide (red line), toluene – FITC (blue line), toluene –FITC - Val-Gln-Asp-Leu-Phe-COOH peptide (green line).

The increased fluorescence in the Toluene-FITC-Peptide solution was attributed to the reaction of fluorescein isotiocyanate with the peptide because the other solutions were not fluorescent. Fluorescein isothiocyanate is commonly used as a fluorescent marker attached to proteins for the reaction of isothiocyanate with the primary and terminal amines in proteins.

In our work, therefore, FITC was used for post-functionalization of the titania mesoporous film and as a marker of the process. On the other hand it was also tried to link the fluorescent marker FITC directly to the peptide that had been previously immobilized on the film but this process was not effective and fluorescence emission was not observed.

For this reason it was tried another route and in particular to link first the peptide with the FITC and, afterwards, trying the immobilization process on the film functionalized with APTES. Mesoporous titania with APTES was immersed in the FITC-peptide solution and the behaviour was studied (Fig. 60).

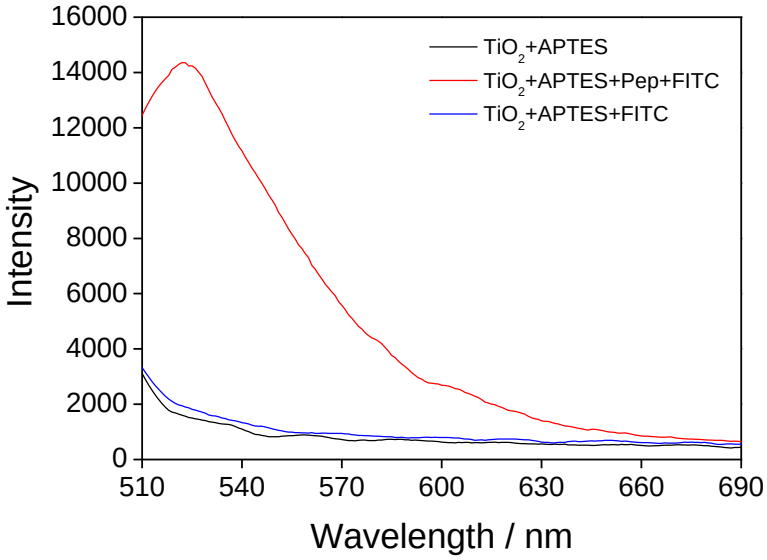

Fig. 60 Fluorescence emission spectra (λ_{ex} = 490 nm) of the mesoporous APTES - titania film after immersion in a solution of toluene–FITC (black line), and toluene–FITC-Val-Gln-Asp-Leu-Phe-COOH peptide (red line). The spectrum of APTES - titania films before immersion (blue line) is also reported as the reference.

After immersion of the films in the different solutions the samples were analyzed by fluorescence spectroscopy; the titania-APTES films immersed in the FITC-peptide solution showed a strong fluorescence with an intense band peaking around 530 nm (red curve), while the samples immersed in the toluene FITC solution did not show any emission band (blue curve) and their spectrum was very similar to that obtained for titania-APTES mesoporous films before immersion (black curve). From the spectra of Fig. 60 it is clear that the APTES amino groups are not effective to bind FITC, while a chemical bond between functionalized film surface and fluorescent dye is only obtained via chemical reaction with the peptide. As a matter of fact, only the samples formed by TiO_2-APTES-Peptide-FITC show a strong increase of the emission properties.

The FTIR and fluorescence data well support, therefore, the successful binding of the peptide to the titania mesoporous films. This process is robust and the samples even after washing in different solvents still show evidence of the presence of the peptide that is not affected by the washing cycle.

The device as created was tested measuring the fluorescence of the titania chip with FITC and Peptide before the linking with TCDD and after the linking of different concentration of TCDD on the film surface. Several trials were carried out on different samples. As reported in Fig.61 it was noted an improvement of the fluorescence emission with the increased concentration of TCDD. A difference between the spectrum without and with TCDD can be distinguishable until a TCDD concentration of 10^{-12}M.

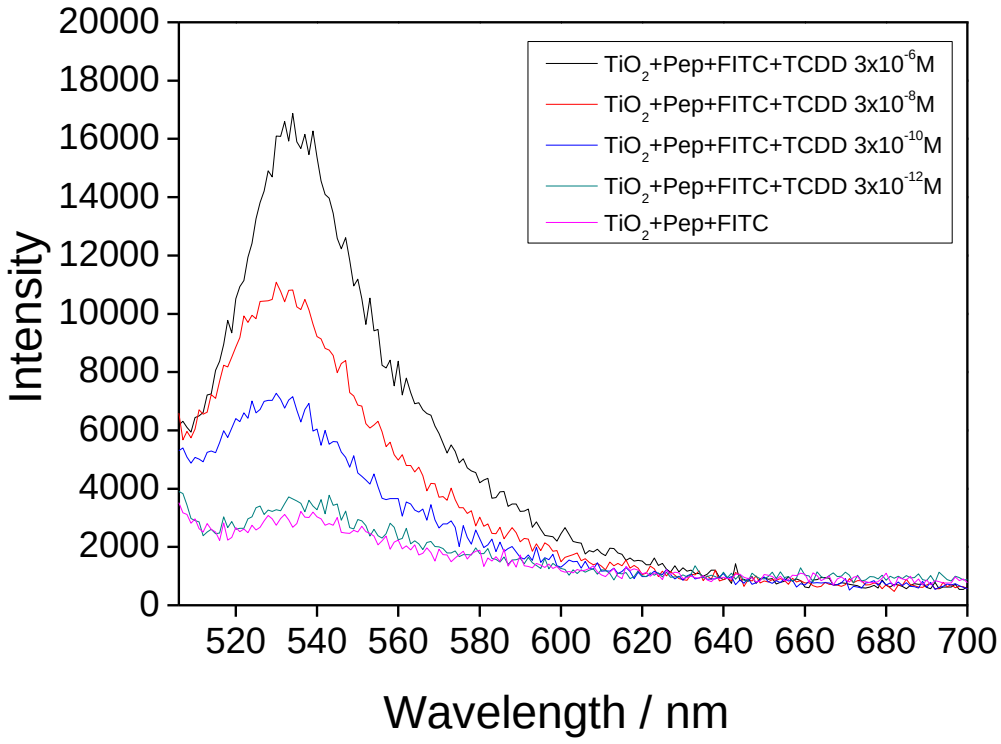

Fig. 61 Fluorescence emission spectra collected at a wavelength of 506-700nm on titania films with peptide and FITC (spectrum pink at the bottom) and after the linking of TCDD to the chip at different concentration increasing from the bottom to the top.

Results

Three pentapeptides that were specific for dioxins detection and in particular for TCDD were synthesized and characterized. The best method to link the peptides to the substrate composed of mesoporous titania film functionalized with APTES was obtained and the peptide with the best binding capacity (the peptide with the Val terminal amino acid) was chosen. A good linking between titania-APTES-peptide was obtained and was demonstrated as this linking was more effective for mesoporous films than for dense films for the major incorporation capacity of porous materials. All these properties were analyzed with FTIR, AFM, spectroscopic ellipsometry and fluorescence. Finally it was demonstrated that the chip was sensitive to the presence of dioxins. In particular the TCDD was tested and it was discovered that after the linking between peptide-TCDD on the film surface there was an increase in the fluorescence spectra proportional to the concentration of dioxins. A limit of detection was obtained at pM level. It was a good result compared to the other methods used so far. In this way it was possible to construct a chip with properties like simplicity, low cost, and sensitivity; furthermore it requests very short time for analysis and it is selective for the presence of peptides. This technique in fact could be used for simple and extensive pre-screening of samples preceding an accurate analysis using HRGC/MS of contaminated samples, reducing in this way time and costs required for analysis.

Part 2 Detection of E.coli using mesoporous titania thin films and antibodies

In the second part of the research work a biosensor for the detection of the pathogen E.coli was developed using FTIR. FTIR spectroscopy was used to provide fingerprints of pathogens eventually present in solution. In fact pathogens differ each other for various functional groups and, their MIR spectra, can be used for the identification and structural characterization of different pathogens but also of different subspecies. The MIR spectra were additive and sensitive and allowed the quantification of the pathogen of interest, transforming the traditional devices to biosensing systems with high sensitivity. In particular mesoporous titania thin films synthesized with the sol-gel method, previously described, were used to encapsulate biomolecules (antibodies and pathogens). This was possible with a high control of the gelation process for the synthesis of titania films and subsequent thermal treatments to avoid the denaturation of biomolecules in environments that have a high alcohol concentration and extreme pH values. For this reason great attention was given to the thermal treatments of mesoporous titania thin films to remove completely EtOH and HCl. Titania was used as substrate for the features described in the synthesis section but also because it has a good biocompatibility and can interact with biological molecules thanks to the formation of coordination linking between titania films and amino or carboxyl groups of the antibodies or of the bacteria. In fact the linking of bacteria was studied directly on titania films, on titania functionalized with APTES and in titania films functionalized with APTES and GA with the antibodies and the best method and the limit of detection of this technique was chosen.

Construction of the devices

Detection of E.coli with TiO_2-APTES-GA-anti E.coli O157:H7 Ab

The first method used provided the detection of E.coli with the immobilization of the antibody on titania films functionalized with APTES and GA as reported in figure 62.

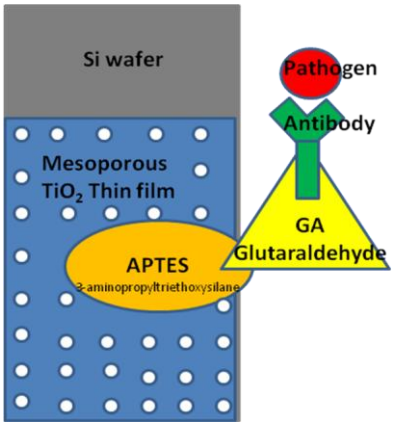

Fig. 62 Design of the biosensor composed of titania mesoporous thin films deposited on a Si wafer and functionalized with APTES, GA, Ab for the final linking of the pathogen.

In the first step titania thin film were functionalized with APTES.

In fig. 63 can be noted the spectra of the films before and after the functionalization process and the corresponding peaks due to APTES: N-H stretching at 3300 cm^{-1}, N-CH_2 stretching around 2800 cm^{-1}, NH_2 scissoring and N-H bending at 1615 cm^{-1}, aliphatic C-N stretching at 1020-1220 cm^{-1}, NH_2 wagging and twisting at 850-750 cm^{-1} and N-H wagging at 715 cm^{-1}.

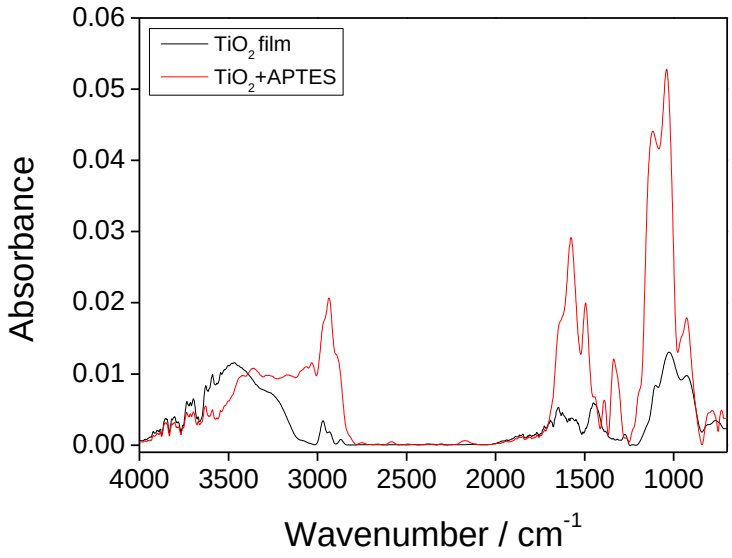

Fig.63 FTIR spectra of mesoporous titania thin films (black) and of the same film after functionalization with APTES (red).

The second step was based on the reaction between APTES and GA that was used to crosslink the APTES with the antibodies thanks to the formation of imide bonds (Fig. 64).

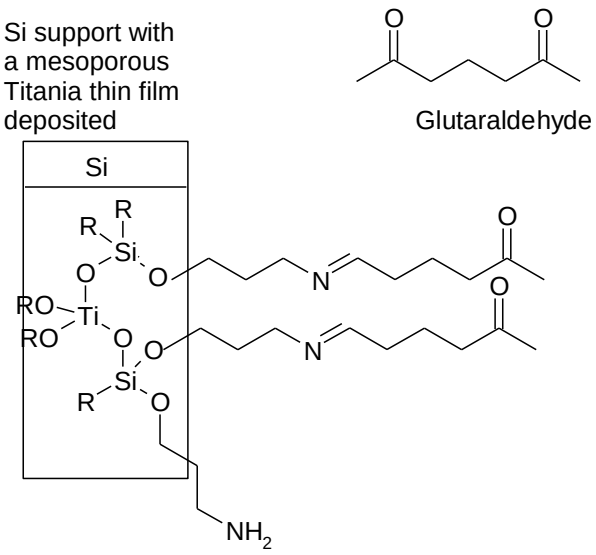

Fig.64 Functionalization of titania films with APTES and GA

In this way the terminal amino groups (APTES) were changed in aldheydic groups that, in the following step, were covalently coupled with the antibody amino groups. The APTES-GA linking is evident in fig.65 in which the bands due to the formation of imines in the area between 1900 and 1600 cm^{-1}, and the bands related to different stretching of the groups C-N, C-O, C-C in the range 1500-1200 cm^{-1} are visible. The GA spectrum was put as reference.

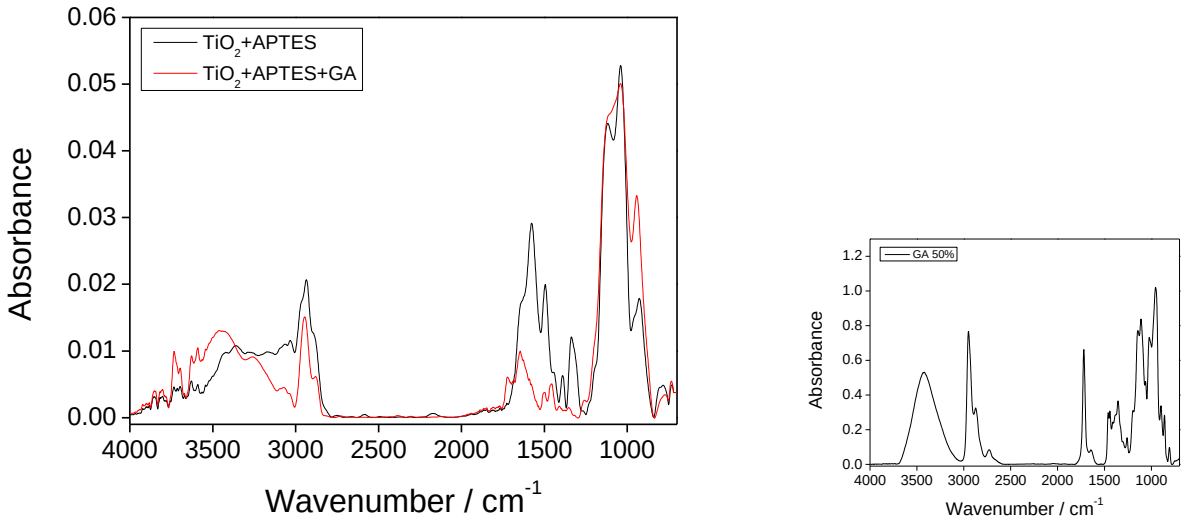

Fig. 65 FTIR spectra of titania films functionalized with APTES (black) and after the linking of Glutharaldheyde (red spectrum). The spectrum of Glutharaldheyde (GA) was reported in the small spectrum on the right as reference.

This linking was also visible with the change of colour of the films as reported in the pictures below (Fig. 66). Starting on the left from mesoporous titania films (yellow), after the functionalization with APTES it was noted a change of colour (pink) and after the linking with GA the final film was blue.

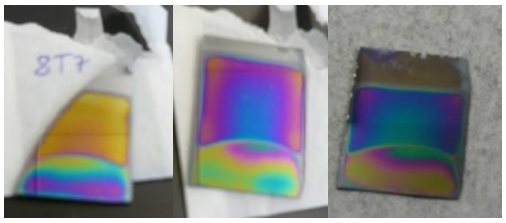

Fig. 66 Titania films before the functionalization (yellow), after the APTES (pink) and after the linking with GA (blue)

To complete the sensor the antibody anti E.coli O157:H7 was linked to the substrate as reported in fig. 67. In this way it was possible a selective detection of the desired pathogen and also of the particular sub-species.

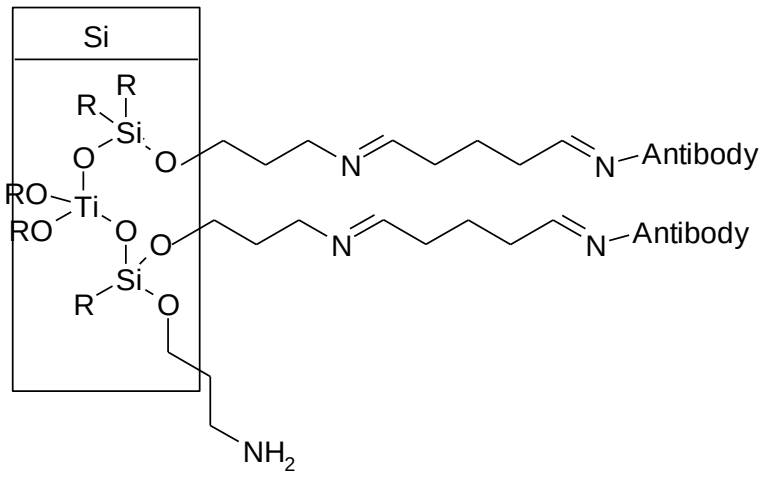

Fig. 67 Linking TiO_2-APTES-GA-Antibody

This linking was followed with FTIR measures as reported in Fig.68.

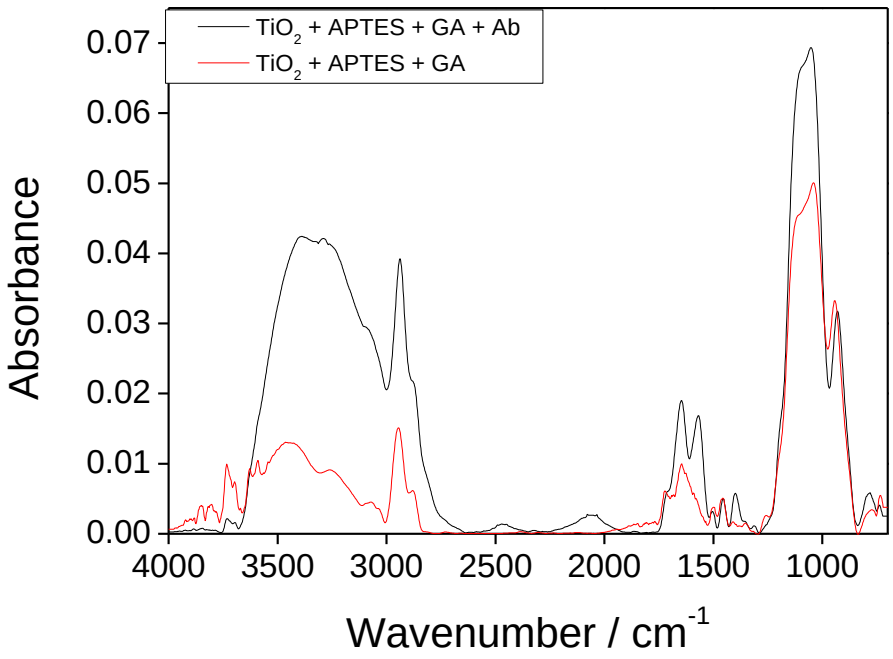

Fig.68 FTIR spectrum of functionalized titania with APTES and GA (red spectrum) and after the linking of the antibody (Ab anti E.coli O157:H7) black spectrum.

Once built the biosensor described above, the method for the final detection of E.coli O157: H7 was developed. The chip was immersed in a buffer with E.coli O157:H7 and was left to react 30 min, washed and analyzed. The reported spectrum (Fig.69) shows for the film with the pathogen very similar peaks to the films without the pathogen but also new peaks appeared and in particular in the region 1300-2000 cm^{-1} (proteic peaks of the bacterium), in the region 3700-4000 cm^{-1} and different peaks intensity in the region 1200-800 cm^{-1} (signals of nucleic acids of the bacterium) that unfortunately in this region overlapped with the spectrum of the Ab and of functionalized titania. In fact the peaks in the 1630-1697 cm^{-1} region are due to the amide I bands of the proteins in the cell and in particular to their secondary structure. While in the region 1402-1457 cm^{-1} the bands due to carbohydrates, glycoproteins and lipids and their characteristic C-O-H in plane bending peaks and $C(CH_3)_2$ symmetric stretching were present. Finally in the range 900-1100 cm^{-1} peaks due to DNA/RNA backbone and phosphate groups of nucleic acids due to the symmetric and asymmetric stretching of P=O and P-O-C groups were present. The spectrum of E.coli deposited on Si, was reported as reference (Fig. 70).

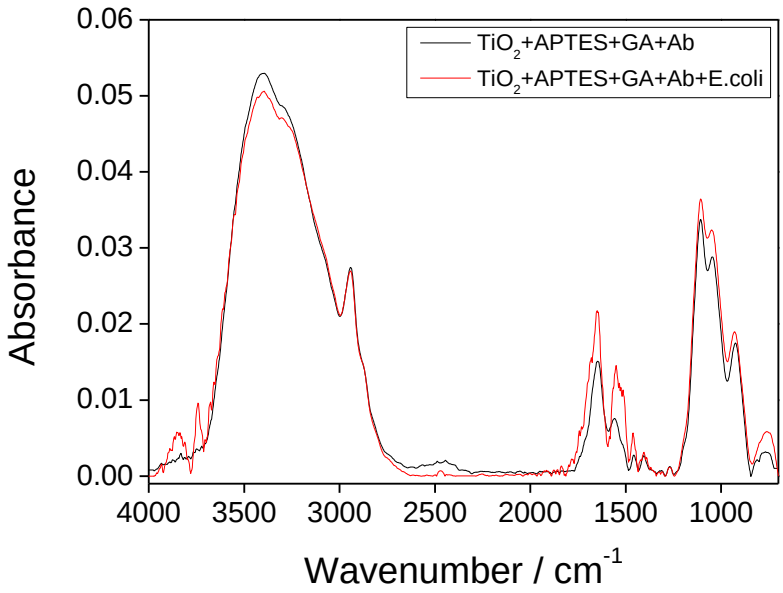

Fig.69 FTIR spectra of titania film functionalized with APTES-GA-Ab (black) and after the linking of E.coli O157:H7.

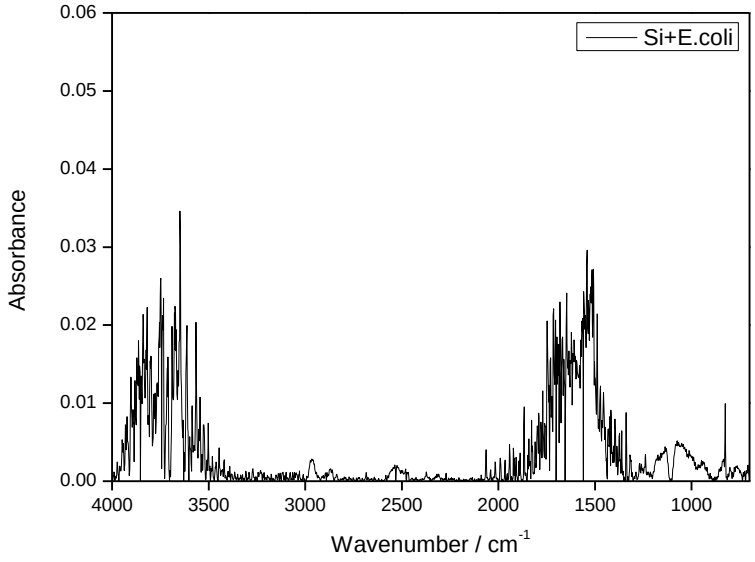

Fig. 70 FTIR spectrum of E.coli O157:H7 on Si wafer.

Detection of E.coli with TiO_2-APTES-anti E.coli O157:H7 Ab

To determine whether this was the best method for the immobilization and detection of E. Coli other routes were tried as the direct link TiO_2-APTES-Ab (without GA). The modification of

titania films using aminosilanes was adopted for the simple immobilization of biomolecules to produce a biosensor. In this case APTES was used as a layer between mesoporous titania films and biomolecules (antibodies in this case and pathogens in the next section). The figure below (Fig. 71) shows the spectra of the films before and after the immobilization of E.coli and it confirms that the peaks due to pathogen were present in the same region of the film with the GA.

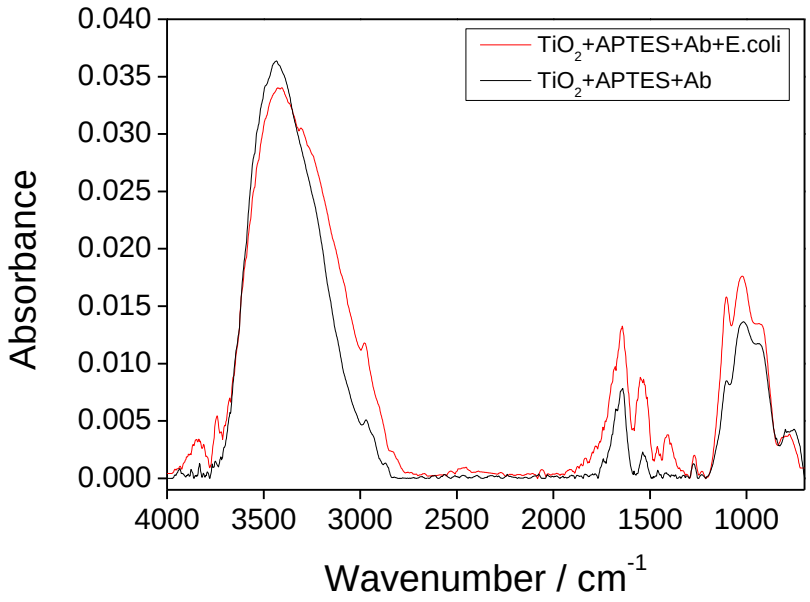

Fig.71 FTIR spectra of titania films with APTES and antibody (black) and after the linking of E.coli (red spectrum).

Detection of E.coli with TiO_2-anti E.coli O157:H7 Ab and with titania thin films

The path of the direct immobilization of the Ab on the film (without APTES and GA) and directly on titania thin film was also tried. In both cases the Ab and the pathogen was adsorbed by electrostatic interactions.

The presence of the pathogen produced a clear spectrum (Fig. 72 and 73).

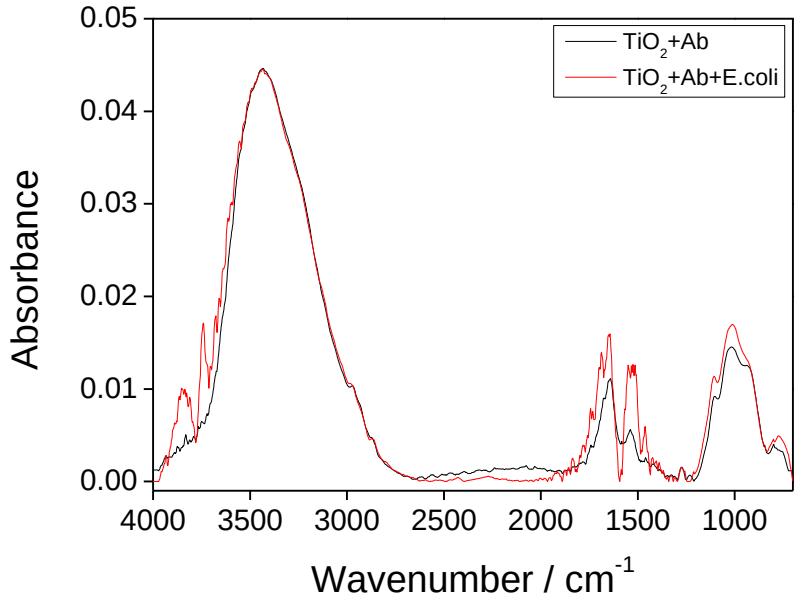

Fig. 72 FTIR spectrum of mesoporous titania films with the antibody anti E.coli (black) and after the immobilization of the pathogen (red spectrum).

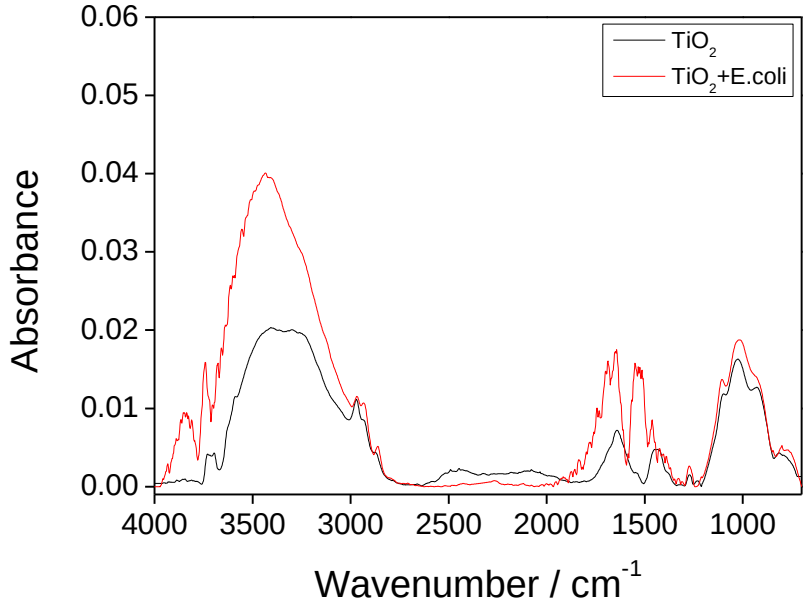

Fig. 73 FTIR spectrum of mesoporous titania films before (black) and after the immobilization of pathogens (red spectrum).

It was also tried to immobilize another subspecies of E.coli (K12) on the same devices but without positive results when the antibody was present in the chip, while the pathogen was immobilized

directly on titania film because in this case there was not a selective molecule for the interaction with the chip.

Comparing the different immobilization techniques of detection, the best result was obtained with the method that provided the covalent binding of the Ab on the film with APTES and GA (black spectrum Fig. 74). The other methods allowed the immobilization of the bacterium, but probably a certain amount of this was lost, leading to a decrease in the relative peaks of the bacterium and thus a lower sensitivity of the device (blue and red spectrum). Finally the direct linking of the pathogen allowed a good immobilization (light blue spectrum) but this was not a selective method.

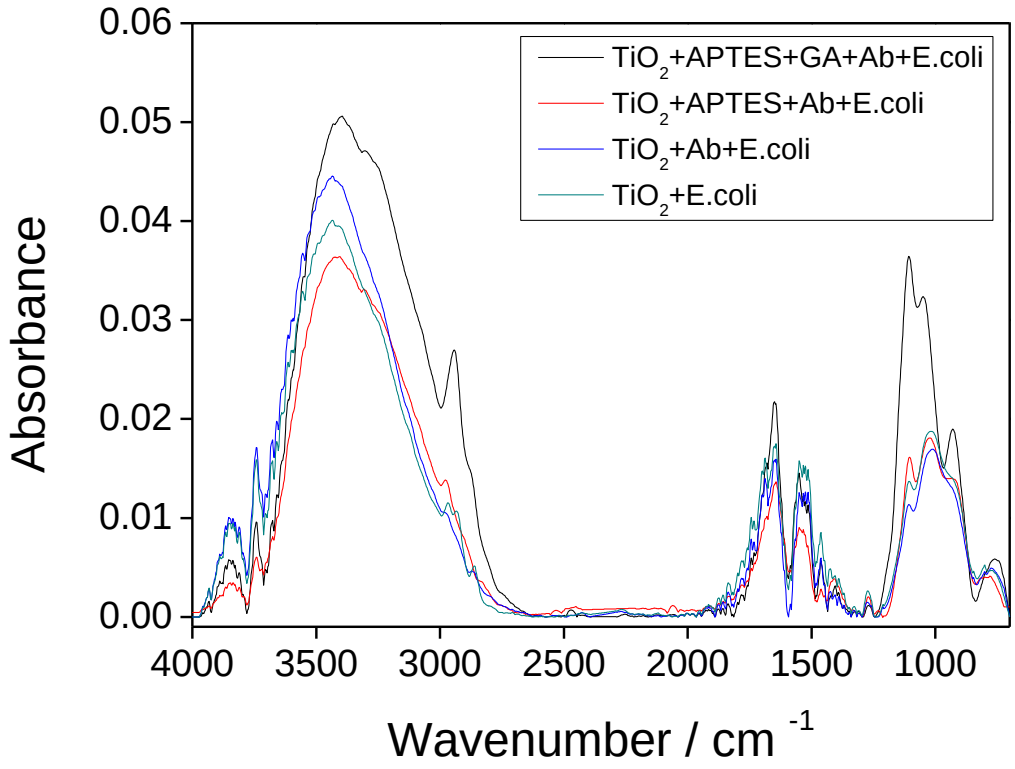

Fig. 74 FTIR spectra of the different devices with the immobilized pathogen O157:H7.

Determination of the Detection Limits of E.coli O157:H7

Tests to establish the detection limit of the devices were carried out starting from the immobilization of E. coli at concentration of $1x10^8$ CFU/ml to a concentration $1x10^2$ CFU/ml. These measures were done directly on mesoporous titania films with the absorbed bacterium (the lower left spectra) or on the films functionalized with APTES, GA, Ab anti E.coli with the

bacterium. In both experiments it was reached a detection limit of $1x10^2$ CFU / ml (Fig. 75 and 76) even if in the films functionalized with APTES-GA-Ab the signal at low concentration was clearer.

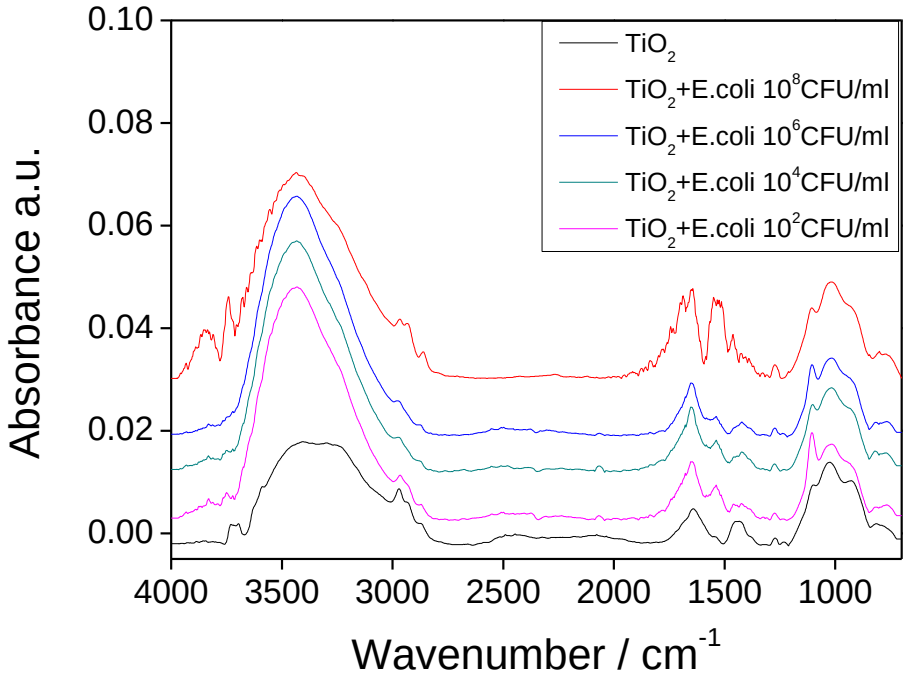

Fig. 75 FTIR of titania films after the exposition to different concentrations of E.coli.

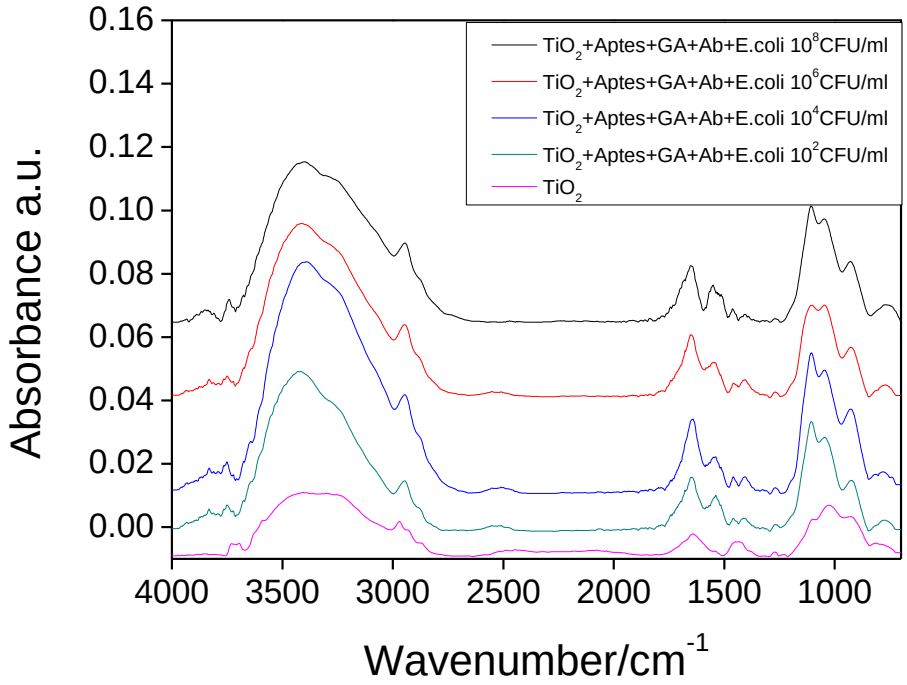

Fig. 76 FTIR of titania film functionalized with APTES, GA and Ab after the exposition to different concentrations of E.coli.

Results

In this work pathogens were detected using their FTIR fingerprints with a label-free method. In particular mesoporous films were functionalized in different ways and new methods were developed to detect and analyse samples in a fast way, reaching low limit of detection. In particular the linking of bacteria was studied directly on titania films, on titania functionalized with APTES and in titania films functionalized with APTES and GA with the antibodies and the last one was chosen as the best method. The reached limit of detection of this technique was 10^2 CFU/ml. Using anti-E. coli O157: H7 immobilized on functionalized mesoporous materials of titania a more effective method was found compared to the traditional. In fact a simple method was realized that requires only a quick sample preparation. Pathogens were identified and classified according to their infrared signatures that can distinguish the species and the strain. Benefits were obtained through the use of nano materials for the immobilization and the detection of pathogens; in fact, thanks to their features it was possible to capture E. coli in less than 30 minutes because of their high surface to volume ratio that provided more surface contact resulting in greater efficiency for the capture. This approach provided specificity due to the characteristic fingerprint and selectivity thanks to the use of species-specific antibodies. It could also be adapted to in-field analysis with portable instruments and, memorizing the spectra for each pathogen and species, it could be created a software that recognises directly the contaminant with a simple method that does not require skilled workers. In this way, changing the recognising molecule, it can be created a rapid, simple, on-site technique for pathogen detection that avoids the distribution of contaminated food, using functionalized chips for in-field use.

Part 3 Development of SERS substrates with mesoporous titania thin films

This part of the work was based on the development of materials that can give a SERS effect for the final detection of food contaminants. In particular it was thought that the previously described mesoporous titania films could be appropriate materials for the development of substrates that can produce a SERS effect. In fact mesoporous films can include molecules into a matrix giving an uniform orientation respect to the surface, as analyzed in the previous parts of the work, and, to achieve this goal, mesoporous titania thin films were modified with nanoparticles to produce nanostructures in a reproducible and not expensive way. In particular films of nanoparticles were created through a bottom-up approach with the growth of nanoparticles into the pores of mesoporous titania, choosing silver among the noble metals, because it produces more intense resonance effects. The grown of silver nanoparticle was followed to obtain a diameter between 20 and 100 nm that is indicated to have a good SERS effect.

The first step in the design of SERS labels was to choose and prepare a suitable SERS substrate because the metallic nanoparticles should possess certain optical properties. In order to achieve SERS signal enhancement required for sensitivity, the analyte must be attached (adsorbed) or in close proximity to a specially prepared surface of a noble metal, as silver (Ag) in our case.

The method used for the preparation was based on impregnation with $AgNO_3$, followed by photo reduction of Ag^+ ions by exposure to UV radiation for different time. Titania, thanks to its photo catalytic properties, produced the reduction of Ag^+ ions to Ag^0 directly on the film without the introduction of a reducing agent, and this property was applied for depositing AgNPs on the surface of nanostructured titania films. Titania films are essential for this process and the photo catalytic activity depends on the titania crystallinity. In our case after the thermal treatment titania is amorphous but it has a minor fraction of anatase that confers the photoactive properties.
The successful reduction was evident on titania films, that only after a few hours of exposure present a change of colour, due to the progressive loading of silver. The film was shown before (film left) and after impregnation with $AgNO_3$ and UV exposure for 6h (Fig. 77), and a metal mirror of silver can be noted only on the film and not on silicon.

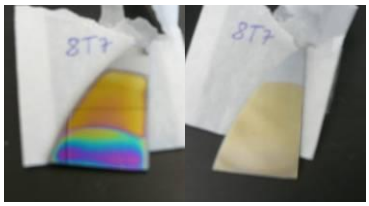

Fig. 77 Picture of titania thin films before (left) and after (right) UV exposure for 6h

Characterization of mesoporous titania films with included silver nanoparticles

The grown of silver nanoparticles on titania surface was followed in different ways. The control of this reduction required a long process in order to obtain Ag nanoparticles (NPs) of the desired size and distribution on the film surface.

For the characterization of mesoporous titania films exposed for different time to UV light, various measures were carried out. First of all, for microscopic investigations the nanoparticles growth were observed by atomic force microscopy (AFM). The changes of conformation were observed before and after AgNPs deposition. In detail in fig. 78 titania films were shown before the inclusion of AgNPs and can be noted as they are porous, highly ordered and have a cubic pore structure with a diameter of about 20 nm.

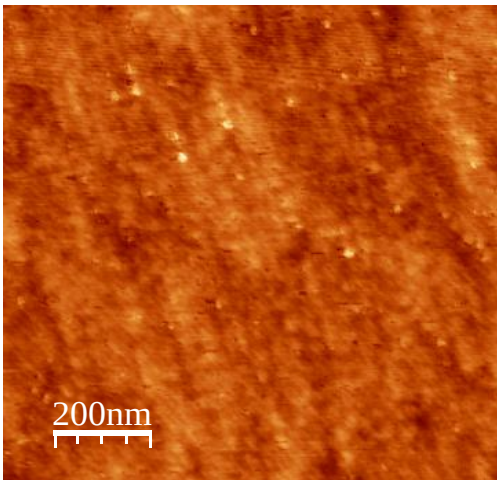

Fig. 78 AFM image of mesoporous titania thin film

The initial growth of Ag NPs inside the pores was followed, after 1h of exposure to UV radiation, by AFM measures. In the image (Fig. 79) NPs of around 20 nm in diameter were visible, forming a continuous and homogeneous layer thanks to the tiania support that acts as a mold within which the nanoparticles grow.

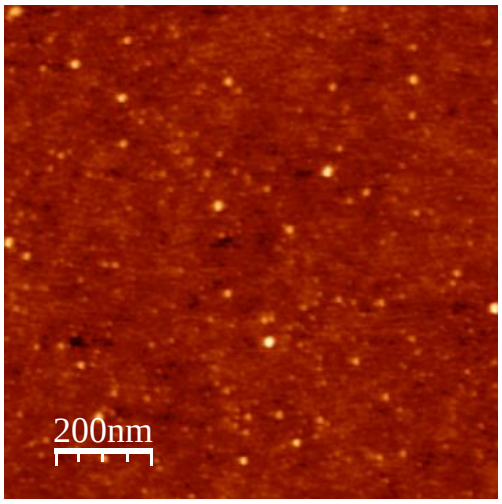

Fig. 79 AFM images of titania thin film with AgNPs after 1h of exposure to UV light

Continuing the exposure to UV radiation after 3h it was observed the growth of nanoparticles and the formation of several layers (Fig. 80). In fact the NPs were primarily formed in the mesopores (1h) and not on the surface, then with a longer UV exposure it was noted the formation of a continuous silver film on the surface. The dimension of NPs at this point were between 50 and 100 nm which were the best size in order to have the SERS effect.

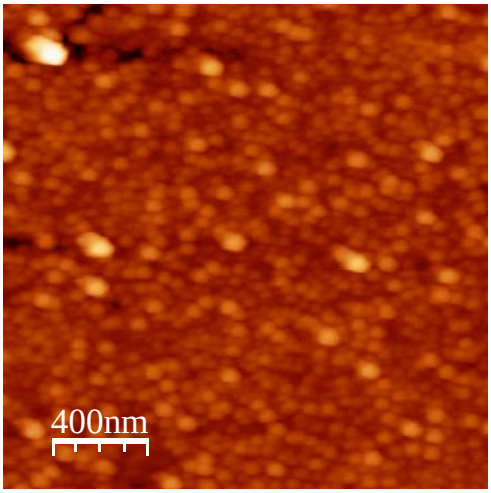

Fig. 80 AFM images of titania thin film with AgNPs after 3h of exposure to UV light

Proceeding further with the exposure to UV, after 6h it was visible the formation of aggregates of nanoparticles of about 100-200 nm in diameter, composed of NPs with size of about 20-50nm (Fig. 81). This proximity was found to be optimal to obtain a significant signal amplification.

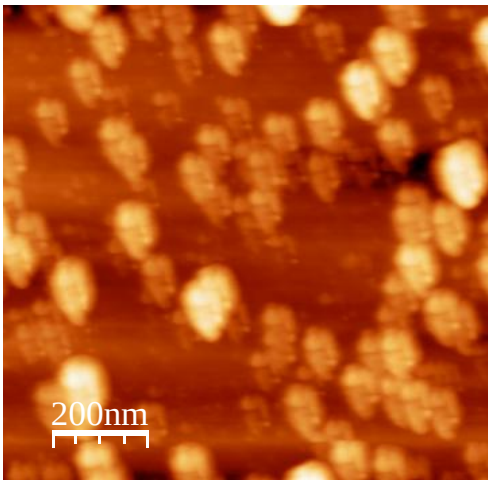

Fig. 81 AFM images of titania thin film with AgNPs after 6h of exposure to UV light

UV-vis measures were also carried out to monitor the changes of spectra after the irradiation with UV light for different time. When AgNPs were included into the film, a very broad band appeared from the near UV to the near infrared regions (300-600 nm), due to the localized surface plasmon resonance peak of spatially confined electrons in Ag^0 deposited on the titania surface (Fig. 82); this confirms the reduction of M^+ ions to M^0.

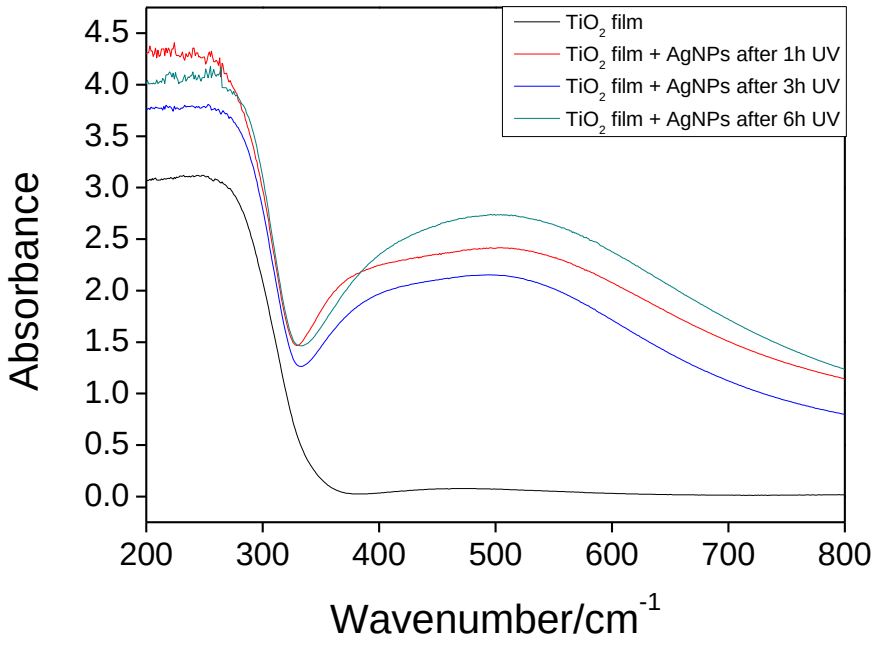

Fig. 82 shows the UV/vis spectrum of the titania mesoporous thin film (Black) and of titania film with AgNPs after the exposure to UV radiation for different times (red 1h, blue 3h, light blue 6h).

Differences in the spectra exposed 1h and 3h with the spectrum after 6h were noted. This difference in the bands of UV was due to the absorption of AgNPs of different sizes. In fact nanoparticles smaller than 20 nm showed an absorption band around 390 nm; this band was present in films exposed for 1h and 3h to UV (similar sizes), while for Ag nanoparticles bigger than 20 nm it could be observed an absorption peak around 530-600 nm, visible in films exposed for 6h. These data confirmed the AFM measures.

FTIR measures were also carried out to monitor changes of spectra after AgNPs deposition. It was noted that in presence of AgNPs there was an increase of the peak around 3200 cm^{-1} and 500 cm^{-1} and also new peaks appeared around 1200-1500 cm^{-1} (Fig. 83). The other peaks were due to Ti-OH stretching at 3250 cm^{-1}, H-O-H bonds of the physisorbed water at 1625 cm^{-1}, moreover the peaks at 2920-2840 cm^{-1} are due to –CH and –COH groups of EtOH adsorbed on the titania surface.

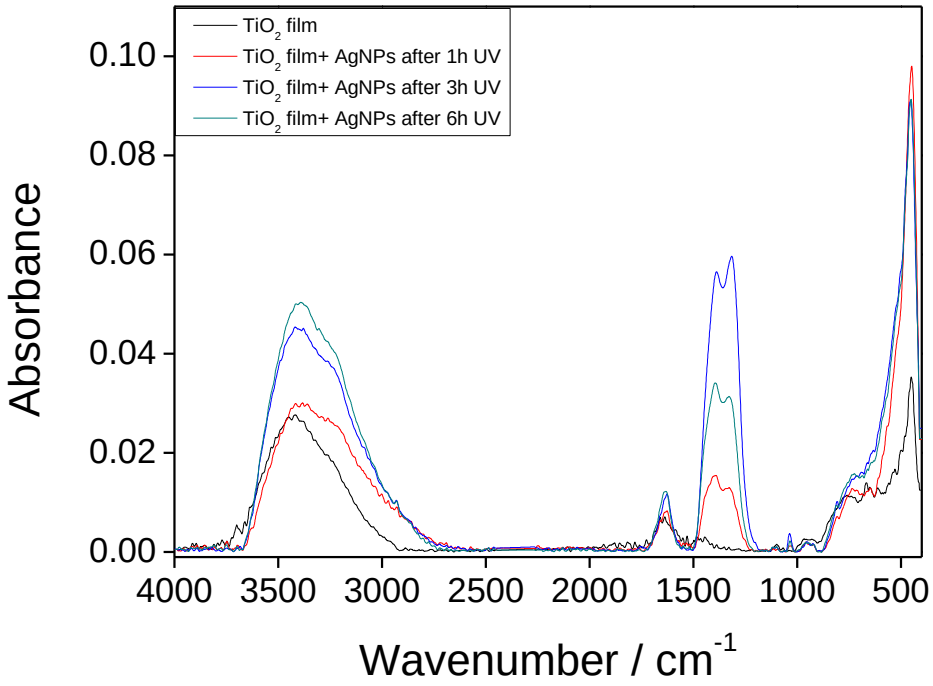

Fig. 83 FTIR spectra of mesoporous titania thin film before (black spectrum) and after the exposition to UV light for different time: 1h (red spectrum), 3h (blue spectrum) and 6h (light blue spectrum).

Finally XRD measures were carried out to monitor which phases and crystallites were present on the film surface and to calculate their dimension.

XRD measures of TiO_2 films with AgNPs left 1h, 3h and 6h under UV light were carried out and, in the spectra, were found the characteristic peaks for the (111), (200), (220), and (311) planes of face centered cubic (fcc) Ag at 2θ= 38°, 44°, 64°, and 77° that confirmed the presence of entrapped silver in the nanocomposite TiO_2-Ag. Peaks due to the formation of oxides were not observed revealing that Ag^0 was not oxidized after grown into TiO_2 films. Small peaks due to the formation of small quantities of anatase were also observed during the calcination process. These characteristic peaks due to anatase TiO_2 nanocrystal were at 2θ= 25.3°, 37.8°, 48.1°, 53.9°, and 62.7°. It was also observed for the sample left 1h and 3h under UV a peak at 2θ around 30° due to $AgNO_3$ unreacted for a total 1% (Fig. 84) that confirmed the UV and AFM spectra that showed for that time an incomplete reaction. While after 6h the peak at 2θ= 30° disappeared for the complete transformation of Ag^+ ion in Ag^0 metal (Fig. 85). Furthermore after 6h two new peaks appeared: a shoulder around 37° and a peak around 50°. The shoulder could be attributed to a small amount of Ag with a hexagonal disposition.

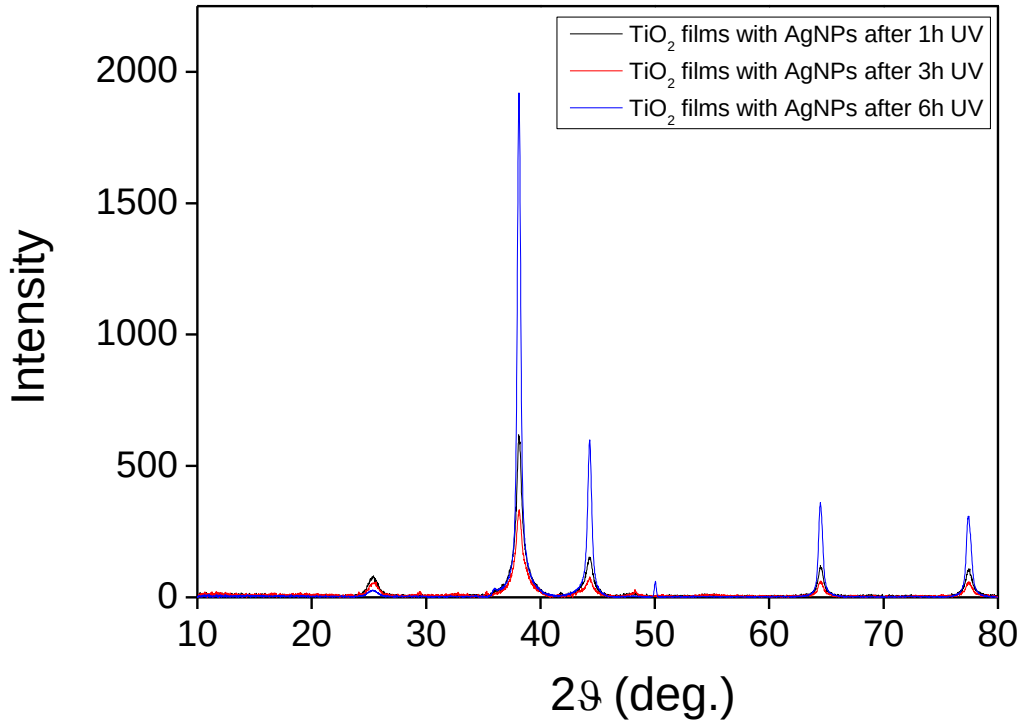

Fig.84 XRD spectra of mesoporous titania films with AgNPs after 1h (black) , 3h (red) and 6h (blue) of UV exposure.

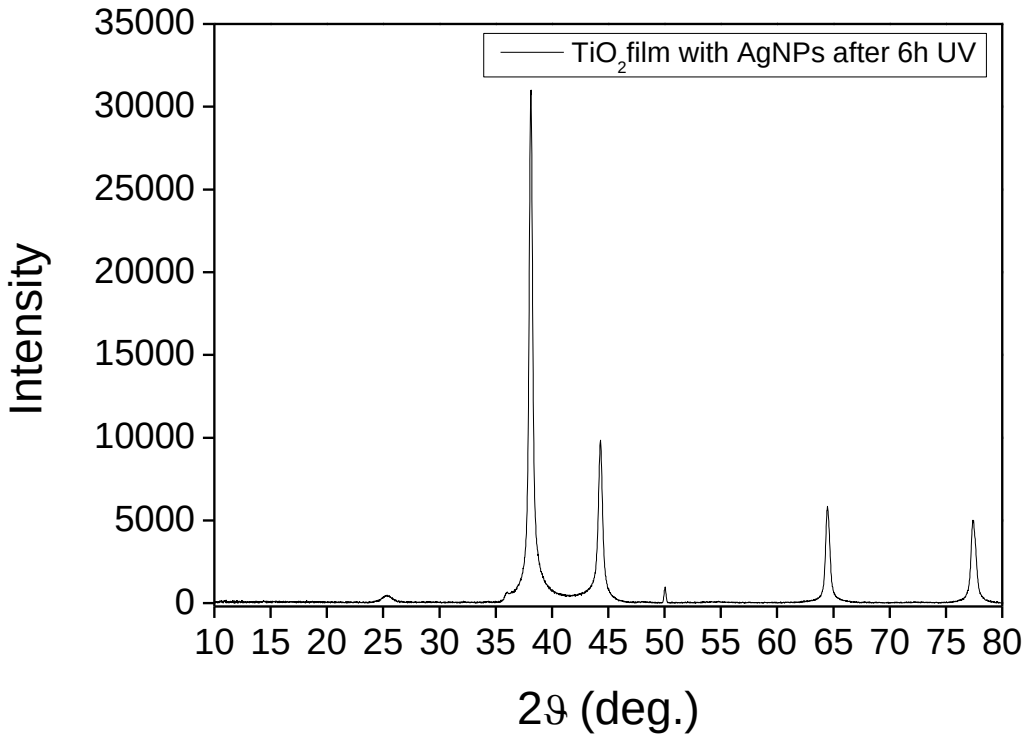

Fig. 85 XRD spectrum of mesoporous titania films with AgNPs after 6h of UV exposure.

Finally the size of crystallites was calculated from XRD spectra in two ways:
A) with Rietveld analysis using the program Maud. The values obtained showed a dimension of crystallites of 12nm for the samples left under UV light for 1h and 3h, while the samples left under UV for 6h showed a dimension of 32-36 nm.

B) The crystallites dimensions were calculated also in a manual way taking from the XRD spectra the FWHM (full width at half maximum) and calculating the dimensions from the Scherrer Equation ($t = \lambda / B \cdot \cos\theta$) with λ=1,54056Å, B that is the full width at half maximum FWHM, and θ the half angle. For this calculation the degrees were converted in radians and it was calculated a mean from the values obtained from the peaks at 25.40°, 38.13°, 44.28°, 64.48°and 77.45°.
The results obtained show a dimension of crystallites comparable with the results obtained with Maud.

Application of titania films with AgNPs for SERS (Surface Enhanced Raman Spectroscopy)

After the creation and characterization of mesoporous titania films with AgNPs the detection of a label was followed with a characteristic Raman vibrational signature, Rhodamine B isothiocyanate (RhBITC) that was used as a probe molecule to characterize the SERS activity. This label was chosen because it can be used in future for the binding of biomolecules and pathogens. Raman spectra of RhBITC were collected and the SERS effect was followed to monitor until which concentration the Rhodamine was discernible. These measures were tried on the films exposed to UV for 1h, 3h and 6h and the best time (6h) and the best conditions for the measures were chosen for the inclusion of the dye and for the setting of the instrument. The measures were carried out and it was reached a limit of detection almost under the femto molar level. The measures were carried out with the laser at 532nm (fig. 86) and with the laser at 633nm (Fig.87).

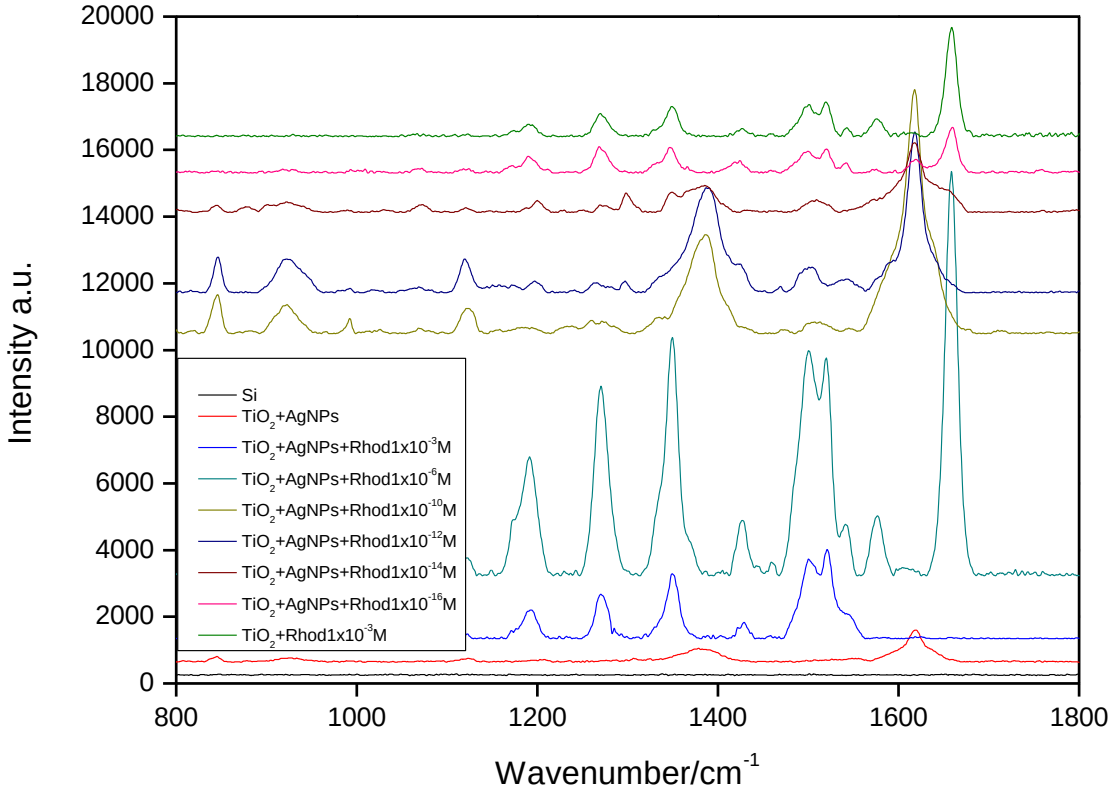

Fig. 86 Raman spectra of RhITC at different concentrations in the range 800-1800 cm^{-1} acquired with the laser at 532nm.

Fig. 86 shows Raman spectra of RhBITC. In detail, observing the spectra from the bottom to the top we can see that the Si raman spectrum (black) does not have significant peaks, the red spectrum of the substrate alone of titania with AgNPs has two main peaks around 1390 cm^{-1} and 1620cm^{-1}. From the blue to the pink spectrum are visible the SERS spectra of the substrates (TiO_2+AgNPs) with different concentration of RhBITC from 10^{-3} to 10^{-6}. The blue spectrum is the typical Raman spectrum for rhodamine that can be observed with a big SERS effect for concentration 10^{-6} M. Further decreasing the concentration (10^{-10} M, 10^{-12} M), the peaks were always observed related to RhBITC but the peaks appeared also due to AgNPs (1390 cm^{-1} and 1620cm^{-1}) that can be found also in FTIR spectra. By reaching the concentration of 10^{-14} M the contribution due to AgNPs decreased until it disappeared for concentration of 10^{-16} M. This last spectrum was a perfect RhBITC SERS spectrum that was possible to measure only on the titania films with silver nanoparticles. The last spectrum (the green spectrum above) was put as reference. It was acquired on titania films (without AgNPs). As shown above the green and the pink spectra are highly comparable with the difference that one (green) was the Raman spectrum obtained for a RhBITC concentration of 10^{-3}M and decreasing the dye concentration it was not possible to see

any rhodamine spectrum on titania films alone, while with SERS substrates (TiO_2+AgNPs) it was possible to obtain a spectrum (pink) for rhodamine concentration until 10^{-16}M, under fM level. To try to not have interference due to AgNPs measures of RhBITC were carried out with the laser at 633nm (Fig. 87).

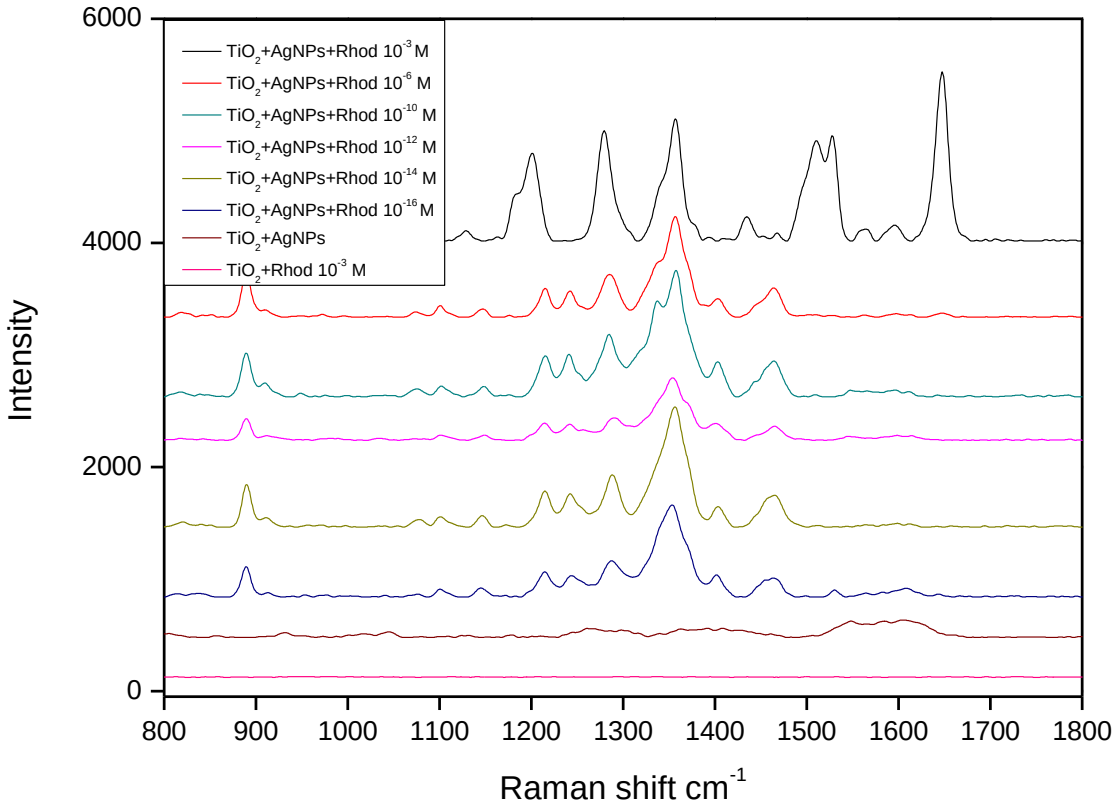

Fig. 87 Raman spectra of RhITC at different concentration in the range 800-1800 cm^{-1} acquired with the laser at 633nm.

These measures showed how the Raman spectrum acquired at concentration 10^{-3}M on titania (pink) had a very low signal and the same was observed for the spectrum of AgNPs alone (brown spectrum). The other spectra are highly clear, reproducible and comparable with the raman spectra present in literature for RhBITC at 633nm, in particular the black spectrum at 10^{-3} M is the clear fingerprint of RhBITC, but it is very intense thanks to the substrate (TiO_2+AgNPs). Decreasing the RhBITC concentration (from 10^{-6} M to 10^{-16} M) it was observed a change in the SERS spectra but the significant peaks were preserved for the detection of rhodamine and also the intensities are highly comparable. Also in this case very low concentrations of RhBITC were detected, confirming the results obtained with the other laser.

To compare the Raman with the SERS spectra and calculate the Analytical enhancement factor the spectra acquired at 532 nm were considered because in this case a good raman spectrum was obtained. In fact ten measures on the films (TiO_2+AgNPs) were carried out with a RhBITC concentration of 10^{-16} M to study the homogeneity of the film and the reproducibility of the measures and those were compared with the spectrum collected on titania with rhodamine 10^{-3} M (Fig.88).

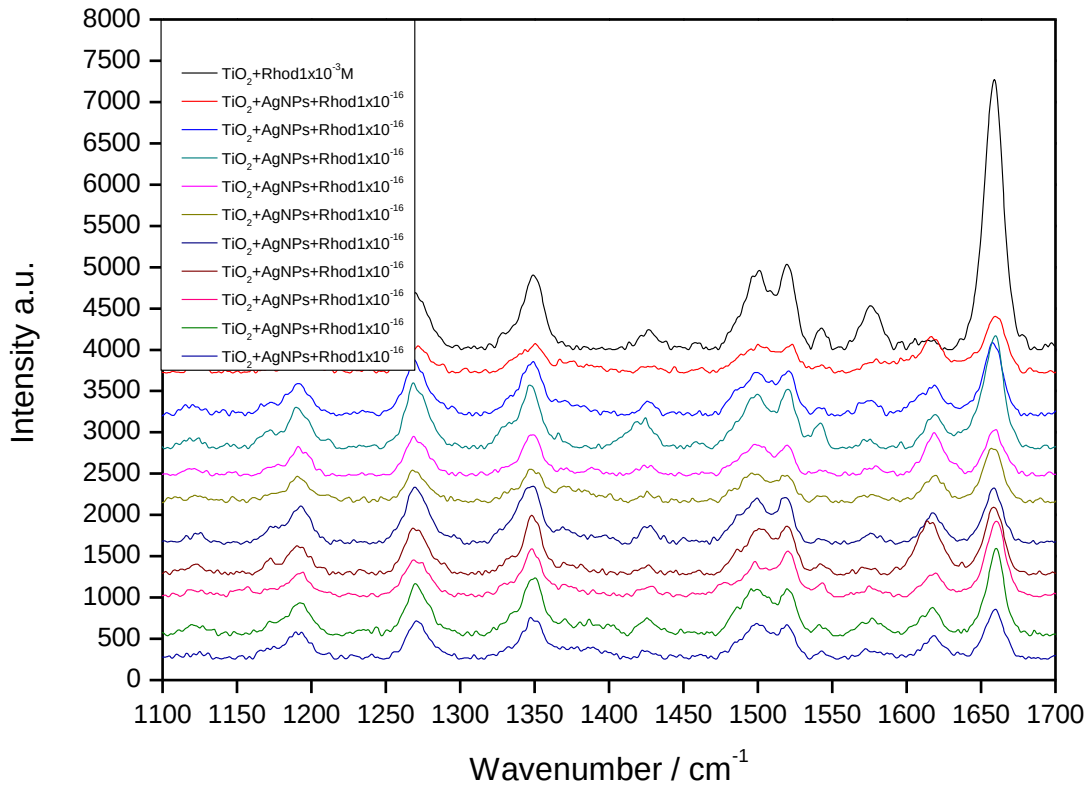

Fig. 88 Raman spectrum of RhBITC at a concentration 10^{-3}M compared with ten SERS measures acquired for rhodamine concentration 10^{-16}M.

As can be seen as follows, making a number of measures within the same sample at concentrations of RhBITC $1x10^{-16}$ M, the results were consistent and reproducible (Tab. 2), indicating a homogeneity of the sample.

	TiO_2+ Rhod $1x10^{-3}$M	TiO_2+Ag + Rhod $1x10^{-16}$ M	TiO_2+Ag + Rhod $1x10^{-16}$ M	TiO_2+Ag + Rhod $1x10^{-16}$ M	TiO_2+Ag + Rhod $1x10^{-16}$ M	TiO_2+Ag + Rhod $1x10^{-16}$ M	TiO_2+Ag + Rhod $1x10^{-16}$ M	TiO_2+Ag + Rhod $1x10^{-16}$ M	TiO_2+Ag + Rhod $1x10^{-16}$ M	TiO_2+Ag + Rhod $1x10^{-16}$ M	TiO_2+Ag + Rhod $1x10^{-16}$ M
Intensity at $1270cm^{-1}$	689.02	297,33	663,70	749,43	447,37	369,52	687,61	540,98	432,46	632,71	457,64
AEF	-	0.43x 10^{13}	0.96x 10^{13}	1.08x 10^{13}	0.64x 10^{13}	0.54x 10^{13}	0.99x 10^{13}	0.78x 10^{13}	0.63x 10^{13}	0.92x 10^{13}	0.66x 10^{13}

Tab. 2 Intensity of the peak at $1270cm^{-1}$ for Raman measures of RhBITC and AEF

To know the "magnitude'' of the enhancement in surface enhanced Raman scattering (SERS) is a really important issue. For many applications it is important to know how much more signal can be expected from SERS as compared to normal Raman under given experimental conditions if we consider an analyte solution with concentration c_{RS}, which produces a Raman signal I_{RS} under non-SERS conditions. Under identical experimental conditions (laser wavelength, laser power, microscope objective or lenses, spectrometer, etc.), and for the same preparation conditions, the same analyte on a SERS substrate, with possibly different concentration (c_{SERS}), now gives a SERS signal I_{SERS}. The analytical enhancement factor (AEF) can then be defined as

$$\mathrm{AEF} = \frac{I_{\mathrm{SERS}}/c_{\mathrm{SERS}}}{I_{\mathrm{RS}}/c_{\mathrm{RS}}}$$

It was calculated doing the average of ten measures at 1270 cm^{-1} considering one of the characteristic peaks of RhBITC.

Average AEF=$0.77x10^{13}$

It was found that the enhancement factor of the signal was of 10^{13} times thanks to the SERS effect compared to samples that do not have AgNPs (Fig. 89).

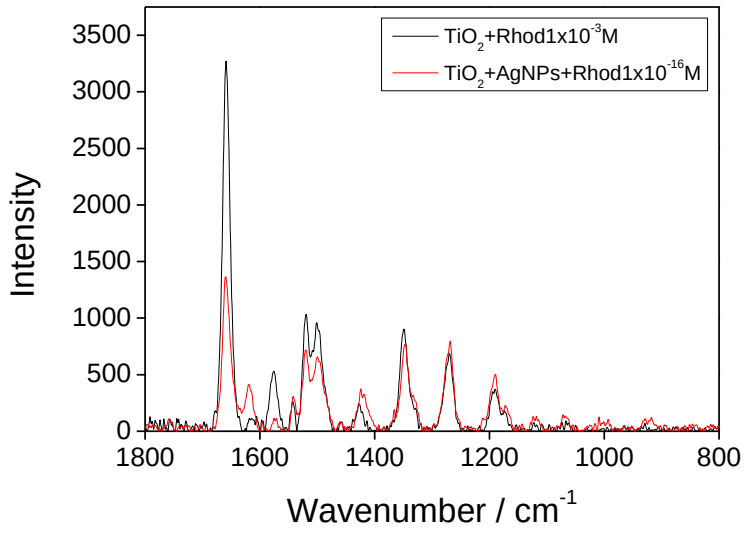

Fig.89 Raman measures of the maximum concentration visible of RhBITC deposited on TiO_2 (black) and on SERS substrates (red spectrum).

The same experiment was carried out, with a label-free technique, for the detection of Cytochrome C, a little protein. It was tried to define also this time the detection limit (Fig. 90).

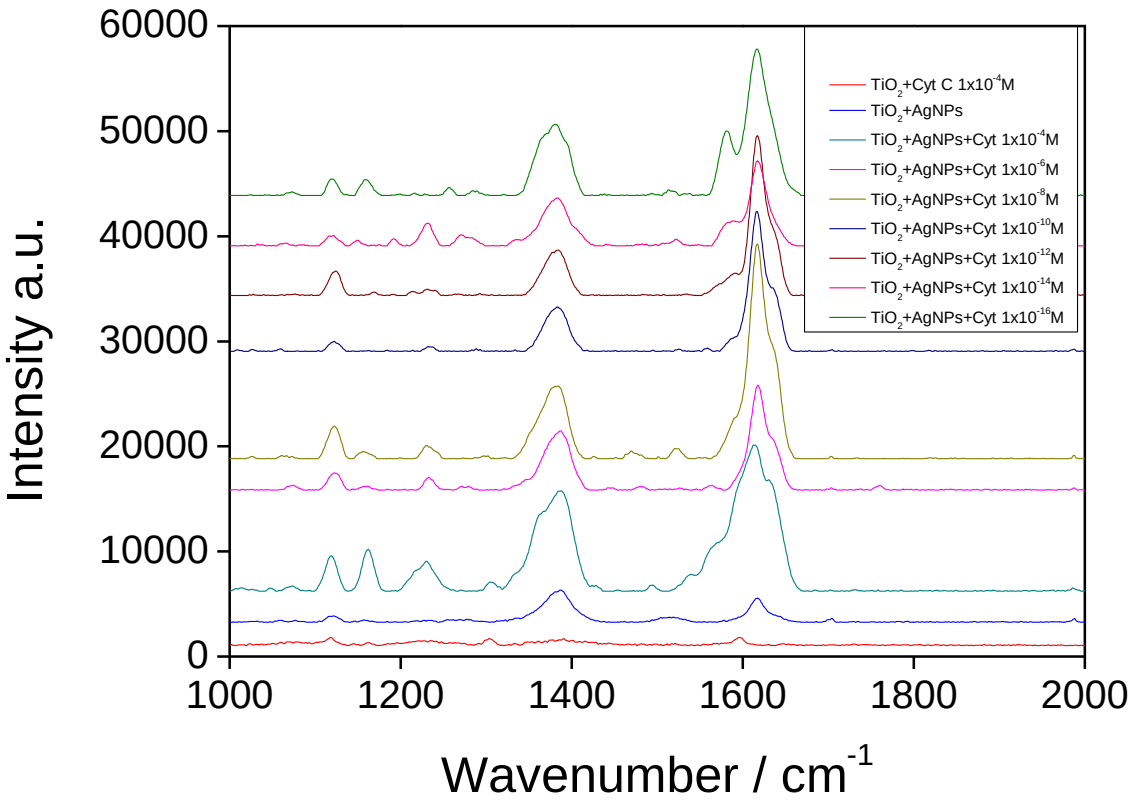

Fig. 90 Raman spectra of CytC at different concentration in the range 1000-2000 cm^{-1} acquired with the laser at 532 nm.

Also this time the Raman spectrum of CytC was measured on titania as reference (red) and it was noted that at this concentration the peaks were low; further decreasing the concentration of CytC the spectra were not visible. The spectrum of AgNPs alone (blue) and all the SERS spectra from a concentration of CytC 10^{-4} M arriving to a concentration 10^{-16} M were also measured. In particular it can be observed the SERS signal of three vibrational fingerprints for CytC at 1130cm^{-1} assigned to in plane vibration of pyrrole half ring, 1310 cm^{-1} due to bending out of plane of CH bonds and 1408 cm^{-1} due to in plane vibrational mode of pyrrole quarter ring and the other typical bends at 1370, 1564, 1585, 1637 cm^{-1}.

SERS spectra were observed for CytC adsorbed on Ag-TiO_2 substrates not only with the 532 nm radiation but also with the 633 nm laser, also if in this case the measures were less good and for this reason not reported. Ten measures were repeated on the same sample at the lower concentration of CytC visible (Fig.91), and also in this case the AEF (Tab.3) was calculated obtaining an enhancement of 10^{13} times (Fig. 92).

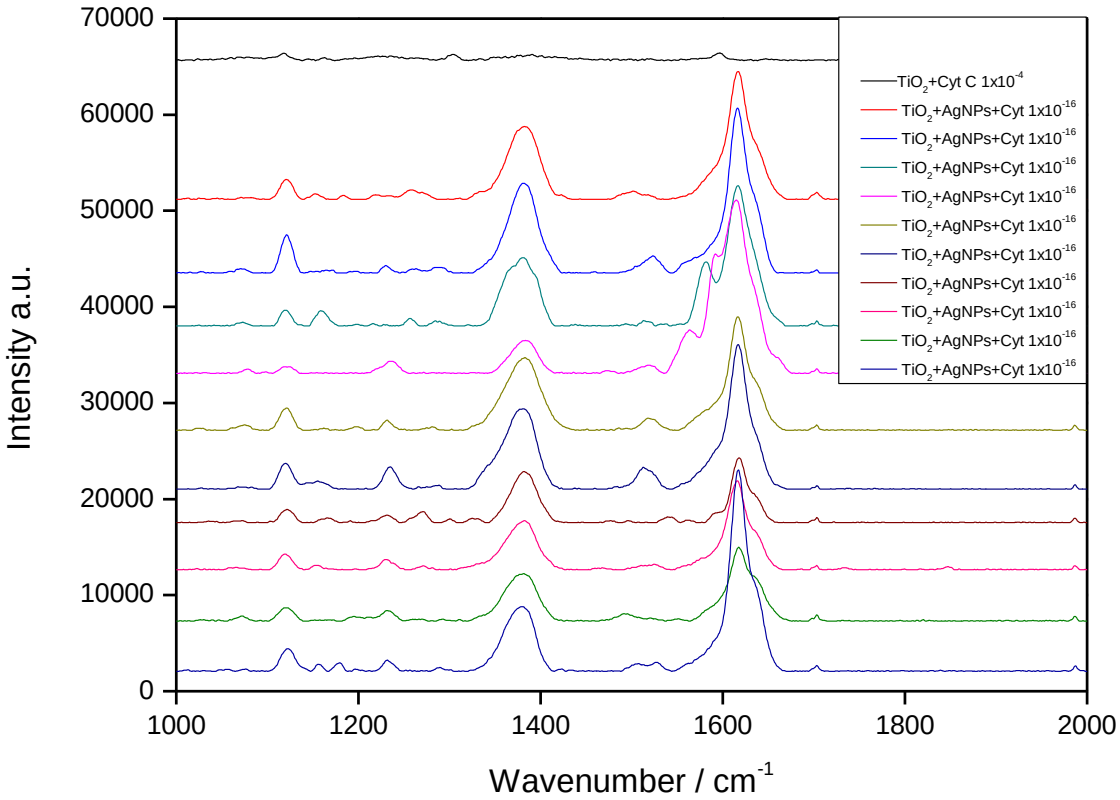

Fig. 91 Raman spectrum of CytC at a concentration 10^{-4}M compared with ten SERS measures acquired for CytC at concentration 10^{-16}M.

	TiO_2+ CytC $1x10^{-4}$ M	TiO_2+Ag+ CytC $1x10^{-16}$ M	TiO_2+Ag+ CytC $1x10^{-16}$ M	TiO_2+Ag+ CytC $1x10^{-16}$ M	TiO_2+Ag+ CytC $1x10^{-16}$ M	TiO_2+Ag+ CytC $1x10^{-16}$ M	TiO_2+Ag+ CytC $1x10^{-16}$ M	TiO_2+Ag+ CytC $1x10^{-16}$ M	TiO_2+Ag+ CytC $1x10^{-16}$ M	TiO_2+Ag+ CytC $1x10^{-16}$ M	TiO_2+Ag+ CytC $1x10^{-16}$ M
Intensity at $1585cm^{-1}$	284.26	2647.26	2710.63	6161.16	8694.03	2207.08	3019.55	418.37	1500.62	1355.81	2393.40
AEF	-	9.31 $x10^{12}$	9.54 $x10^{12}$	21.67 $x10^{12}$	30.58 $x10^{12}$	7.76 $x10^{12}$	10.62 $x10^{12}$	1.47 $x10^{12}$	5.28 $x10^{12}$	4.77 $x10^{12}$	8.42 $x10^{12}$

Tab. 3 Intensity of the peak at 1585 cm^{-1} for Raman measures of CytC and AEF

Average AEF=1.09 $x10^{13}$.

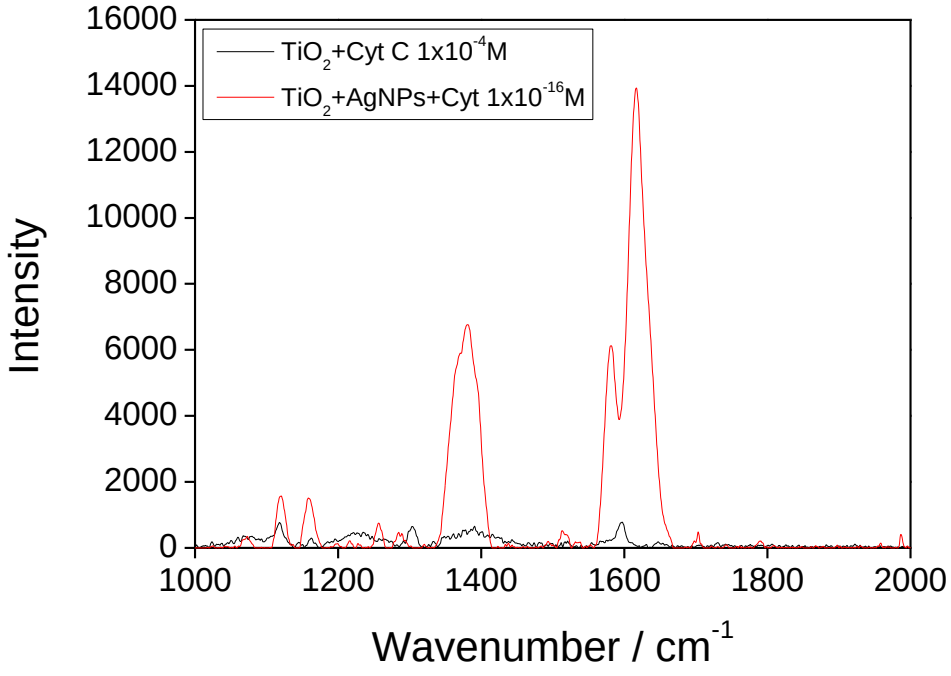

Fig. 92 Raman measures of the maximum concentration visible of CytC deposited on TiO_2 (black) and on SERS substrates (red spectrum).

Results

New mesoporous films were developed as starting materials for the inclusion of nanoparticles in order to obtain the size (20-100 nm) and the distance between nanoparticles useful for a SERS effect. The mesoporous structure acted as a mold in which NPs were grown in an orderly and reproducible way. The uniform distribution of silver nanoparticles deposited into the pores and on the titania surface was confirmed by AFM measures. Different trials were done for the characterization of these substrates and the best results were obtained with 6h of UV exposure leading to the formation of NPs of dimension about 30nm, that formed cluster on the film surface. A self-assembled layer of AgNPs, in fact, provided several advantages in terms of sensitivity, quantification and multiplexing, getting a good signal and improving significantly the limit of detection of analytes deposited on them, leading to a good EF (enhancement factor) of the signal. Thanks to nanofabrication using mesoporous materials it was possible to obtain a greater control over geometry, shapes and distances between the metal nanoparticles avoiding the problems of precipitation and aggregation, present in solution. In this way, substrates prepared with bottom-up approach allowed good phenomena of SERS enhancement. The use of silver as noble metals in the form of nanostructured substrates led to a Raman amplification of analytes up to 13 orders of magnitude. This result was important for the detection of RhBITC and CytC but also because it can be applied to biological analysis providing information at high spectral resolution, at room temperature, without water interference and not suffering from rapid photobleaching commonly observed in fluorescence spectroscopy. The advantages of SERS reached with this project, compared to the current labelling approaches, included: low-cost and fast analysis of samples, the excellent ability to amplify the signal arriving to a single molecule level, the quantification of analytes using the characteristic SERS spectra and the high photostability. Additionally, this is a highly innovative technique that can be applied for the detection of pathogens or food contaminants in a very fast way.

Conclusions

For the construction of biosensors were synthesized, with a sol-gel method, mesoporous thin films of transition metal oxides and silica, using the evaporation induced self-assembly approach. The best conditions for the synthesis, deposition and post treatments have been found. To use these substrates for the construction of biosensors it was necessary to study their stability in PBS solutions to simulate the biological environment. Different trials were carried out to monitor the thickness of the films after immersion in solution from 1 to 48h and the result obtained was that zirconia and especially silica films were not stable, instead titania and hafnia were stable also after a long immersion in solution. Mesoporous titania was chosen as the adequate material for the final construction of the devices thanks to its hydrolytic stability in water and in physiological solutions and for the simplicity of the synthesis. These materials were characterized with FTIR measures to obtain the complete template removal allowing the maximum surface area for the following step of functionalization. From TEM measures the films resulted porous and ordered with a pore distance of 8.5nm, data that was confirmed by GISAXS measures that attributed to the porous titania a cubic disposition, contracted for the thermal treatment, to form a unit cell of 7 x 3 nm. To understand the morphology of the material were carried out FIR measures that showed as the material was composed of small crystallites of anatase in an amorphous matrix, that for its very small size was not visible by GISAXS. For the incorporation of biomolecules on the film surface it was necessary to functionalize the surface with a linker, in particular APTES and APTMS were used to obtain a film with exposed amino groups. Two routes were followed to functionalize the mesoporous surface: the “one pot” synthesis with organosilane molecules and the “post-synthesis” process with grafting groups. The first method did not allow to remove completely the template because the film was synthesized together with the organic functional group that would be destroyed if treated at 350°C. For this reason the films without all the thermal treatments were less stable and dissolved in solution; it was visible by ellipsometric measures that showed a consistent thickness reduction of the one pot films if immersed in solution. Furthermore with this method the organic functions were incorporated not only on the pore surface but also into the material framework, not allowing a big amount of functionalities available for the linking. For all these reasons the post-synthesis method was chosen to anchor organic groups to the pore wall of mesoporous titania film. This was possible with a hydrolysis-condensation reaction that was monitored with FTIR, AFM, and ellipsometry measures. The functionalization process of non porous (dense) with porous materials was compared, obtaining dramatic differences in FTIR spectra due to the different amount of organic functions incorporated only on the surface or on the

surface and inside the pore system. Once obtained the functionalized materials the films were used as substrates for the coupling and detection of additional molecules (first and second part of the work) or as building units for the assembly of nanoscaled structures (third part of the work).

In the first part of the work new devices for the detection of dioxins and in particular the most dangerous molecule TCDD, were developed. Three peptides were used as recognising element of the device. They were synthesized, purified and characterized with HPLC and MALDI-TOF MS. After that the peptides were immobilized on titania films functionalized with APTES and the best linking was found for the peptide with the terminal Valine, while the other peptides did not furnish positive results. The presence of peptides was monitored with FTIR measures and the linking for porous and dense titania was analyzed obtaining a good amount of peptide only in porous films. This revealed the excellent possibility to immobilize biomolecules on these porous materials thanks to their high surface area and pore volume. This linking was evident also by ellipsometric measures that showed a film thickness for calcined mesoporous titania of 180nm, after the linking with APTES of 270nm and after the peptide immobilization of 350nm. The linking of APTES and peptide was also monitored by AFM, to avoid the formation of aggregates on the film surface that do not guarantee the film homogeneity. The linking of the peptide to the film was also followed by fluorescence measures. These measures were first done in solution where FITC was identified as a good probe for the linking of peptides and for the TCDD detection. Finally the peptide was labelled with FITC, and the linking to the substrate was followed by florescence. The variation of fluorescence wad also detected after the linking of the TCDD on the device. With the created biosensor were read different concentrations of TCDD and the detection limit that produced an increase of fluorescence after the dioxins binding was at pM concentrations. This device can be a detection technique for simple and extensive pre-screening method, to monitor, by fluorescence measures, if a sample was contaminated or not. This detection limit can discriminate many samples, but for a more accurate analysis they can be submitted to HRGC/MS. The final device can be useful for the short time required for the analysis (less than 1 min), for the low cost, for the simplicity of use (the chip can just be immersed into the samples for a few minutes, washed, dried and analyzed), for the sensitivity (detection at pM level) and specificity (for the presence of peptides that bind only dioxins molecules).

The second part of the work was based on the detection of pathogens and in particular E.coli O157:H7 with FTIR, through the encapsulation of biological molecules in sol-gel materials and in particular in mesoporous titania thin films. Titania, in fact, in addition to the properties due to the pores (surface area and volume) is also a biocompatible material that can coordinate with the

biomolecules and keep their bioactivity. This is what was tried to obtain with our device for the direct linking of pathogens on titania surface and on a functionalized device. In detail different routes were tried and the linking TiO_2-APTES-GA-Ab-E.coli led to the best results. In fact thanks to a cross linker, the GA, was possible to link the functionalized titania to the specific antibody for the final step of detection. It was possible to link directly the pathogen on titania film but in this way it was not possible to obtain a selective device for the detection of a pathogen. With the functionalized device a detection limit of 10^2 CFU/ml was reached and it was possible to discriminate not only the pathogen (with the specific antibody) but also the subspecies. In future it could be created chips divided in different sections that contain different antibodies for the simultaneous detection of different pathogens; in fact thanks to the recent development in the FTIR instruments is possible to have a clear fingerprint of the pathogen and also of the subspecies that could be memorized in software to have a direct identification of the pathogen after the measure. In this way a device that required a quick sample preparation was obtained; in fact the pathogen was linked to the substrate in less than 30 minutes, thanks to the nanostructured substrate that provided a big surface coverage, leading to a greater efficiency for the capture. These chips could be used in field with portable instruments; they would be low cost, quick, highly specific and with a good sensibility and would not require skilled workers (a software could directly recognize the pathogen spectra).

In the third part of the work the aim was to overcome the limitations encountered in the other parts of the work and in particular the detection limit. In fact mesoporous materials for the construction of substrates were applied because their properties give a relevant enhancement of the Raman signal for the detection of molecules that are absorbed on them. In particular, for the development of these SERS substrates AgNPs were grown on mesoporous titania films with a bottom up approach. In this way it was possible to control the geometry, the shapes and the distance of nanoparticles that started growing into the pores with cubic geometry at definite distance and continued growing in the same way on the film surface until forming clusters of nanoparticles with the same dimension. All this process was followed with AFM measures. The UV-vis measures confirmed the reduction of Ag^+ to Ag^0 leading to AgNPs of dimension bigger than 20nm and through XRD analysis the formation of face centred cubic Ag with the same cubic disposition of titania, in anatase form, was revealed. After 6h of UV reaction the peak due to $AgNO_3$ disappeared due the complete reduction of silver ion. After that were calculated the crystallites dimension that were around 32-36nm; result that agrees with the previous UV and AFM measures. After the characterization of the material, SERS measures were tried, and in particular for the first trial RhBITC was used as a prototype dye, because when it is absorbed on a SERS substrate it produces

a very intense SERS spectrum not only at 532nm but also at 633nm. In this way, covering the film with this dye, a level of detection under the femtomolar (concentration of 10^{-16} M) was reached. The reproducibility, homogeneity of distribution and consistency of the results was also confirmed, by repeating the measures different times on the same sample, obtaining a final enhancement factor compared to non SERS substrate bigger of 10^{13} order of magnitude. The same experiment was also tried without a dye for the detection of a protein (CytC) and the same detection limit and enhancement factor were reached. The results showed that TiO_2 with AgNPs synthesized in this way is an excellent SERS substrate, that allows to obtain a new detection method in a fast way (the measure requires less than 2 min), that does not need sample preparation (the sample is just deposited on the substrate), that does not have signal by water molecules (important for biological sample rich in water) and furthermore it is highly photostable, low cost, reproducible, homogeneous and gives an immense amplification of the signal. In this way, this device can be applied for the detection of molecules with or without a SERS enhancer (rhodamine), and in particular for the detection of environmental toxins or biomolecules. Thanks to their properties of high spectral resolution, high sensibility (it can detect analytes at single molecule levels), simple analysis at room temperature, capability of avoiding different problems, as the photobleaching (that can be found e.g. in fluorescence measures), it can be a valuable tool. In this way, with these substrates very low detection limits were reached in a simple way and the next research will be based on the detection of food pathogen and contaminants with the construction of new devices.

List of symbols and abbreviations

AFM Atomic force microscopy

Ah aryl hydrocarbon

AhR Ah receptor

ANS 1-anilino-naphthalene-8-sulfonic acid

APTES 3-aminopropyltriethoxysilane

APTMS 3-aminopropyltrimethoxysilane

Arnt Ah receptor nuclear translocator

BEIA bioluminescent enzyme immunoassay

BSE bovine spongiform encephalopathy

CALUX chemically activated luciferase expression

CDR complementarity determining region

CFU colony-forming units

C_{mc} critical micelle concentration

CYP1A1 cytochrome P4501A1

CytC cytochrome c

DCM dichloromethane

DIPEA *N*-Ethyldiisopropylamine

DMF Dimethylformamide

DMSO dimethyl sulfoxide

DRE dioxin responsive element

EIA enzyme immunoassay

EISA evaporation-induced self assembly

ELFA enzyme-linked fluorescent assay

ELIMCL enzyme-linked immunomagnetic chemiluminescence

ELISA enzyme linked immunosorbent assay

EROD 7-ethoxyresorufin O-deethylase

FDA Food and drug administration

FIR far infrared

FITC Fluorescein isothiocyanate

FT-IR Fourier Transform Infrared

FWHM full width at half maximum

GA Glutaraldehyde

GISAXS grazing incidence small angle X-ray scattering

HACCP hazard analysis in critical control point

HAHs halogenated aromatic hydrocarbons

HATU *N,N,N′,N′*-Tetramethyl-*O*-(7-azabenzotriazol-1-yl)uronium hexafluorophosphate

HOBt 1-hydroxybenzotriazole hydrate

HRGC/MS high-resolution gas chromatography / mass spectrometry

Hsp heat shock protein

IARC International Agency for Research on Cancer

ICG immunochromatography strip test,

ISO International Organization for Standardization

ITEQ International Toxic Equivalent

IUPAC International Union of Pure and Applied Chemistry

LIA line immunoassay

MIR middle infrared

MSE mean square error

n Refractive index

NMP 1-methyl-2- pyrrolidone

NPs nanoparticles

PBS phosphate buffered saline

PCBs Polychlorinated biphenyls

PCDDs polychlorinated dibenzo para dioxins

PCDFs polychlorinated dibenzofurans

PCR polymerase chain reaction

PEO polyethylene oxide

POPs Persistent Organic Pollutants

PPO polypropylene oxide

PZT Piezoelectric Transducer

RH relative humidity

RhBITC rhodamine B isothiocyanate

RIA radio-immunoassays

RIBA recombinant immunoblot assay

RT-PCR reverse transcriptase PCR

SERS surface-enhanced Raman spectroscopy

SPR surface plasmon resonance

TCDD 2,3,7,8- tetrachlorodibenzo-para-dioxin

TDI tolerable daily intake

TEFs toxicity equivalency factors

TEM transmission electron microscopy

TEOS tetraethoxysilane

TEQ toxic equivalency

TFA trifluoroacetic acid

TIS triisopropylsilane

TMO transition metal oxides

TO transverse optical

TQM Total Quality Management

vCJD human variant Creutzfeldt-Jakob Disease

WHO World Health Organisation

XAP X-associated cellular protein

XRD X-ray diffraction

λ (wavelength)

References

[1] FDA Centre for Food Safety and Applied Nutrition (2007) www.cfsan.fda.gov/ebam/bam-a1.html. Accessed 13 Nov 2007

[2] Alocilja EC, Radke SM. Market analysis of biosensors for food safety. Biosens Bioelectron. 2003, 18:841–6

[3] Chemburu S, Wilkins E, Abdel-Hamid I. Detection of pathogenic bacteria in food samples using highly-dispersed carbon particles. Biosens Bioelectron. 2005, 21:491–9.

[4] Belson K, Fahim K. After extensive beef recall, Topps goes out of business. The New York Times [Newspaper]. 2007.

[5] Ivnitski D, Abdel-Hamid I, Atanasov P, Wilkins E, Biosensors for detection of pathogenic bacteria. Biosensors & Bioelectronics. 1999, 14 599–624

[6] Griffin, P.M., Tauxe, R.V.. The epidemiology of infections caused by E. coli 0157:H7 and other Enterohemorrhagic E. coli, and the associated hemolytic-uremic syndrome. Epidemiol. 1991, 13, 60–98.

[7] Buchanan, R. L., Doly, M.P.. Foodborne desease significance of E. coli O157:H7 and other enterohemorrhagic E. coli. Food Technol. 1997, 51 (10), 69–76.

[8] Rowe, P.C., Orrbine, E., Wells, G.A. Epidemiology of hemolytic-uremic syndrome in Canadian children from 1986 to 1988. J. Pediatr. 1991, 119, 218–224.

[9] Kay D, Crowther J, Fewtrell L, Francis CA, Hopkins M, Kay C, et al. Quantification and control of microbial pollution from agriculture: a new policy challenge? Environ Sci Policy 2008, 11:171–84

[10] Mucchetti G, Bonvini B, Francolino S, Neviani E, Carminati D. Effect of washing with a high pressure water spray on removal of Listeria innocua from Gorgonzola cheese rind. Food Control. 2008, 19:521–5.

[11] Umali-Deininger D, Sur M. Food safety in a globalizing world: opportunities and challenges for India. Agric Econ. 2007, 37:135–47.

[12] Jin SS, Zhou J, Ye J. Adoption of HACCP system in the Chinese food industry: a comparative analysis. Food Control. 2008, 19:823–8.

[13] Taylor E. A new method of HACCP for the catering and food service industry. Food Control. 2007, 19:126–34.

[14] Piatek, D. R. and Ramaen, D. L. J. Method for controlling the freshness of food products liable to pass an expiry date, uses a barcode reader device that reads in a conservation code when a product is opened and determines a new expiry date which is displayed [Patent Number: FR2809519-A1]. 2001.

[15] DeBoer E, Beumer RR. Methodology for detection and typing of foodborne microorganisms. Int J Food Microbiol. 1999, 50:119–30.

[16] Artault S, Blind JL, Delaval J, Dureuil Y, Gaillard N. Detecting Listeria monocytogenes in food. Int Food Hyg. 2001, 12:23

[17] Ayçiçek H, Aydogan H, Küçükkaraaslan A, Baysallar M, Basustaoglu AC. Assessment of the bacterial contamination on hands of hospital food handlers. Food Control. 2004, 15:253–9.

[18] Sanders SQ, Boothe DH, Frank JF, Arnold JW. Culture and detection of Campylobacter jejuni within mixed microbial populations of biofilms on stainless steel. J Food Prot. 2007, 70:1379–85.

[19] Weagant SD. A new chromogenic agar medium for detection of potentially virulent Yersinia enterocolitica. J Microbiol Methods. Feb 2008, 72:185–90.

[20] Stephan R., Schumacher S., Zychowska M.A. The VITR technology for rapid detection of Listeria monocytogenes and other Listeria spp. Int J Food Microbiol. 2003, 89:287–90.

[21] Brooks BW, Devenish J, Lutze-Wallace CL, Milnes D, Robertson RH, Berlie-Surujballi G. Evaluation of a monoclonal antibody-based enzyme-linked immunosorbent assay for detection of Campylobacter fetus in bovine preputial washing and vaginal mucus samples. Vet Microbiol. 2004, 103:77–84.

[22] Velusamy V, Arshak K, Korostynska O, Oliwa K, Adley C. An overview of foodborne pathogen detection: In the perspective of biosensors. Biotechnology Advances. 2010, 232–254.

[23] Iqbal SS, Mayo MW, Bruno JG, Bronk BV, Batt CA, Chambers JP. A review of molecular recognition technologies for detection of biological threat agents. Biosens Bioelectron. 2000, 15:549–78.

[24] Leonard P, Hearty S, Brennan J, Dunne L, Quinn J, Chakraborty T, et al. Advances in biosensors for detection of pathogens in food and water. Enzyme Microb Technol. 2003, 32:3-13.

[25] Meng JH, Doyle MP. Introduction. Microbiological food safety. Microb Infect. 2002, 4: 395–7.

[26] Murphy NM, McLauchlin J, Ohai C, Grant KA. Construction and evaluation of a microbiological positive process internal control for PCR-based examination of food samples for Listeria monocytogenes and Salmonella enterica. Int J Food Microbiol. 2007, 120:110–9.

[27] Touron A, Berthe T, Pawlak B, Petit F. Detection of Salmonella in environmental water and sediment by a nested-multiplex polymerase chain reaction assay. Res Microbiol. 2005, 156:541–53.

[28] Liem AKD and van Zorge JA. Dioxins and related compounds: status and regulatory aspects. Environ. Sei. Pollo Res. 1995, 2, 46-56.

[29] Van den Berg M, Birnbaum L, Bosveld ATC, Brunström B, Cook P, Feeley M, Giesy JP, Hanberg A, Hasegawa R, Kennedy SW, Kubiak T, Larsen JC, Leeuwen FXR, Liem AKD, Nolt C, Peterson RE, Poellinger L, Safe S, Schrenk D, Tillitt D, Tysklind M, Younes M, Wærn F, Zacharewski T, Toxic Equivalency Factors (TEFs) for PCBs, PCDDs, PCDFs for Humans and Wildlife. Environ Health Perspect. 1998, 106:775-792.

[30] Rappe C and Buser HR. Occupational exposure to polychlorinated dioxins and dibenzofurans. ln: Choudhar G, ed., Chemical Hazards in the Workplace - Measurement and Control (ACS Symposium Series No. 149), Washington DC, American Chemical Society. 1981 pp. 319-342

[31] Safe S, Bandiera S, Sawyer T, Robertson L, Safe L, Parkinson A, Thomas PE, Ryan DE, Reik LM, Levin W, et al. PCBs: Structure-function relationships and mechanism of action. Environ. Health Perspect. 1985, 60, 47–56.

[32] WHO/EURO (World Health Organisation/Regional Office for Europe) (1987). Dioxins and Furans from Municipal Incinerators (Environmental Health Series 17), Copenhagen

[33] Gillespie WJ and Gellman L. Dioxin in pulp and paper products: incidence and risk. ln: Bleaching: a TAPPl Press Anthology, TAPPl Proceedings. Bleach Plant Operation. 1989, pp. 658-663.

[34] ATSDR (2001). Polychlorinated biphenyls. Accessed at http : // www.atsdr.cdc.gov/tfacts17.pdf.

[35] WHO Dioxins and their effects on human health. May 2010. Fact sheet N°225

[36] Monitoring of Dioxins in Food and Feed EFSA Journal 2010; 8(3):1385 7-35

[37] Ahlborg UG, Brouwer A, Fingerhut MA, Jacobson JL, Jacobson SW, Kennedy SW, Kettrup AAF, Koeman JH, Poiger H, Rappe C, Safe SH, Seegal RF, Tuomisto J, van den Berg M. Impact of polychlorinated dibenzo-p-dioxins, dibenzofurans and biphenyls on human and environmental health, with special emphasis on application of the toxic equivalency factor concept. Europ. J. PharmcoL.-environ. ToxicoL. PharmcoL. 1992, 228, 179-199.

[38] IARC. Monographs on the evaluation of carcinogenic risks to humans. Volume 69, Polychlorinated dibenzo-para-dioxins and polychlorinated dibenzofurans, Lyon. 1997, pp 33-343.

[39] Poland A., J.C. Knutson, 2,3,7,8-Tetrachlorodibenzo-thorn-Dioxin and Related Halogenated Aromatic Hydrocarbons: Examination of the Mechanism of Toxicity, Annu. Rev. Pharmacol. Toxicol. 1982, 517

[40] Safe SH. Comparative toxicology and mechanism of action of polychlorinated dibenzo-p-dioxins and dibenzofurans. Annu. Rev. Pharmacol. Toxicol. 1986, 371–399.

[41] White JC, Parrish ZD, Isleyen M, Gent MP, Iannucci-Berger W, Eitzer BD, Kelsey JW and Mattina MI. Influence of citric acid amendments on the availability of weathered PCBs to plant and earthworm species. Int. J. Phytoremediation. 2005, 8, 63-79.

[42] Poland A, Knutson J, and Glover E. Studies on the mechanism of action of halogenated aromatic hydrocarbons. Clin. Physiol. Biochem. 1985, 3, 147–154.

[43] Safe S., Development, validation and limitations of toxic equivalency factors,Crit. Rev. Toxicol. 1990, 51

[44] Denison M.S., C.F. Elferink, D. Phelan, in: M.S. Denison, W.G. Helferich (Eds.), Toxicant–Receptor Interactions in the Modulation of Signal transduction and Gene Expression, Taylor & Francis, Bristol, PA. 1998, p. 3.

[45] Pongratz P.I., G.G.F. Mason, L. Poellinger, Dual roles of the 90-kDa heat shock protein hsp90 in modulating functional activities of the dioxin receptor. Evidence that the dioxin receptor functionally belongs to a subclass of nuclear receptors which require hsp90 both for ligand binding activity and repression of intrinsic DNA binding activity. J. Biol. Chem. 1992, 13728-34

[46] Chen H.-S., G.H. Perdew, Subunit composition of the heteromeric cytosolic aryl hydrocarbon receptor complexJ. Biol. Chem. 1994, 269 27554-58

[47] Meyer B.K., M.G. Pray-Grant, J.P. Vanden Heuvel, G.H. Perdew, Hepatitis B virus X-associated protein 2 is a subunit of the unliganded aryl hydrocarbon receptor core complex and exhibits transcriptional enhancer activity Mol. Cell Biol. 1998, 18 978-88.

[48] Kazlauskas A., L. Poellinger, I. Pongratz, Evidence That the Co-chaperone p23 Regulates Ligand Responsiveness of the Dioxin (Aryl Hydrocarbon) Receptor J. Biol. Chem. 1999, 274 13519

[49] Whitlock Jr. J.P., Induction of cytochrome P4501A1, Ann. Rev. Pharmacol. Toxicol. 1999, 39 103-25

[50] Denison M. S., Zhao B., Baston D.S., Clark G.C., Murata H., Hana D., Recombinant cell bioassay systems for the detection and relative quantitation of halogenated dioxins and related chemicals , Talanta. 2004, 63 1123–1133

[51] Safe SH. Polychlorinated biphenyl (PCBs). Environmental impact, biochemical and toxic responses, and implications for risk assessment. Crit Rev Toxicol. 1994, 24(2):87 – 149.

[52] Harrison RO, Carlson RE. Immunoassay analysis of dioxin in soil: validation of TEQ screening at 500 ppt using rapid extraction clean up. Organohalogen Compd. 1999, 40:31 – 4

[53] Anderson JW, Jones JM, McCoy DL. Cost-effective dioxin site characterization using a P450 human reporter gene system (HRGS; EPA 4425).Organohalogen Compd. 2000, 45:208– 11.

[54] Jones JM, Anderson JW, Tukey RH. Using the metabolism of PAHs in a human cell line to characterize environmental samples. Environ Toxicol Pharmacol. 2000, 8:119–26.

[55] El-Fouly MH, Richter C, Giesy JP, Denison M. Production of a novel recombinant cell line for use as a bioassay system for detection of 2,3,7,8-TCDD-like chemicals. Environ Toxicol Chem. 1994, 13:1581–8.

[56] Nagy SR, Lui G, Lam K, Denison MS. A green fluorescent protein based recombinant cell bioassay for the detection of activators of the Ah receptor: application of screening of 1,5-dialkylamino-2,4-dinitrobenzene combinatorial chemical library. Organohalogen Compd. 2000, 45:232– 5.

[57] Kobayashi Y. et al. Evaluation of Ah-Immunoassay as a screening method for dioxins and co-PCBs in environmental samples, in: Proceedings of the DXN2002 Conference. 2003.

[58] Uchiyama K., Yang M., Sawazaki T., Shimizu H., Ito S. Development of a Bio-MEMS for Evaluation of dioxin toxicity by immunoassay method, Sensors and Actuators, B 103. 2004, 200–205

[59] Kobayashi Y. et al. Dioxin screening in environmental samples using the Ah-Immunoassay, in: the Proceedings of the DXN2002 Conference. 2002, pp. 337–340.

[60] Vanderlaan M, Watkins BE, Stanker L. Environmental monitoring by immunoassay. Environ Sci Technol 1988, 22(3):247–54.

[61] Sadik O, Witt DM. Monitoring Endocrine-disrupting chemicals. Environ Sci Technol. 1999, 368:A-374 (A News, Sept. 1).

[62] Clark GC, Brown DJ, Seidel SD, Phelan D, Denison MS. Characterisation of the CALUX and GRAB bioassays for sensitivity and specificity in the detection of pharmacological agents that activate the Ah receptor signalling system. Organohalogen Compd 1999, 42:309– 12.

[63] Seidel SD, Li V, Winter GM, Rogers WJ, Martinez EI, Denison MS. Ah receptor-based chemical screening bioassays: application and limitations for the detection of Ah receptor agonists. Toxicol Sci. 2000, 55: 107– 15.

[64] Afshari CA, Nuwaysir EF, Barrett JC. Application of complementary DNA microarray technology to carcinogen identification, toxicology and drug safety evaluation. Cancer Res. 1999, 59(19):4759– 60.

[65] Takhistov Paul, Biosensors technology for food processing, safety and packaging from Y.H.Hui, Handbook of food science technology and engineering. 2006, Cap.128, Vol.3

[66] Lazcka O, Del Campo FJ, Munoz FX. Pathogen detection: a perspective of traditional methods and biosensors. Biosens Bioelectron. 2007, 22:1205–17.

[67] Vo-Dinh T, Cullum B. Biosensors and biochips: advances in biological and medical diagnostics. Fresenius J Anal Chem. 2000, 366:540–51

[68] Lim DV. Detection of microorganisms and toxins with evanescent wave fiber-optic biosensors. Proc IEEE 2003, 91:902–7.

[69] Taylor AD, Ladd J, Yu QM, Chen SF, Homola J, Jiang SY. Quantitative and simultaneous detection of four foodborne bacterial pathogens with a multi-channel SPR sensor. Biosens Bioelectron. 2006, 22:752–8.

[70] Waswa J, Irudayaraj J, DebRoy C. Direct detection of E-Coli O157: H7 in selected food systems by a surface plasmon resonance biosensor. Lwt-Food Sci Technol. 2007, 40:187–92.

[71] Campbell GA, Mutharasan R. Detection of pathogen Escherichia coli O157: H7 using selfexcited PZT-glass microcantilevers. Biosens Bioelectron. 2005, 21:462–73.

[72] Pal S, Alocilja EC, Downes FP. Nanowire labeled direct-charge transfer biosensor for detecting Bacillus species. Biosens Bioelectron. 2007, 22:2329–36.

[73] Guntupalli R, Hu J, Lakshmanan RS, Huang TS, Barbaree JM, Chin BA. A magnetoelastic resonance biosensor immobilized with polyclonal antibody for the detection of Salmonella typhimurium. Biosens Bioelectron. 2007, 22:1474–9.

[74] Tokarskyy O, Marshall DL. Immunosensors for rapid detection of Escherichia coli O157: H7 —perspectives for use in the meat processing industry. Food Microbiol. 2008, 25:1-12.

[75] Coons AH, Creech HJ, Jones RN, Berliner E. The demonstration of pneumococcal antigen in tissues by the use of fluorescent-antibody. J Immunol. 1942, 45:159–70.

[76] Weller TH, Coons AH. Fluorescent antibody studies with agents of varicella and herpes zoster propagated in vitro. Proc Soc Exp Biol Med. 1954, 86:789–94.

[77] Rule K.L., and Vikesland P. J., Surface-Enhanced Resonance Raman Spectroscopy for the Rapid Detection of Cryptosporidium parvum and Giardia lamblia, Environ. Sci. Technol. 2009, 43, 1147–1152

[78] Aroca, R. Surface Enhanced Vibrational Spectroscopy; 2006, Wiley: Chichester.

[79] Stiles P. L., Dieringer J. A., Shah N. C., Van Duyne R. P., Surface-Enhanced Raman Spectroscopy Annu. Rev. Anal. Chem. 2008, 1, 601–626.

[80] Kustner B., Gellner M., Schutz M., Schoppler F., Marx A., Strobel P., Adam P., Schmuck C., Schlucker S., SERS Labels for Red Laser Excitation: Silica-Encapsulated SAMs on Tunable Gold/Silver Nanoshells Angew. Chem. 2009, 121, 1984–1987

[81] Ni J., Lipert R. J., Dawson G. B., Porter M. D., Immunoassay readout method using extrinsic Raman labels adsorbed on immunogold colloidsAnal. Chem. 1999, 71, 4903–4908.

[82] Goeller LJ, Riley MR. Discrimination of bacteria and bacteriophages by Raman spectroscopy and surface-enhanced Raman spectroscopy. Appl Spectrosc. 2007, 61:679–85.

[83] Grow AE, Wood LL, Claycomb JL, Thompson PA. New biochip technology for label-free detection of pathogens and their toxins. J Microbiol Methods. 2003, 53:221–33.

[84] Kalasinsky KS, Hadfield T, Shea AA, Kalasinsky VF, Nelson MP, Neiss J, et al. Raman chemical imaging spectroscopy reagentless detection and identification of pathogens: signature development and evaluation. Anal Chem. 2007, 79:2658–73

[85] Schmilovitch Z, Mizrach A, Alchanatis V, Kritzman G, Korotic R, Irudayaraj J, et al. Detection of bacteria with low-resolution Raman spectroscopy. Trans ASAE. 2005, 48: 1843–50.

[86] Siebert F., Infrared spectroscopy applied to biochemical and biological problems, Methods Enzymol. 1995, 501–526.

[87] Aroca R., Surface-Enhanced Vibrational Spectroscopy, Wiley, New York. 2006.

[88] Kneipp K., Kneipp H., Itzkan I., Dasari R.R., Feld M.S., Ultrasensitive chemical analysis by Raman spectroscopy, Chem. Rev. 1999, 2957– 2976

[89] Kneipp K.. Surface-Enhanced Raman Scattering, Physics Today . 2007, vol.60 Iss.11 pp.40-47 .

[90] Le Ru E. C., Blackie E., Meyer M., and Etchegoin P. G., Surface Enhanced Raman Scattering Enhancement Factors: A Comprehensive Study J. Phys. Chem. C, 2007Vol. 111, No. 37.

[91] Lin S.-Y., Li M.-J., Cheng W.-T., FT-IR and Raman vibrational microspectroscopies used for spectral biodiagnosis of human tissues, Spectroscopy. 2007, 21 1–30.

[92] Liu Y., Chao K., Nou X., Chen Y.R., Feasibility of colloidal silver SERS for rapid bacterial screening, Sens. & Instrumen. Food Qual. 2009, 3:100–107

[93] Naumann D. FT-infrared and FT-Raman spectroscopy in biomedical research, in: H.U. Gremlich, B. Yan (Eds.), Infrared and Raman Spectroscopy of Biological Materials, Marcel Dekker Inc. New York. 2001, pp. 323–377.

[94] Nie S., Emory S.R., Probing single molecules and single nanoparticles by surface-enhanced Raman scattering, Science. 1997, 275 1102– 1106.

[95] Schlucker S., Kiefer W. In Frontiers of Molecular Spectroscopy "Selective Detection of Proteins and Nucleic Acids with Biofunctionalized SERS Labels": (Ed.: J. Laane), Elsevier, Amsterdam. 2009, pp. 267–288.

[96] Schlücker S. SERS Microscopy: Nanoparticles probes and biomedical applications, ChemPhysChem. 2009, 10, 1344-1354.

[97] Arrondo J.L.R., Muga A., Castresana J., Goñi F.M. Quantitative studies of the structure of proteins in solution by Fourier-transform infrared spectroscopy, Prog. Biophys. Mol. Biol. 1993, 59 23–56.

[98] Blackie E. Quantification of the enhancement factor in surface enhanced raman scattering. 2010, PhD Thesis.

[99] Xu H., Aizpurua J., Kell M., Apell P. Electromagnetic contributions to single-molecule sensitivity in surface-enhanced Raman scattering, Phys. Rev. 2000, E 62 4318–4324;

[100] Arrondo J.L.R., Goñi F.M. Structure and dynamics of membrane proteins as studied by infrared spectroscopy, Prog. Biophys. Mol. Biol. 1999, 72 367–405.

[101] Barth A. IR spectroscopy, in: V.N. Uversky, E.A. Permyakov (Eds.), Protein Structures: Methods in Protein Structure and Stability Analysis, Nova Science Publishers, 2006.

[102] Barth A., Infrared spectroscopy of proteins, Biochimica et Biophysica Acta 1767. 2007, 1073–1101

[103] Fabian H.,. Mäntele W, Infrared spectroscopy of proteins, in: J.M. Chalmers, P.R. Griffiths (Eds.), Handbook of Vibrational Spectroscopy, John Wiley & Sons, Chichester, 2002, pp. 3399–3426.

[104] Yu CX, Irudayaraj J, Debroy C, Schmilovtich Z, Mizrach A. Spectroscopic differentiation and quantification of microorganisms in apple juice. J Food Sci. 2004, 69:S268–72.

[105] Al-Holy MA, Lin M, Cavinato AG, Rasco BA. The use of Fourier transform infrared spectroscopy to differentiate Escherichia coli O157: H7 from other bacteria inoculated into apple juice. Food Microbiol. 2006, 23:162–8.

[106] Lin MS, Al-Holy M, Al-Qadiri H, Kang DH, Cavinato AG, Huang YQ, et al. Discrimination of intact and injured Listeria monocytogenes by Fourier transform infrared spectroscopy and principal component analysis. J Agric Food Chem. 2004, 52: 5769–72.

[107] Ellis DI, Broadhurst D, Kell DB, Rowland JJ, Goodacre R. Rapid and quantitative detection of the microbial spoilage of meat by Fourier transform infrared spectroscopy and machine learning. Appl Environ Microbiol. 2002, 68:2822–8.

[108] Ellis DI, Broadhurst D, Clarke SJ, Goodacre R. Rapid identification of closely related muscle foods by vibrational spectroscopy and machine learning. Analyst. 2005, 130:1648–54.

[109] Shahzad A., Köhler G., Knapp M., Gaubitzer E., Puchinger M. and Edetsberger M.; Emerging applications of fluorescence spectroscopy in medical microbiology field, Journal of Translational Medicine. 2009, 7, 99.

[110] Scott, N.R. Nanotechnology and animal health. Rev. sci. tech. Off. int. Epiz. 2005, 24(1): 425-432.

[111] Warad, H.C. and J. Dutta. Nanotechnology for agriculture and food systems – a view. Proc. 2nd International Conference on Innovations in Food Processing Technology and Engineering. Bangkok, Thailand. 2005.

[112] Lu G Q, X S Zhao. Nanoporous materials: Science and engineering. 2004.

[113] Forster S. and Thomas Plantenberg, From Self-Organizing Polymers to Nanohybrid and Biomaterials, Angew. Chem. Int. Ed. 2002, 41, 688 ± 714

[114] Beck J S, Vartuli J C, Roth W J, Leonowicz M E, Kresge C T, Schmitt K D, Chu C T W, Olson D H, Sheppard E W, McCullen S B, Higgins J B, Schlenker J L. A new family of mesoporous molecular sieves prepared with liquid crystal templates. J Am Chem Soc, 1992, 114: 10834—10843

[115] Brinker C. J., A. J. Hurd, K. J. Ward in Ultrastructure Processing of Advanced Ceramics, eds. J. D. Mackenzie and D. R. Ulrich, Wiley, New York. 1988, 223.

[116] Satcher. Sol- gel chemistry, 2005.

[117] Wright J. D. and Nico A.J.M. Sommerdijk. Sol-gel materials, Chemistry and Applications, Gordon & Breach Sci. 2001, P, 88(19), 197401-1/197401-4.

[118] Whitesides G M, Grzybowski B A. Self-assembly at all scales. Science. 2002, 295: 2418—2421

[119] Ringsdorf H, Simon J. Molecular self-assembly-snap-together vesicles. Nature. 1994, 371: 284284

[120] Rodriguez-Mozaz, S; Marco, MP; de Alda, MJL; Barcelo, D. Biosensors for environmental applications: Future development trends. Pure and applied chemistry. 2004, 723 -732.

[121] Angelomè P. C. and Galo J. de A. A. Soler-Illia. Ordered mesoporous hybrid thin films with double organic functionality and mixed oxide frame work, J. Mater. Chem. 2005, 15, 3903–3912 | 3903

[122] Boettcher S W, Fan J, Tsung C K, Shi Q, Stucky G D. Harnessing the sol-gel process for the assembly of non-silicate mesostructured oxide materials. Acc Chem Res, 2007, 40: 784—792

[123] Brinker C. J., Scherrer G. W. Sol- gel materials, Chemistry and Applications, Sol-Gel Science, The Physics and Chemistry of Sol–Gel Processing. 1990.Academic Press, San-Diego, CA.

[124] Calvo, P. C. Angelome´, V. M. Sanchez, D. A. Scherlis, F. J. Williams, and G. J. A. A. Soler-Illia. Mesoporous Aminopropyl-Functionalized Hybrid Thin Films with Modulable Surface and Environment-Responsive Behavior Chem. Mater. 2008, 20, 4661–4668

[125] Crepaldi E. L., G. J. de A. A. Soler-Illia, D. Grosso, F. Cagnol, F. Ribot, and C. Sanchez. Highly Organized Mesoporous Titania Thin Films, J. Am. Chem. Soc. 2003, 125 (32), pp 9770–9786

[126] Fujita S, Inagaki S. Self-organization of organosilica solids with molecular- scale and mesoscale periodicities. Chem Mater. 2008, 20: 891—908

[127] Hatton B, Landskron K, Whitnall W, Perovic D, Ozin G A. Past, present, and future of periodic mesoporous organosilicass−the PMOs. Acc Chem Res. 2005, 38: 305—312

[128] Hoffmann F, Cornelius M, Morell J, Fröba M. Silica-based mesoporous organic-inorganic hybrid materials. Angew Chem Int Ed. 2006, 45: 3216—3251

[129] He X, Antonell D. Recent advances in synthesis and applications of transition metal containing mesoporous molecular sieves. Angew Chem Int Ed. 2002, 41: 214—229

[130] Hunks W J, Ozin G A. Challenges and advances in the chemistry of periodic mesoporous organosilicas (PMOs). J Mater Chem. 2005, 15: 3716—3724

[131] Kickelbick G. Hybrid inorganic-organic mesoporous materials. Angew Chem Int Ed. 2004, 43: 3102—3104

[132] Li L L, Duan, W T, Yuan Q, Li Z X, Duan H H, Yan C H. Hierarchical γ-Al2O3 monoliths with highly ordered 2D hexagonal mesopores in macroporous walls. Chem Commun. 2009, 6174—6176

[133] Moller K, Bein T. Inclusion chemistry in periodic mesoporous hosts. Chem Mater. 1998, 10: 2950—2963

[134] Monnier A, Schüth F, Huo Q, Kumar D, Margolese D, Maxwell R S, Stucky G D. Krishnamurty M, Petroff P, Firouzi A, Janicke M, Chmelka B. Cooperative formation of inorganic-organic interfaces in the synthesis of silicate mesostructures. Science. 1993, 261; 1299—1303

[135] Sanchez C, Boissière C, Grosso D, Laberty C, Nicole L. Design, synthesis, and properties of inorganic and hybrid thin films having periodically organized nanoporosity. Chem Mater. 2008, 20: 682—737

[136] Schmidt H., M. Mennig. Wet Coating Technologies for Glass. 2000. The sol-gel gateway.

[137] Schüth F. Non-siliceous mesostructured and mesoporous materials. Chem Mater. 2001, 13: 3184—3195

[138] Scott B J, Wirnsberger G, Stucky G D. Mesoporous and mesostructured materials for optical applications. Chem Mater. 2001, 13: 3140—3150

[139] Soler-Illia G. J. A. A. and P. Innocenzi. Mesoporous Hybrid Thin Films: The Physics and Chemistry Beneath Chem. Eur. J. 2006, 12, 4478 – 4494

[140] Wan Y, Shi Y F, Zhao D Y. Designed synthesis of mesoporous solids via nonionic-surfactant-templating approach. Chem Commun. 2007, 897—926

[141] Wan Y, Yang H F, Zhao D Y. "Host-guest" chemistry in the synthesis of ordered nonsiliceous mesoporous materials. Acc Chem Res. 2006, 39: 423—432

[142] Yang P D, Zhao D Y, Margolese D I, Chmelka B F, Stucky G D. Generalized syntheses of large-pore mesoporous metal oxides with semicrystalline frameworks. Nature. 1998, 396; 152—155

[143] Yuan Q, Liu Q, Song W G, Feng W, Pu W L, Sun L D, Zhang Y W, Yan C H. Ordered mesoporous Ce1−xZrxO2 solid solutions with crystalline walls. J Am Chem Soc. 2007, 129: 6698—6699

[144] Yuan Q, Yin A X, Luo C, Sun L D, Zhang Y W, Duan W T, Liu H C, Yan C H. Facile synthesis for ordered mesoporous γ-aluminas with high thermal stability. J Am Chem Soc. 2008, 130: 3465—3472

[145] Ying J Y, Mehnert C P, Wong M S. Synthesis and applications of supramolecular-templated mesoporous materials. Angew Chem Int Ed. 1999, 38: 56—77

[146] Zhao L. et al. Preparation of mesoporous titania film using non-ionic triblock copolymer as surfactant template/ Applied Catalysis A: General. 2004, 263 171–177

[147] Li L., L. Sun, Y. Zhang, C. Yan, Functional-template directed self-assembly (FTDSA) of mesostructured organic-inorganic hybrid materials, Sci China Ser B-Chem. 2009, vol. 52, n°11, 1759-1768

[148] Flodstrom K., V. Alfredsson, Influence of the block length of triblock copolymers onthe formation of mesoporous silica, Microporous and Mesoporous Materials. 2003, 59, 167–176

[149] Smarsly et Antonietti, Block copolymer assemblies as templates for the generation of mesoporous inorganic materials and crystalline films, Eur. J. Inorg. Chem. 2006, 6,111-119,

[150] Soler-Illia G.J.d.A. et al. Block copolymer-templated mesoporous oxides, Current Opinion in Colloid and Interface Science. 2003, 8 109–126)

[151] Zhao D Y, Feng J L, Huo Q S, Melosh N, Fredrickson G H, Chmelka B F, Stucky G D. Triblock copolymer syntheses of mesoporous silica with periodic 50 to 300 Å pores. Science. 1998, 279: 548—552

[152] Lu Y, Ganguli R, Drewien CA, Anderson MT, Brinker CJ, Gong W, Guo Y, Soyez H, Dunn B, Huang MH, Zink JI Continuous formation of supported cubic and hexagonal mesoporous films by sol-gel dip-coating. Nature. 1997, 389:364–368

[153] Lu Y, Fan H, Stump A, Ward TL, Rieker T, Brinker CJ, Aerosol-Assisted Self-Assembly of Mesostructured Spherical Nanoparticles. Nature. 1999, 398:223–226

[154] Attard G S, Glyde J C, Göltner C G. Liquid-crystalline phases as templates for the synthesis of mesoporous silica. Nature. 1995, 378: 366—368

[155] Brinker C. J., Y. Lu, A. Sellinger, H. Fan, Evaporation-Induced Self-Assembly: Nanostructures Made EasyAdv. Mater. 1999, 11, 579-585.

[156] Lu G Q, X S Zhao. Nanoporous materials: Science and engineering. 2004.

[157] Inuyama Y.; Nakamura C.; Oka T.; Yoneda Y.; Obataya I.; Santo N.; Miyake J. Simple and high-sensitivity detection of dioxin using dioxin-binding peptapetide. Biosensors and bioelectronics. 2007, 22, 2093-2099.

[158] Nakamura C.; Inuyama Y.; Goto H.; Obataya I.; Kaneko N.; Nakamura N.; Santo N.; Miyake J. Dioxin-binding pentapeptide for use in a high-sensitivity on-bead detection assay. Anal. Chem. 2005, 77, 7750-7757

[159] Jang L. S.; Liu H. J.; Fabrication of protein chips based on 3-aminopropyltriethoxysilane as monolayer. Biomed Microdevices. 2009, 11, 331-338.

[160] Topoglidis E.; Cass A. E. G.; Gilardi G.; Sadeghi S.; Beaumont N.; Durrant J. Protein Adsorption on nanocrystalline TiO_2 films: an immobilization strategy for bioanalytical devices. Anal. Chem. 1998, 70, 5111-5113

[161] Calvo A.; Joselevich M.; Soler- Illia, G. J. d. A. A.; Williams F. J. Chemical reactivity of amino-functionalized mesoporous silica thin films obtained by co-condensation and post-grafting routes. Microporous and mesoporous materials. 2009, 121, 67-72.

[162] Howarter J.; Youngblood J. P. Optimization of silica silanization by 3-Aminopropyltriethoxysilane. Langmuir. 2006, 22, 11142-11147.

Ringraziamenti

Ringrazio per questo lavoro in primo luogo la mia relatrice, la Prof.ssa Silvia Pagani ed i miei correlatori il Prof. Gian Franco Greppi ed il Prof. Plinio Innocenzi, per avermi dato l'opportunità ed i mezzi per svolgere e concludere al meglio questo percorso di dottorato.

In particolare ringrazio il Prof. Greppi per essermi stato sempre accanto ed avermi guidato sempre in modo amorevole e propositivo nelle scelte quotidiane; inoltre lo ringrazio per aver creduto in me e per tutte le esperienze formative a cui mi ha consentito di partecipare durante questo periodo.

Ringrazio il Prof. Innocenzi per la sua disponibilità e per esser stato una guida fondamentale nel "nanomondo" ancora difficile da comprendere. Con lui ringrazio tutto il LMNT (Laboratorio di Scienza dei Materiali e Nanotecnologie) ed in particolare Tongjit, Luca, Cristiana, Daniela, Barbara, Alessandra, Davide e Stefano per tutte le stupende esperienze condivise in questi anni.

Vorrei anche ringraziare per la loro disponibilità e per l'amore nel trasmettere la scienza il Dott. Sabato D'Auria dell' IBP (Istituto di Biochimica delle Proteine) del CNR di Napoli presso cui ho svolto due periodi di questo dottorato e tutto il suo gruppo di ricerca che mi ha fatto sempre sentire a casa.

Ringrazio il Prof. Joseph Irudayaraj per avermi dato l' opportunità di svolgere parte di questo dottorato presso l'Agricultural and Biological Engineering Department della Purdue University (USA), e con lui tutto lo staff del Nanobiosensors Lab che mi ha consentito di vedere un'altra realtà ed ampliare enormemente le mie conoscenze.

Inoltre ringrazio i miei colleghi di dottorato milanesi ed in particolare Valentina per essere sempre stata disponibile ed ospitale. Infine ringrazio in modo particolare Sonia con cui ho condiviso davvero tanto anche al di fuori del lavoro e tutti gli altri miei colleghi con cui ho percorso questo cammino tra cui Vanna, Massimo, Giuseppina, Paola, Dionigia, Anna Maria, e tutto il personale di Porto Conte Ricerche.

Dedico questo lavoro a Salvatore, e lo ringrazio per avere sempre creduto in me e per avermi sempre accompagnato nella strada che porta alla mia realizzazione personale anche se le scelte che abbiamo dovuto prendere hanno incluso tanti sacrifici, tra cui lunghi periodi di distanza.Gli dico un GRAZIE immenso per esserci sempre stato e per non aver mai posto limiti e condizioni.

La mia dedica va anche ai miei genitori e a Gabriele che hanno vissuto con me tutti i periodi di gioia e preoccupazione che questo lavoro ha comportato e li ringrazio di cuore per tutto.

Insieme a loro ringrazio tutta la mia famiglia, miei padrini, cugini, nipotini e la mia famiglia acquisita, miei suoceri e mia cognata per avere condiviso con me ogni passo e per avermi sempre dimostrato la loro stima.

Infine, ma non meno importanti, ringrazio i miei amici ed in particolare Marco, Claudia, Davide per esser stati sempre presenti ed in particolare Tania che è stata immersa con me nella estenuante correzione di questo testo… alla fine questo lavoro è anche suo!

Mi scuso per tutti coloro che avrò di sicuro dimenticato e ringrazio tutti per aver percorso con me questo tratto di strada a volte in salita, a volte impervio ma al contempo ricco di tante scoperte e soddisfazioni che mi ha fatto immergere appieno nella mia infinita passione per la ricerca.